UNIVERSITY OF CALIFORNIA
RIVERSIDE

Climate Impacts of Biomass Burning Aerosols: Constraining the Chemicophysical Properties of Fresh and Aged Particles

A Dissertation submitted in partial satisfaction
of the requirements for the degree of

Doctor of Philosophy

in

Chemical and Environmental Engineering

by

Michael Giordano

June 2014

Dissertation Committee:
Dr. Akua Asa-Awuku, Chairperson
Dr. David Cocker
Dr. Roya Bahreini

The Dissertation of Michael Giordano is approved:

_____

_____

_____

Committee Chairperson

University of California, Riverside

Acknowledgements

This dissertation is the culmination of the time and work I have put in at UC Riverside. I owe many people my sincere gratitude for helping me make my time here fruitful and productive. Without the training, support, and guidance I have received, this dissertation would not have been possible.

First and foremost, I would like to thank my advisor Dr. Akua Asa-Awuku. Her support, guidance, and advice have helped me become not only a better scientist, engineer, and academic but also a better all-around person. I owe the growth of my abilities to identify research questions, form hypothesis, and design experiments to the time we have spent together. Most of all, however, she has my sincere gratitude for letting me find my own path in my graduate studies while still focusing me on the bigger picture. I will be forever thankful for the opportunities I was given to do field work alongside lab work in one of the premier environmental chambers in the world. Additionally, Dr. Asa-Awuku's ability to help me think through any questions and problems I was encountering myself is something I hope to be able to pass on to my own future mentees. I would also like to thank her for the ability to mentor a number of undergraduate students.

I would also like to thank Dr. David Cocker. His expertise in the aerosol field and his openness to share his knowledge with students has helped me greatly in my time at UCR. Without his support too, this dissertation would not have been possible.

Dr. Lelia Hawkins, at Harvey Mudd College, is subject to my thanks as well. Her lending of her instrument, as well as the training and aid in data analysis of it, has been a

key part of part of this dissertation. I would also like to thank Dr. Hawkins' student, Mrs. Madeline Hartley, for her help in data analysis.

Operation of the Atmospheric Processes Lab would be impossible with only one person. The knowledge and skills passed on by former students are a key component in keeping the lab in running order. In particular, I would like to thank Dr. Shunsuke Nakao, Dr. Xiaochen (Esther) Tang, Dr. Ping (Annie) Tang, and Dr. Seyedehsan Hosseini for the institutional knowledge they carried on and passed down to the current generation of graduate students. Without them, learning the operation of the lab and its instruments would have been nearly impossible in the time frame of my graduate work. Many of my contemporary graduate students must be thanked for their aid and dedication to the lab as well. My contemporary graduate students include Mrs. Chia-Li (Candice) Chen, Mr. Vincent Chen, Mr. Carlos Espinoza, Mrs. Mary Kacarab, Mr. Derek Price, Mr. Daniel Short, and Mrs. Diep Vu. Many current and former undergraduate students have also contributed to the operation of the lab and data analysis presented in this dissertation. Mr. Tyler Berte, Mr. William Lichtenberg, Mr. Gary Liu, and Mr. Ali Roohani all deserve special thanks here.

Mr. Kurt Bumiller has been instrumental in helping me solve a number of obstacles in my time in the Atmospheric Processes Lab and also deserves special thanks. His experience, laboratory skills, and hardware skills have been invaluable.

I would also like to express my sincere gratitude to my advisory committee member, Dr. Roya Bahreini, for her time and aid in developing this dissertation.

For funding and supporting this work, I would also like to thank the W.M. Keck Foundation, the National Science Foundation, the Environmental Protection Agency, the United States Department of Agriculture, the California NASA Space Grant Consortium, and the UCR Department of Chemical and Environmental Engineering.

The text of this dissertation, in part, is a reprint of the material as it appears in Giordano et al. (Env. Sci. & Tech., 47(19), 10980–10986, 2013), Giordano et al. (Atmos. Chem. Phys., in review, 2014), Giordano et al. (Geophys. Res. Lett., in preparation, 2014), and Giordano et al. (in preparation, 2014). The co-author listed in that publication directed and supervised the research which forms the basis for this dissertation.

ABSTRACT OF THE DISSERTATION

Climate Impacts of Biomass Burning Aerosols: Constraining the Chemicophysical Properties of Fresh and Aged Particles

by

Michael Giordano

Doctorate of Philosophy, Graduate Program in Chemical and Environmental Engineering
University of California, Riverside, June 2014
Dr. Akua Asa-Awuku, Chairperson

Biomass burning is one of the largest contributors of particles and trace gases to the atmosphere. This work focuses on constraining the impacts that biomass burning has on Earth's climate through two effects: scattering or absorption of light by particles and particle impacts on cloud formation. To explore biomass burning light interaction and hygroscopicity, a series of environmental chamber experiments were carried out using fuels common to the southwest U.S. This work includes the effects that photochemical aging has on the emissions to provide a realistic assessment of the emissions' lifetime in the atmosphere.

The work done on the cloud formation properties of the emissions shows that two common assumptions applied to the emissions misrepresent their cloud forming abilities. The first assumption, that surface active compounds are negligible in cloud activation, is shown to not apply to biomass burning aerosols. Not accounting for the presence of surface active compounds over estimates the hygroscopicity of the aerosols by up to 30%. The second assumption, that the volume of the particles is well characterized by the

electrical mobility diameter, is also shown to not apply to the system. Making the second assumption when parameterizing the hygroscopicity of the aerosols underestimates the hygroscopicity by up to 50%. Accounting for both assumptions is shown to have a greater impact at the point of emission than after six hours of photochemical aging. Therefore, the age of the aerosols must be taken into account when predicting the indirect effects of biomass burning aerosol.

This work also explores the light absorption of biomass burning aerosol and its reaction to photochemical aging. The results indicate that the aerosol is light absorbing and the magnitude of absorption can change with photochemical exposure. This work also shows that the absorption of the aerosol evolves with the volatility and surface active compounds present in the aerosol.

The final part of this work demonstrates that the local air quality that biomass is grown in can have an impact when that biomass is burned. Biomass grown in a polluted area is shown to emit more NO_x than biomass grown in a clean area and that the aerosols are less volatile.

Table of Contents

List of Tables

List of Figures

List of Abbreviations

°C	Degree Centigrade
APM	Aerosol Particle Mass (analyzer)
ATD	Arizona Test Dust
CCN	Cloud Condensation Nuclei
CCNC	Cloud Condensation Nuclei Counter
CERT	Center for Environmental Research and Technology
CN	Condensation Nuclei
CPC	Condensation Particle Counter
DMA	Differential Mobility Analyzer
DMT	Droplet Measurement Technologies
HTDMA	Hygroscopicity Tandem Differential Mobility Analyzer
HULIS	Humic-Like Substances
MCE	Modified Combustion Efficiency
OC	Organic Carbon
OM	Organic Matter
PILS	Particle Into Liquid Sampler
S-L	Szyszkowski–Langmuir
SMCA	Scanning Mobility CCN Analysis
SMPS	Scanning Mobility Particle Sizer
ST	Surface Tension
TEM	Transmission Electron Microscope

UCR	University of California, Riverside
UV	Ultraviolet
VFR	Volume Fraction Remaining
Vis	Visible
VTDMA	Volatility Tandem Differential Mobility Analyzer
WSOC	Water soluble organic carbon
WSOM	Water soluble organic matter

1 Introduction

1.1 Introduction of Dissertation

Atmospheric aerosols, solid or liquid particles suspended in the atmosphere, play a key role in the global radiative forcing budget through both direct and indirect mechanisms (Forster et al., 2007). The "direct effect" of aerosols in the atmosphere refers to aerosols' ability to scatter or absorb solar and terrestrial radiation (McCormick and Ludwig; 1967, Atwater, 1970). The aerosol "indirect effect" refers to aerosols' ability to act as cloud condensation nuclei which affects the formation and properties of clouds (Twomey, 1977; Albrecht, 1989). The total climate impacts of aerosols, through both the direct and indirect effects, remains difficult to constrain and, is still the greatest source of uncertainty in the Earth's energy balance. The list of causes for the uncertainty in both direct and indirect effects is extensive. Parameters such as particle size and number distribution, particle composition, particle morphology, and particle lifetime and altitude in the atmosphere, just to name a few, all modulate the heating and cooling effects that aerosols have on the Earth (Haywood and Boucher, 2000, and references therein). Beyond climate impacts, aerosols can also have health impacts on both humans and terrestrial ecosystems and effect regional visibility (Miller, 1973; Pope and Dockery, 2006; Forster et al., 2007).

An important area in the study of atmospheric aerosols is the concept of photochemical aging, sometimes referred to as oxidative aging. Photochemical aging refers to chemical

and physical transformational processes initiated by absorption of solar radiation. The process is important in the aerosol phase directly and indirectly since photochemistry is important in the production of gas-phase atmospheric oxidants (e.g. the OH radical) which can interact with the aerosol phase (Seinfeld and Pandis, 2012). Photochemical aging has been shown to alter the chemistry of existing atmospheric aerosols and produce new aerosols from oxidizing semi-volatile gas-phase species (Robinson et al., 2007 and references therein).

One of the largest contributors to the global aerosol load is biomass burning, which occurs in both the developing and developed worlds. Biomass burning encompasses domestic applications (home cook/heating stove use), anthropogenic events (agricultural field burning/prescribed burns) and biogenic events (wildland fires). Biomass burning is estimated to release 2-5 PgC yr^{-1} to the atmosphere, and global climate change is predicted to increase that number (Crutzen and Andreae, 1990; Yokelson et al., 1996 Andreae, et al., 2004; Reid et al., 2005; van der Werf et al., 2006; Forster et al., 2007). The significant amounts of aerosol and trace gases that biomass burning releases to the atmosphere can have serious impacts on the atmosphere's chemical composition and therefore Earth's climate (Simpson et al., 2006). The total climatic impacts of biomass burning remain hard to quantify due to the variation in aerosol emissions between biomass burning events. Emissions can vary in both composition and amount depending on a number of factors. The biomass species being burned, composition and moisture of the fuel, packing ratio of the fire, and the fire regime (e.g. flaming, smoldering, or mixed

phase) all affect the emissions properties of biomass burning (Andreae and Merlet, 2001; Petters et al., 2009; Thonicke et al., 2010; Hosseini et al., 2013). Additionally, biomass burning aerosol properties have been shown to be modified by photochemical aging in the atmosphere (Hennigan et al., 2011; Engelhart et al., 2012; Giordano et al., 2013; Giordano et al., 2014; Zhong and Jang, 2014).

Biomass burning aerosol has been suggested as a nonnegligible contributor to the total aerosol direct effect. The light absorption of biomass burning is pronounced in the ultraviolet (UV) and near-ultraviolet visible wavelengths with 49% of total aerosol light absorption being attributed between 300 and 400 nm (Kirchstetter and Thatcher, 2012). Ambient studies and laboratory mimic studies are the most common forms of studying the direct effect of biomass burning aerosol though a number of chamber studies have been conducted (Del Vecchio and Blough, 2004; Hoffer et al., 2006; Moosmuller et al., 2011; Kirchstetter and Thatcher, 2012; Lack et al., 2012, Zhong and Jang, 2014).

Hygroscopicity is a measure of a particle's affinity for water and, in the atmosphere, a measure of a particle's ability to become a cloud droplet. Biomass burning aerosol has shown to have a range of hygroscopicity values. Studies on biomass burning hygroscopicity have been conducted both through field measurements and controlled laboratory studies. Results indicate that biomass burning aerosol can range anywhere from very hygroscopic (good at forming clouds) to very non-hygroscopic (poor at forming clouds) (e.g. Petters et al., 2009; Hennigan et al., 2011). The variation in

hygroscopicity values is partly due to the complex aerosol chemistry from different fuel types and the impact of photochemical aging (DeCarlo et al., 2010; Janhäll et al., 2010; Engelhart et al., 2012).

This study provides new insights into both the indirect and direct effects of aerosols from biomass burning and identifies a novel parameter that impacts the composition of the emissions. Special attention is paid to the impacts of photochemical aging on both effects. Two biomass species common to the southwest US, manzanita (*Arctostaphylos glandulosa*) and chamise (*Adenostoma fasciculatum*) were used to explore novel aspects of the direct and indirect effects of biomass burning aerosol. Forest litter from a mixed conifer forest was also used to explore the impacts of chronic air pollution on biomass burning emissions. All species were collected in southern California with the aid of the U.S. Department of Agriculture Forest Service. All experiments were conducted at the University of California-Riverside, College of Engineering – Center for Environmental Research and Technology.

Chapter 2 explores the presence of surface active compounds in biomass burning aerosol and their effect on a common hygroscopicity parameterization. The results clearly show that surface active compounds are present in both manzanita and chamise and that their concentration changes with photochemical exposure. The analysis revealed that the true hygroscopicity is lower than the calculated hygroscopicity and helps rectify differences between different methods of measuring hygroscopicity.

Chapter 3 characterizes how the shape of an aerosol impacts its hygroscopicity. The work presented is a novel measurement of particle shape for biomass burning aerosol and the first to apply experimentally derived results to hygroscopicity calculations. Results show that the current norm for analysis severely under predicts hygroscopicity for biomass burning aerosol.

Chapter 4 combines the results and analysis from Chapters 2 and 3 to provide an improved measurement of biomass burning hygroscopicity.

Chapter 5 explores the light absorption characteristics of biomass burning aerosol and their evolution with photochemical aging. The results presented indicate that photochemical aging increases the light absorption ability of biomass burning aerosol. The increase in absorption is coupled with a decrease in the volatility of the aerosol.

Chapter 6 explores how biomass grown in areas of chronic air pollution has different biomass burning emissions than biomass grown in clean areas. The results show that there is a significant difference in the NO_x emissions, particle number emissions, and particle volatilities.

Chapter 7 summarizes the findings of this dissertation and presents conclusions.

1.2 References

Albrecht, B. A.: Aerosols, cloud microphysics, and fractional cloudiness, *Science*, 245, 1227–1230, 1989.

Andreae, M. O., and Merlet, P.: Emission of trace gases and aerosols from biomass burning, Global Biogeochemical Cycles, 15, 955-966, 2001.
Andreae, M. O., Rosenfeld, D., Artaxo, P., Costa, A. A., Frank, G. P., Longo, K. M., and Silva-Dias, M. A. F.: Smoking rain clouds over the Amazon, *Science*, 303, 1337–1342, doi:10.1126/science.1092779, 2004.

Atwater, M. A.: Planetary albedo changes due to aerosols, *Science*, 170(3953), 64–66, 1970.

Crutzen, P. J. and Andreae, M. O.: Biomass burning in the tropics: Impact on atmospheric chemistry and biogeochemical cycles, *Science*, 250, 1669–1678, doi:10.1126/science.250.4988.1669, 1990.

DeCarlo, P. F., Ulbrich, I. M., Crounse, J., de Foy, B., Dunlea, E. J., Aiken, A. C., Knapp, D., Weinheimer, A. J., Campos, T., Wennberg, P. O., and Jimenez, J. L.: Investigation of the sources and processing of organic aerosol over the Central Mexican Plateau from aircraft measurements during MILAGRO, *Atmos. Chem. Phys*., 10, 5257–5280; DOI 10.5194/acp-10-5257- 2010, 2010.

Del Vecchio**,** R. and Blough, N.V.: On the Origin of the Optical Properties of Humic Substances, *Environmental Science & Technology***,***38* (14), 3885-3891, 2004.

Engelhart, G. J., Hennigan, C. J., Miracolo, M. A., Robinson, A. L., and Pandis, S. N.: Cloud condensation nuclei activity of fresh primary and aged biomass burning aerosol, *Atmospheric Chemistry and Physics*, *12*(15), 7285-7293, 2012.

Forster, P., Ramaswamy, V., Artaxo, P., Berntsen, T., Betts, R., Fahey, D. W., Haywood, J., Lean, J., Lowe, D. C., Myhre, G., Nganga, J., Prinn, R., Raga, G., Schulz, M., and Van Dorland, R.: Changes in atmospheric constituents and in radiative forcing, in: Climate Change 2007: The Physical Science Basis, Contribution of Working Group I to the Fourth Assessment Report of the Intergovernmental Panel on Climate Change, edited by: Solomon, S., Qin, D., Manning, M., Chen, Z., Marquis, M., Averyt, K. B., Tignor, M., and Miller, H. L., Cambridge University Press, Cambridge, UK and New York, NY, USA, 131–215, 2007.

Giordano, M.R., Short, D.Z., Hosseini, S., Lichtenberg, W., and Asa-Awuku, A.: Changes in droplet surface tension affect the observed hygroscopicity of photochemically aged biomass burning aerosol, *Env. Sci. & Tech.,* 47(19), 10980–10986, doi:10.1021/es401867j, 2013.

Giordano, M.R., Espinoza, C., and Asa-Awuku, A.: Experimentally measured morphology of biomass burning aerosol and its impacts on CCN ability, *Atmos. Chem. Phys. Discuss*., acp-2014-293, 2014.

Haywood, J. and Boucher, O.: Estimates of the direct and indirect radiative forcing due to tropospheric aerosols: A review, *Reviews of Geophysics*, *38*(4), 513-543, 2000.

Hennigan, C. J., Miracolo, M. A., Engelhart, G. J., May, A. A., Presto, A. A., Lee, T., Sullivan, A. P., McMeeking, G. R., Coe, H., Wold, C. E., Hao, W.-M., Gilman, J. B., Kuster, W. C., de Gouw, J., Schichtel, B. A., J. L. Collett Jr., Kreidenweis, S. M., and Robinson, A. L.: Chemical and physical transformations of organic aerosol from the photo-oxidation of open biomass burning emissions in an environmental chamber, *Atmos. Chem. Phys.*, 11, 7669-7686; doi:10.5194/acp-11-7669-2011, 2011.

Hoffer, A., Gelencsér, A., Guyon, P., Kiss, G., Schmid, O., Frank, G. P., Artaxo, P., and Andreae, M. O.: Optical properties of humic-like substances (HULIS) in biomass-burning aerosols, *Atmos. Chem. Phys*., 6, 3563-3570, doi:10.5194/acp-6-3563-2006, 2006.

Hosseini, S., Urbanski, S.P., Dixit, P., Qi, L., Burling, I., Yokelson, R., Shrivastava, M., Jung, H., Weise, D. R., Miller, W., Cocker, D.: Laboratory characterization of PM emissions from combustion of wildland biomass fuels. *J. Geophys. Res.*, DOI:10.1002/jgrd.50481, 2013.

Janhäll, S., Andreae, M. O., and Pöschl, U.: Biomass burning aerosol emissions from vegetation fires: particle number and mass emission factors and size distributions, *Atmos. Chem. Phys*., 10, 1427-1439; DOI 10.5194/acp-10-1427-2010, 2010.

Kirchstetter, T. W. and Thatcher, T. L.: Contribution of organic carbon to wood smoke particulate matter absorption of solar radiation, *Atmos. Chem. Phys*., 12, 6067-6072, doi:10.5194/acp-12-6067-2012, 2012.

Lack, D. A., Langridge, J. M., Bahreini, R., Cappa, C. D., Mid dlebrook,A. M., and Schwarz, J. P.: Brown carbon and internal mixing in biomass burning particles, *P. Natl. Acad. Sci.*, 109,14802–14807, doi:10.1073/pnas.1206575109, 2012.

McCormick, R. A. and Ludwig, J. H.: Climate modification by atmospheric aerosols, *Science*, 156(3780), 1358–1359, 1967.

Miller, P. R.: Oxidant-induced community change in a mixed conifer forest. *Advan. Chem. Ser.*, 122, 101-17, 1973.

Moosmüller, H., Chakrabarty, R. K., Ehlers, K. M., and Arnott, W. P.: Absorption Ångström coefficient, brown carbon, and aerosols: basic concepts, bulk matter, and spherical particles, *Atmos. Chem. Phys*., 11, 1217-1225, doi:10.5194/acp-11-1217-2011, 2011.

Petters, M. D., Carrico, C. M., Kreidenweis, S. M., Prenni, A. J., DeMott, P. J., Collett, J. L., and Moosmüller, H.: Cloud condensation nucleation activity of biomass burning aerosol, *J. Geophys. Res.*, 114, D22205, doi:10.1029/2009JD012353, 2009.

Pope, C.A and Dockery, D.W.: Health effects of fine particulate air pollution: Lines that connect, J. Air Waste Management, 56, 709-742, 2006.
Reid, J. S., Koppmann, R., Eck, T. F., and Eleuterio, D. P.: A review of biomass burning emissions part II: intensive physical properties of biomass burning particles, *Atmos. Chem. Phys.*, 5, 799– 825, doi:10.5194/acp-5-799-2005, 2005.

Robinson, A. L., Donahue, N. M., Shrivastava, M. K., Weitkamp, E. A., Sage, A. M., Grieshop, A. P., Lane, T. E., Pierce, J. R., and Pandis, S. N.: Rethinking organic aerosols: Semivolatile emissions and photochemical aging. *Science*, 315(5816), 1259-1262, 2007.

Seinfeld, J. H., & Pandis, S. N.: *Atmospheric chemistry and physics: from air pollution to climate change*. John Wiley & Sons, Hoboken, New Jersey, 2012.

Simpson, I. J., Rowland, F. S., Meinardi, S., and Blake, D. R.: Influence of biomass burning during recent fluctuations in the slow growth of global tropospheric methane, Geophys. Res. Lett., 33, L22808, 10.1029/2006gl027330, 2006.
Thonicke, K., A. Spessa, I. C. Prentice, S. P. Harrison, L. Dong, and C. Carmona-Moreno. "The influence of vegetation, fire spread and fire behaviour on biomass burning and trace gas emissions: results from a process-based model." *Biogeosciences* 7(6), 2010.

Twomey, S.: The influence of pollution on the shortwave albedo of clouds, *J. Atmos. Sci.*, 34, 1149–1152, 1977.

van der Werf, G. R., Randerson, J. T., Giglio, L., Collatz, G. J., Kasibhatla, P. S., and Arellano Jr., A. F.: Interannual variability in global biomass burning emissions from 1997 to 2004, *Atmos. Chem. Phys*., 6, 3423-3441, doi:10.5194/acp-6-3423-2006, 2006.

Yokelson, R. J., Griffith, D. W. T., and Ward, D. E.: Open-path Fourier transform infrared studies of large-scale laboratory biomass fires, *J. Geophys. Res*., 101, 067-21080, 1996.

Zhong, M. and Jang, M.: Dynamic light absorption of biomass-burning organic carbon photochemically aged under natural sunlight, *Atmos. Chem. Phys*., 14, 1517-1525, doi:10.5194/acp-14-1517-2014, 2014.

2 Changes in Droplet Surface Tension Affect the Observed Hygroscopicity of Photochemically Aged Biomass Burning Aerosol

2.1 Introduction

Biomass burning can generate significant amounts of aerosol (2–5 Pg yr^{-1}) (Crutzen and Andreae, 1990; Andreae et al., 2004; Reid et al., 2005; van der Werf et al., 2006). The aerosol formed during burning events has the ability to modify cloud properties and indirectly impact climate radiative forcing (IPCC, 2004; Reutter et al., 2009; Liu and Wang, 2010). Given the significant contribution of biomass burning emissions to the organic aerosol budget, further constraining their hygroscopicity in global models will help reduce uncertainty in simulated aerosol indirect forcing (Liu and Wang, 2010).

Previous works have investigated the cloud condensation nuclei (CCN) properties of biomass burning aerosol. The hygroscopicity of biomass smoke, as represented by the single hygroscopicity parameter κ, has shown a range of values. Much of the variation can be linked to differences in fuels and in burn conditions (e.g. but not limited to Petters et al., 2009; Carrico et al., 2010). The studies range from field measurements to controlled laboratory studies (online and offline measurements). The variation is partly due to the complex aerosol chemistry from different fuel types and the impact of photochemical aging (e.g., DeCarlo et al., 2010; Janhäll et al., 2010). Petters et al. (2009) measured the CCN activity of 24 biomass fuels (hard and soft woods, shrubs, and grasses); the aerosol ranged from weakly hygroscopic ($\kappa \sim 0.06$) to strongly hygroscopic

($\kappa \sim 0.7$). Novakov and Corrigan (1996) concluded that the water-soluble organic species from biomass burning are primarily responsible for their CCN activity. Although, recent research suggests inorganic species may also be important if present in enough concentration (Hand et al., 2005; Levin et al., 2010). Furthermore, primary emissions of biomass burning aerosol can produce additional secondary organic aerosol (SOA) (i.e., Eatough et al., 2003; de Gouw and Jimenez, 2009; Yokelson et al., 2009; Hennigan et al., 2010). Engelhart et al. (2012) measured changes in fresh and aged CCN activity of 12 different fuels (hard and soft woods, shrubs, and grasses) and concluded that decreases in activation were driven by the photochemical production of SOA and the CCN activity of the 12 fuels converged to similar hygroscopicity values ($\kappa \sim 0.2 \pm 0.1$) after a few hours of photochemical processing. Dusek et al. (2011) analyzed the subsaturated and supersaturated hygroscopicity of four (2 hard and 2 soft) wood fuels. The hygroscopicity of the smoke from the wood was similar to those reported by Petters et al. (2009), $0.2 > \kappa > 0.05$. However, the supersaturated (CCN derived) hygroscopicity of small particles (50 nm) was twice that of subsaturated (H-TDMA) measurements. The authors concluded that the discrepancy was partially due to surface tension effects that can lead to an overprediction of particle hygroscopicity from CCN measurements; without accounting for surface tension, the true hygroscopicity of the solute composition is not well understood (Dusek et al., 2011).

Surface active material may be present in atmospheric aerosol. Ruehl et al. (2012) found strong evidence that surface tension reduction can occur in microscopic droplets. This

surface tension reduction could therefore augment the hygroscopicity of CCN active particles. However, online experimental evidence of surface tension depression in microscopic droplets has remained elusive.

Previous work has shown that the composition of the aerosols from biomass burning has a large impact both on hygroscopicity and surface tension. The majority of biomass burning aerosol particulate mass is carbonaceous material (Artaxo et al., 2002; Decesari et al., 2006). Both the primary and secondary carbonaceous components contain complex material called HUmic-LIke Substances (HULIS). HULIS contains slightly soluble substances (mainly dicarboxylic acids) that have been shown to be surface active, range in densities, and modify hygroscopicity and CCN activity (e.g., but not limited to, Kiss et al., 2005; Dinar et al., 2006a; Dinar et al., 2006b; Asa-Awuku et al., 2008). HULIS has been isolated from river samples, derived from mimics, and/or extracted from biomass burning filter studies; yet again, CCN derived hygroscopicity has varied from $0.06 < \kappa < 0.34$ (Dinar et al., 2006b, Asa-Awuku et al., 2008; Ziese et al., 2008; Fors et al., 2010; Kristensen et al., 2012). X-ray microscopy and spectroscopy has also confirmed HULIS in biomass burning tar balls (Tivanski et al., 2007). To the best of our knowledge, the existence of strong surfactants and HULIS in biomass burning aerosol has been mostly garnered from filter extracts. Field measurements and chamber CCN studies have assumed negligible surface tension depression in supersaturated regimes.

In this work, we use a semicontinuous method to measure surfactant properties and the CCN activity of biomass burning aerosol as it ages with photochemistry. We provide evidence to support the existence of surfactants as well as evidence that photochemical aging can modify aerosol surface tension. We then discuss the importance of surfactants to the CCN ability of these aerosols. Köhler theory analysis is performed to demonstrate the effects of including or excluding surface tension in CCN κ calculations. We also discuss how the variation in biomass burning hygroscopicity can be attributed to the evolution of the surface active material.

2.2 Theory for CCN Activation

2.2.1 Köhler Theory and Single Parameter Hygroscopicity, κ

Köhler theory calculates the saturation ratio, *S*, over an aqueous droplet as follows:

$$S = a_w \exp\left(\frac{4\sigma_{s/a} M_w}{RT\rho_w D}\right) \qquad \text{Eq. 2.1}$$

where a_w is the activity of water in solution, ρ_w is the density of water, M_w is the molecular weight of water, $\sigma_{s/a}$ is the surface tension of the solution/air interface, R is the universal gas constant, T is the temperature, and D is the wet diameter of the droplet.

A single parameter, κ, can parameterize hygroscopicity (Petters and Kreidenweis, 2007):

$$\kappa = \frac{4A^3}{27 D_d^3 ln^2 s_c} \;;\; \text{where } A = \frac{4\sigma_{s/a} M_w}{RT\rho_w} \qquad \text{Eq. 2.2}$$

where D_d is the dry particle diameter, and s_c is the critical supersaturation required to activate a particle with size D_d. D_d is the measured mobility diameter that is calculated as

the 50% efficiency for which half of all particles activate at s_c, the instrument supersaturation. From Eq. 2.2, κ is interpolated using a linear regression of experimental D_d and calibrated s_c.

κ-Köhler theory works well for ideal droplet water activity conditions, when the growing cloud droplet exists as an aqueous solution and all available solute is dissolved. κ-Köhler theory also applies the ideal surface tension of water, $\sigma_{s/a} = 0.072$ J m^{-2}. This approximation may not be applicable in the presence of strong surface active compounds.

For completely soluble CCN, s_c scales with $D_d^{-3/2}$. This relationship changes if an aerosol exhibits limited solubility (Padró et al., 2007; Petters and Kreidenweis, 2008). At a characteristic dry diameter of a slightly soluble aerosol, d^*, if $D_d < d^*$ then the amount of water available at the activation point is insufficient to dissolve all solute (changing the s_c-d dependence) and if $D_d > d^*$ then there is sufficient water to dissolve all solute (s_c scales with $D_d^{-3/2}$). The solubility limit of the solute therefore corresponds to $D_d = d^*$ and can be calculated. At the point of complete dissolution, the mass of dissolved solute in the aerosol is

$$m = \frac{\pi}{6} \varepsilon_s \rho_s d^{*3} \qquad \text{Eq. 2.3}$$

where ε_s and ρ_s are the volume fraction and density of solute, respectively. Applying Köhler theory, the droplet volume at critical diameter (V_d) can be calculated. If assumed to be approximately equal to the volume of water in the activated droplet, C_{eq} is estimated as follows (Padró et al., 2007):

$$C_{eq} = \frac{27}{8}\varepsilon_s \frac{\rho_s}{\rho_w}\frac{d^{*3}s_c^{*3}}{A^3} \quad \text{Eq. 2.4}$$

C_{eq} is used to calculate the average concentration of organic solute at activation and the amount of solute for effective surface tension depression.

2.2.2 Surface Tension

The Szyszkowski–Langmuir (S-L) equation (Eq. 2.5) is used to empirically fit the data over a range of concentrations (Szyskowski, 1908):

$$\sigma_{s/a} = \sigma_o - \alpha T * \ln(1 + \beta C) \quad \text{Eq. 2.5}$$

where σ_o is the reference surface tension of pure water, T the temperature in K, C is the water-soluble organic concentration, and α and β are the maximum adsorption density and Langmuir equilibrium adsorption constant, respectively. The latter two variables are calculated with linearly regressed fits of experimental data. Table 2S.1 shows the α and β parameters of Eq. 2.5 as a function of water-soluble organic matter (WSOM). For each s_c-D_d, $\sigma_{s/a}$ at activation is computed iteratively by optimizing the relationships between the Kelvin term, A, concentration at activation C_{eq} (Eq. 2.4), and the Eq. 2.5 parameters α and β. Additional information about the method can be found in Padró et al. (2007).

Due to the different assumptions κ can be calculated under, subscripts are used to clarify the discussion. $\kappa_{apparent}$ refers to a κ-value assuming $\sigma_{s/a} = \sigma_o$. κ_{st} refers to a surface tension corrected hygroscopicity value calculated by assuming a soluble solute with constant

surface tension depression. κ_{corr} refers to a surface tension corrected hygroscopicity value calculated by assuming a soluble solute with surface tension depression of the applied Eq. 2.5 fit within the same 1–2 h of filter measurement.

2.3 Experimental methods and Instrumentation

A series of biomass burning experiments were carried out at the University of California, Riverside College of Engineering, Center for Environmental Research and Technology (UCR CE-CERT) atmospheric processes lab from summer 2011 to spring 2012. Chamise (*Adenostoma fasciculatum*) and manzanita (*Arctostaphylos glandulosa*), shrubs common to the California chaparral biome, were burned in a wood-burning stove. Both chamise and manzanita were collected on Bureau of Land Management land near the San Bernardino National Forest (approximately 33.84°, −116.88° and the surrounding area). The collection site is approximately 3600–3900 feet in elevation. Chaparral species such as chamise, manzanita, scrub oak, and ceanothus surround the area. Both manzanita and chamise burned in the flaming regime. The flame integrated modified combustion efficiencies (MCE) of both fuels were greater than 0.98 (where MCE ≡ $(\Delta CO_2)/(\Delta CO_2 + \Delta CO)$) (Ward and Hao, 1991).

The smoke was diluted first with an injection system then with a Venturi tube and injected into a 12 m^3 Teflon chamber with final concentration of 50–100 μg m^{-3}. The chamber concentration is within range of ambient and plume-like concentrations also used in previous chamber studies (Hennigan et al., 2011). The sample was injected with a

10:1 total to sample flow ratio. As short of a copper transfer line as possible was used for the smoke injection, approximately 7 m in length. The enclosure is surrounded by 170 ultraviolet (UV) lights with peak intensity of 350 nm (350 BL, Sylvania). UV lights were turned on 1 h after injection to promote photochemistry and remained on until the experiment concluded. The chamber was flushed and filled with filtered air prior to injection. The temperature of the chamber ranged approximately from 20 to 27 °C during the experiment.

The experiment was operated until the chamber was empty (up to 6 h). Chemical aging was monitored with Teledyne carbon monoxide (CO) and ozone (O_3) gas analyzers and suggested realistic aging occurred in the chamber (Figure 2S.1). Previous studies have used similar measurements to monitor plume age in ambient studies. Yokelson et al. (2009) reported $\Delta O_3/\Delta CO \approx 0.25$ for a 1.5 h old plume in the Yucatan. The chamber aging process is similar for manzanita; the $\Delta O_3/\Delta CO = 0.20$ after 1.5 h of irradiation. $\Delta O_3/\Delta CO$ steadily increased to 0.5. For chamise, $\Delta O_3/\Delta CO$ also displayed a steady rise though it was delayed for a number of hours. Chamise had an order of magnitude greater formation of O_3 than manzanita, leading to a $\Delta O_3/\Delta CO > 6.0$ at the end of the experiment. The comparison of chamber $\Delta O_3/\Delta CO$ data with field measurements suggests that realistic aging can be achieved in the chamber system.

Scanning Mobility CCN Analysis (SMCA) was used to obtain fast size-resolved CCN activity of the aging system (Moore et al., 2010). The sampled aerosol was size-classified

using a Scanning Mobility Particle Sizer (SMPS, TSI 3080/3081). The monodisperse stream from the classifier was split, and one stream entered a condensation particle counter (TSI 3772) while the other stream was sampled with a DMT Continuous Flow Streamwise Thermal Gradient Chamber CCN counter (CCNC) (Roberts and Nenes, 2005; Rose et al., 2008). The CCNC instrument was operated at a 10:1 sheath-to-aerosol ratio with a sample flow of 0.5 L min^{-1}. The total concentration (CN) of sized particles measured by the CPC determined the ratio of CCN/CN. For each supersaturation, s_c, the activation diameter, $D_{d,}$ was defined as the diameter for which CCN/CN = 0.5. The experimental setup was calibrated with ammonium sulfate ($(NH_4)_2SO_4$) aerosol. CCNC calibration information is provided in Table 2S.2.

Teflon filter samples were taken during lights off (the first hour of the experiment) and lights on (the remainder of the experiment). For offline analysis, the filters were sonicated in Millipore DI water (18 mΩ, TOC ~ 3 ppb) for 1 h. The aqueous extracts were then filtered using a Whatman 25 mm syringe filter to remove large nondissolved particles. Then, samples were diluted into 10 mL DI water at ratios of 1:3, 1:4, 1:5, and 1:6. The surface tension of each sample was then measured with a pendant drop tensiometer (Attension Theta 200, Biolin Scientific, Sweden). The optical tensiometer captures at least 100 images of the droplet and computes droplet surface tension through application of the Young–Laplace equation; the standard deviations for $\sigma_{s/a}$ are less than 0.05 mN m^{-1} for a given sample at one concentration (Andreas et al., 1937; Fordham, 1948). The water-soluble organic carbon (WSOC) concentrations of each sample were

measured using a Total Organic Carbon analyzer (Sievers 900, GE). The error associated with TOC measurements is ±2%. Organic carbon (OC) concentration (taken as WSOC here) was converted to organic mass (OM) concentration using an OM/OC measurement from an Aerodyne High-Resolution Particle Time-of-Flight Aerosol Mass Spectrometer (HR-PToF AMS) connected directly to the environmental chamber (DeCarlo et al., 2006). OM/OC values were 1.46 ± 0.064 and 1.41 ± 0.057 for chamise and manzanita, respectively.

2.4 Results

In both fuel species, photochemistry modifies the presence of surface active material found in biomass burning aerosol. This work shows that surface active materials are present in aerosol generated from chamber biomass burning experiments. The effective surface tension depression, $((\sigma_o - \sigma_{s/a})/\sigma_o) \times 100$, is plotted as a function of the concentration of water-soluble organic carbon (Figure 2.1). Up to 30% surface tension depression is observed from the filter extracts. The surface tension depression from filter extracts is consistent with previous works. Asa-Awuku et al.(2008) observed biomass burning extract samples that exhibited a surface tension depression of nearly 20% at their measured concentration. Salma et al. (2006) found up to 30% surface tension depression from atmospheric humic-like substances. Kiss et al. (2005) showed that HULIS extracts of atmospheric aerosols depressed surface tension by up to 42%. Facchini et al. (2000) reported that polyacidic compounds from aerosols, as HULIS are, depressed surface tension by nearly 25%. The surface tension data and WSOC data is fit to the

Szyszkowski–Langmuir (S-L) equation. Chamise aerosol sampled in the dark chamber is less surface active than aerosol sampled after two and four hours of photochemistry (Figure 2.1). Conversely, manzanita aerosol displays the opposite trend. Manzanita aerosol irradiated for five hours is less surface active than aerosol sampled from a dark chamber, with intermediate stages that are only slightly less active than nonaged particles (Figure 2.1).

The CCN activity is also modified by photochemistry. s_c-D_d pairs for chamise and manzanita are shown in Figure 2.2 (where s_c is the critical supersaturation at which a particle activates). The critical diameter, D_d, required for activation at a given s can span 50 nm during a 4 h photochemical experiment. Freshly emitted aerosol appears to be hygroscopic; D_d for chamise and manzanita can be greater or equal to $\kappa = 0.4$. The greatest variability in D_d for both fuel types occurs at lower instrument s of 0.25% and 0.46%. The average best fit $\kappa_{apparent}$ is 0.098 ± 0.001 and 0.238 ± 0.001 for chamise and manzanita, respectively. Petters et al. (2009) reported a κ of 0.10 for manzanita branches from a stack burn. This differs from our average value of 0.238 from the environmental chamber burn study of manzanita branches and leaves. Additionally, Petters et al. (2009) note that manzanita is a species that is well characterized by a range $0.05 < \kappa < 0.19$. From Figure 2.2, it can be seen that for the majority of the experiment our measurements fall within this range. This is especially true of photochemically aged measurements. Our nonphotochemically aged CCN measurements have higher average $\kappa_{apparent}$ values.

For chamise, Petters et al. (2009) reported a wide range of κ values for stack burns of chamise, ~$0.2 < \kappa < 0.5$, and also for chamber burns, ~ $0.2 < \kappa < 0.35$. Engelhart et al. (2012) reported a similar range for primary emissions of chamise, approximately $0.3 < \kappa < 0.5$, and for oxidized emissions, $0.15 < \kappa < 0.25$, reported at two different supersaturations. Our reported values are in line with both of these measurements (e.g., photochemical aging driving $\kappa_{apparent}$ values down (Figure 2.2)). Our lower bound $\kappa_{apparent}$ value is lower than both Petters et al. (2009) and Engelhart et al. (2012). The discrepancy may be due to fuel condition (water content) upon burning or fire conditions (e.g., MCE) (Carrico et al., 2010). It is noted that wood-stove burning can result in higher MCE than open burning. Petters et al. (2009) reported 5–10 min of flaming followed by 5–10 min of smoldering as compared to our consistently flaming phase for injection of the smoke into the smog chamber. Engelhart et al. (Hennigan et al., 2011 reported in Engelhart et al., 2012) reported a MCE of 0.94, compared to our MCE > 0.98. Comparisons of $\kappa_{apparent}$ biomass species suggest differing amounts of hygroscopic material are produced during burns of the same fuel.

The average reported $\kappa_{apparent}$ is sensitive to changes in surface tension. In Table 2.1, the overall average κ_{st} and A_{st} are calculated for the corresponding data in Figure 2.2 by applying constant values for $\sigma_{s/a}$. The average κ_{st} can be ≤ 0.1 for a 25% surface tension depression (Table 2.1). $\kappa_{st} \leq 0.1$ is similar to subsaturated H-TDMA measurements of biomass burning aerosol (Dusek et al., 2011; Martin et al., 2013).

Figure 2.3 shows both $\kappa_{apparrent}$ and κ_{corr} for manzanita and chamise aerosol as a function of time. Both fuels show dependence of hygroscopicity with photochemistry; $\kappa_{apparent}$ before irradiation is higher than after photochemistry for both manzanita and chamise. Both species decrease $\kappa_{apparent}$ by a factor of 2 or more with photochemical activity (Figure 2.3). $\kappa_{apparent}$ for chamise is 0.21 ± 0.11 in the dark and an average of 0.09 ± 0.06 after irradiation. For manzanita, $\kappa_{apparent}$ is 0.33 ± 0.11 in the dark and an average of 0.12 ± 0.04 after irradiation. Stronger surfactants (indicative of HULIS) are present during the aging of chamise aerosol (Figure 2.1). As a result, κ_{corr} decreases. The changes in surface activity could be due to the chemical processing of HULIS during photochemical aging.

κ_{corr} values of chamise aerosol indicate the composition of aerosol ranges from slightly soluble to wettable and insoluble. If $\sigma_{s/a}$ is accounted for, the κ_{corr} for chamise becomes 0.10 ± 0.06 in the dark and reduces to an average κ_{corr} 0.02 ± 0.02 (Figure 2.3a) during aging. The change in κ_{corr} is comparable for manzanita, where κ_{corr} is 0.12 ± 0.05 in the dark and reduces to an average κ_{corr} 0.06 ± 0.04 after lights on (Figure 2.3b). In the case of manzanita, the presence of surfactants decreases with photochemical aging (Figure 2.1). κ_{corr} indicates that the aerosol solute from both fuels becomes less hygroscopic with aging.

The results presented here support the growing body of evidence that surface active materials are present in biomass burning emissions. The surfactant effects are real and can be observed from semicontinuous measurements of offline filter extracts of environmental chamber aerosol. The aerosol formed from the combustion of chamise and manzanita is able to depress droplet surface tension up to 30% at concentrations relevant for droplet activation. Köhler theory when combined with measurements of surface tension, solubility, and CCN activity can aid our understanding of organic solute hygroscopicity. The inclusion of surfactant parameters is in agreement and consistent with findings that show that the organic component of the aerosol has soluble properties with a κ hygroscopicity parameter of ≤ 0.1. In both cases, aging of the primary aerosol produces less hygroscopic material.

The majority of aerosol formed in these experiments is organic (Figure 2S.2). The presence of nitrates, sulfates, and other inorganic salts from wild fire events could potentially induce surface tension salting out effects (Asa-Awuku et al., 2008). This would likely increase soluble material and $\kappa_{apparent}$ values. However, only 5% of the total aerosol needs to be surface active for closure of sub- and supersaturated hygroscopicity measurements to disagree (Dusek et al., 2011). Surface tension properties in biomass burning systems should be accounted for when estimating hygroscopicity from supersaturated data sets. There are additional factors that can affect both sub- and supersaturated κ, including both fractal dimension (particle shape) and particle

composition. However, surface tension has the greatest impact in the supersaturated regime and appears to reconcile the differences in previously reported κ values.

Our analysis confirms that hygroscopicity derived from CCN activity can be overestimated by a factor of 2 if surface tension effects are not accounted. The findings are consistent with the recent work of Martin et al. (2013) and Kristenen et al. (2012) who found that subsaturated hygroscopicity for biomass burning and HULIS is less than CCN derived values. Semicontinuous surface tension analysis can account for the presence and evolution of surfactants. It may also bridge the gap between subsaturated and supersaturated hygroscopicity measurements. Unifying the two regimes may reduce uncertainties in the prediction of indirect forcing of biomass burning aerosol.

2.5 Acknowledgements

Many thanks to David Weise and Joey Chong of the USDA Forest Service, Pacific Southwest Research Station in Riverside, CA, for their advice and pivotal role in the acquisition of fuels. The authors would also like to thank David Cocker and the Keck Foundation for use of the environmental chamber. MG and DS would like to thank California NASA Space Grant Consortium for partially supporting this work. MG and AA would also like to thank the U.S Environmental Protection Agency for funding this work made possible by EPA grant number 83504001. SH would like to thank W. Miller and the Strategic Environmental Research and Development Program (SERDP) projects SI-1648 and SI-1649. W. Lichtenberg thanks the National

Science Foundation (1032388) for undergraduate research support. Any opinions, findings, and conclusions expressed in this material are those of the authors and do not necessarily reflect the views of NSF, NASA, or EPA.

2.6 References

Andreae, M. O., Rosenfeld, D., Artaxo, P., Costa, A. A., Frank, G. P., Longo, K. M., and Silva-Dias, M. A. F.: Smoking rain clouds over the Amazon, *Science*, 303, 1337–1342, doi:10.1126/science.1092779, 2004.

Andreas, J.M., Hauser, E.A., and Tucker, W.B.: Boundary tension by pendant drops, *J. Phys. Chem.*, 42(8), 1001-1019, DOI 10.1021/j100903a002, 1937.

Artaxo, P., Martins, J.V., Yamasoe, M.A., Procopio, A.S., Pauliquevis, T.M., Andreae, M.O., Guyon, P., Gatti, L.V., and Leal, A.M.C.: Physical and chemical properties of aerosols in the wet and dry seasons in Rondonia, Amazonia, *J. Geophys. Res.-Atmos.*, 107(D20), 8081, DOI 10.1029:2001JD000666, 2002.

Asa-Awuku, A., Sullivan, A. P., Hennigan, C. J., Weber, R. J., and Nenes, A.: Investigation of molar volume and surfactant characteristics of water-soluble organic compounds in biomass burning aerosol, *Atmos. Chem. Phys.*, 8, 799-812, DOI 10.5194/acp-8-799-2008, 2008.

Carrico, C. M., Petters, M. D., Kreidenweis, S. M., Sullivan, A. P., McMeeking, G. R., Levin, E. J. T., Engling, G., Malm, W. C., and Collett, J. L.: Water uptake and chemical composition of fresh aerosols generated in open burning of biomass, *Atmos. Chem. Phys.*, 10, 5165– 5178, doi:10.5194/acp-10-5165-2010, 2010.

Climate Change 2007: The Physical Science Basis. Contribution of Working Group I to the Fourth Assessment Report of the Intergovernmental Panel on Climate Change; Intergovernmental Panel on Climate Change: Geneva, Switzerland, 2007.

Crutzen, P. J. and Andreae, M. O.: Biomass burning in the tropics: Impact on atmospheric chemistry and biogeochemical cycles, *Science*, 250, 1669–1678, doi:10.1126/science.250.4988.1669, 1990.

DeCarlo, P.F., Kimmel, J.R., Trimborn, A., Northway, M.J., Jayne, J.T., Aiken, A.C., Gonin, M., Fuhrer, K., Horvath, T., Docherty, K.S., Worsnop, D.R., and Jimenez, J.L.: Field-deployable, high-resolution, time-of-flight aerosol mass spectrometer, *Anal. Chem*., 78(24), 8281-8289, DOI 10.1021/ac061249n, 2006.

DeCarlo, P. F., Ulbrich, I. M., Crounse, J., de Foy, B., Dunlea, E. J., Aiken, A. C., Knapp,D., Weinheimer, A. J., Campos, T., Wennberg, P. O., and Jimenez, J. L.: Investigation of the sources and processing of organic aerosol over the Central Mexican Plateau from aircraft measurements during MILAGRO, *Atmos. Chem. Phys.*, 10, 5257–5280, doi:10.5194/acp-10-5257-2010, 2010.

de Gouw, J. and Jimenez, J. L.: Organic Aerosols in the Earth's Atmosphere, *Environ. Sci. Technol*., 43, 7614–7618; DOI 10.1021/es9006004, 2009.

Decesari, D., Fuzzi, S., Facchini, M.C., Mircea, M., Emblico, L., Cavalli, F., Maenhaut, W., Chi, X., Schkolnik, G., Falkovich, A., Rudich, Y., Claeys, M., Pashynska, V., Vas, G., Kourtchev, I., Vermeylen, R., Hoffer, A., Andreae, M.O., Tagliavini, E., Moretti, F., and Artaxo, P.: Characterization of the organic composition of aerosols from Rondonia, Brazil, during the LBA-SMOCC 2002 experiment and its representation through model compounds, *Atmos. Chem. Phys.*, 6, 375-402, DOI 10.5194/acp-6-375-2006, 2006.

Dinar, E., Taraniuk, I., Graber, E. R., Katsman, S., Moise, T., Anttila, T., Mentel, T. F., and Rudich, Y.: Cloud Condensation Nuclei properties of model and atmospheric HULIS, *Atmos. Chem. Phys*., 6, 2465–2481; DOI 10.5194/acp-6-2465-2006, 2006a.

Dinar, E., Mentel, T. F., and Rudich, Y.: The density of humic acids and humic like substances (HULIS) from fresh and aged wood burning and pollution aerosol particles, *Atmos. Chem. Phys.*, 6, 5213–5224; DOI 10.5194/acp-6-5213-2006, 2006b.

Dusek, U., Frank, G. P., Massling, A., Zeromskiene, K., Iinuma, Y., Schmid, O., Helas, G., Hennig, T., Wiedensohler, A., and Andreae, M. O.: Water uptake by biomass burning aerosol at sub- and supersaturated conditions: closure studies and implications for the role of organics, *Atmos. Chem. Phys*., 11, 9519-9532; DOI 10.5194/acp-11-9519-2011, 2011.

Eatough, D. J., Eatough, N. L., Pang, Y., Sizemore, S., Kirchstetter, T. W., Novakov, T., and Hobbs, P. V.: Semi volatile particulate organic material in southern Africa during SAFARI 2000, *J. Geophys. Res*., 108(D13), 8479; DOI 10.1029/2002JD002296, 2003.

Engelhart, G. J., Hennigan, C. J., Miracolo, M. A., Robinson, A. L., and Pandis, S. N.: Cloud condensation nuclei activity of fresh primary and aged biomass burning aerosol, *Atmos. Chem. Phys*., 12, 7285-7293; DOI 10.5194/acp-12-7285-2012, 2012.

Facchini, M.C., Decesari, S., Mircea, M., Fuzzi, S., and Loglio, G.: Surface tension of atmospheric wet aerosol and cloud/fog droplets in relation to their organic carbon content and chemical composition, *Atmos. Env.*, 34, 4853-4857, 2000.

Fordham, S.: On the calculation of surface tension from measurements of pendant drops, *Proc. R. Soc. Lond. A*, 194, DOI 10.1098/rspa.1948.0063, 1948.

Fors, E. O., Rissler, J., Massling, A., Svenningsson, B., Andreae, M. O., Dusek, U., Frank, G. P., Hoffer, A., Bilde, M., Kiss, G., Janitsek, S., Henning, S., Facchini, M. C., Decesari, S., and Swietlicki, E.: Hygroscopic properties of Amazonian biomass burning and European background HULIS and investigation of their effects on surface tension with two models linking H-TDMA to CCNC data, *Atmos. Chem. Phys*., 10, 5625-5639; DOI 10.5194/acp-10-5625-2010, 2010.

Hand, J. L., Malm, W. C., Laskin, A., Day, D., Lee, T., Wang, C., Carrico, C., Carrillo, J., Cowin, J. P., Collett, J., Iedema, M. J.: Optical, physical, and chemical properties of tar balls observed during the Yosemite aerosol characterization study, *J. Geophys. Res.: Atmos.*, 110 (D21), doi:10.1029/2004JD005728, 2005.

Hennigan, C. J., Miracolo, M. A., Engelhart, G. J., May, A. A., Presto, A. A., Lee, T., Sullivan, A. P., McMeeking, G. R., Coe, H., Wold, C. E., Hao, W.-M., Gilman, J. B., Kuster, W. C., de Gouw, J., Schichtel, B. A., J. L. Collett Jr., Kreidenweis, S. M., and Robinson, A. L.: Chemical and physical transformations of organic aerosol from the photo-oxidation of open biomass burning emissions in an environmental chamber, *Atmos. Chem. Phys.*, 11, 7669-7686; DOI 10.5194/acp-11-7669-2011, 2011.

Janhäll, S., Andreae, M. O., Pöschl, U.: Biomass burning aerosol emissions from vegetation fires: Particle number and mass emission factors and size distributions, *Atmos. Chem. Phys.*, 10, 1427– 1439, doi:10.5194/acp-10-1427-2010, 2010.

Köhler, H.: The nucleus in and the growth of hygroscopic droplets, *Transactions of the Faraday Society*, 43, 1152–1161, 1936.

Liu, X.; Wang, J.How important is organic aerosol hygroscopicity to aerosol indirect forcing?, *Environ. Res. Lett.*, 5(4), doi:10.1088/1748-9326/5/4/044010, 2010.

Kiss, G., Tombácz, E., Hansson, H-C.: Surface tension effects of humic-like substances in the aqueous extract of tropospheric fine aerosol, *J. of Atmos. Chem.*, 50(3), 279-294, 2005.

Kristensen, T. B., Wex, H., Nekat, B., Nøjgaard, J. K., Pinxteren, D., Lowenthal, D. H., Mazzoleni, L. R., Dieckmann, K., Koch, C.B., Mentel, T. F., Herrmann, H., Hallar, A. G., Stratmann, F., and Bilde, M.: Hygroscopic growth and CCN activity of HULIS from different environments, *J. of Geophys. Res-Atmos*, 117(D22); DOI 10.1029/2012JD018249, 2012.

Levin, E. J. T., McMeeking, G. R., Carrico, C. M., Mack, L. E., Kreidenweis, S. M., Wold, C. E., Moosmüller, H., Arnott, W. P., Hao, W. M., Collett Jr., J. L., and Malm, W. C.: Biomass burning smoke aerosol properties measured during fire laboratory at Missoula experiments (FLAME), *J. Geophys. Res.-Atmos.*, 115(D18), DOI 10.1029/2009JD013601, 2010.

Martin, M., Tritscher, T., Jurányi, Z., Heringa, M. F., Sierau, B., Weingartner, E., Chiricob, R. , Gysel, M. S.H., Prévôt, A. S. H., Baltenspergerb, U., and Lohmann, U.: Hygroscopic properties of fresh and aged wood burning particles, *Journal of Aerosol Science*, 56, 15-29, DOI 10.1016/j.jaerosci.2012.08.006, 2013.

Moore, R. H., Nenes, A., and Medina, J.: Scanning mobility CCN analysis—a method for fast measurements of size-resolved CCN distributions and activation kinetics, *Aerosol Science & Tech.*, 44(10), 861-871, DOI 10.1080/02786826.2010.498715, 2010.

Novakov, T. and Corrigan, C. E.: Cloud condensation nucleus activity of the organic component of biomass smoke particles, *Geophys. Res. Lett.*, 23, 2141–2144, doi:10.1029/96GL01971, 1996.

Padró, L. T., Asa-Awuku, A., Morisson, R., and Nenes, A.: Inferring Thermodynamic Properties from CCN Activation Experiments: Single-component and Binary Aerosols, *Atmos. Chem. Phys.*, 7, 5263–5274; DOI 10.5194/acp-7-5263-2007, 2007.

Petters, M. D. and Kreidenweis, S. M.: A single parameter representation of hygroscopic growth and cloud condensation nucleus activity, *Atmos. Chem. Phys.*, 7, 1961–1971, DOI 10.5194/acp-7-1961-2007, 2007.

Petters, M. D. and Kreidenweis, S. M.: A single parameter representation of hygroscopic growth and cloud condensation nucleus activity – part 2: including solubility, *Atmos. Chem. Phys.*, 8, 6273-6279, DOI 10.5194/acp-8-6273-2008, 2008.

Petters, M. D.; Carrico, C. M.; Kreidenweis, S. M.; Prenni, A. J.; DeMott, P. J.; Collett, J. L.; Moosmüller, H.: Cloud condensation nucleation activity of biomass burning aerosol, *J. Geophys. Res.*, 114, D22205, doi:10.1029/2009JD012353, 2009.

Reid, J. S.; Koppmann, R.; Eck, T. F.; Eleuterio, D. P.: A review of biomass burning emissions. Part II: Intensive physical properties of biomass burning particles, *Atmos. Chem. Phys.*, 5, 799– 825, doi:10.5194/acp-5-799-2005, 2005.

Roberts, G. C. and Nenes, A.: A continuous-flow streamwise thermal-gradient CCN chamber for atmospheric measurements, *Aerosol Sci. Tech*., 39(3), 206–221; DOI 10.1080/027868290913988, 2005.

Rose, D., Gunthe, S. S., Mikhailov, E., Frank, G. P., Dusek, U., Andreae, M. O., and Pöschl, U.: Calibration and measurement uncertainties of a continuous-flow cloud condensation nuclei counter (DMT-CCNC): CCN activation of ammonium sulfate and sodium chloride aerosol particles in theory and experiment, *Atmos. Chem. Phys*., 8, 1153–1179, DOI 10.5194/acp-8-1153-2008, 2008.

Ruehl, C. R., Chuang, P. Y., Nenes, A., Cappa, C. D., Kolesar, K. R., and Goldstein, A. H.: Strong evidence of surface tension reduction in microscopic aqueous droplets. *Geophysical Research Letters*, 39 (23), DOI: 10.1029/2012GL053706, 2012.

Reutter, P.; Su, H.; Trentmann, J.; Simmel, M.; Rose, D.; Gunthe, S. S.; Wernli, H.; Andreae, M. O.; Pöschl, U.Aerosol- and updraft-limited regimes of cloud droplet formation: Influence of particle number, size and hygroscopicity on the activation of cloud condensation nuclei (CCN), *Atmos. Chem. Phys.*, 9, 7067– 708010.5194/acp-9-7067-2009, 2009.

Salma, I., Ocskay, R., Varga, I., Maenhaut, W.: Surface tension of atmospheric humic-like substances in connection with relaxation, dilution, and solution pH, *J. Geophys. Res.*, 111, D23205, DOI 10.1029/2005JD007015, 2006.

Szyskowski, B. V.: Experimentelle studien über kapillare eigenschaften der wässerigen lösungen von fettsauren, *Zeitschrift für Physikalische Chemie*, 64, 385–414, 1908.

Tivanski, A.V., Hopkins, R. J., Tyliszczak, T., and Gilles, M. K.: Oxygenated interface on biomass burn tar balls determined by single particle scanning transmission x-ray microscopy, *J. Phys. Chem. A*, 111(25), 5448-5458; DOI 10.1021/jp070155u, 2007.

van der Werf, G. R.; Randerson, J. T.; Giglio, L.; Collatz, G. J.; Kasibhatla, P. S.; Arellano,A. F., Jr.Interannual variability in global biomass burning emissions from 1997 to 2004, *Atmos. Chem. Phys.*, 6, 3423– 344110.5194/acp-6-3423-2006, 2006.

Ward, D.E. and Hao, W.M.: Projections of emissions from burning of biomass for use in studies of global climate and atmospheric chemistry, Proceedings of the 84th Annual Meeting and Exhibition Air & Waste Management Association, Volume 19, 16-21 June 1991, Vancouver, British Colombia, Canada.

Yokelson, R. J., Crounse, J. D., DeCarlo, P. F., Karl, T., Urbanski, S., Atlas, E., Campos, T., Shinozuka, Y., Kapustin, V., Clarke, A. D., Weinheimer, A., Knapp, D. J., Montzka, D. D., Holloway, J., Weibring, P., Flocke, F., Zheng, W., Toohey, D., Wennberg, P. O., Wiedinmyer, C., Mauldin, L., Fried, A., Richter, D., Walega, J., Jimenez, J. L., Adachi, K., Buseck, P. R., Hall, S. R., and Shetter, R.: Emissions from biomass burning in the Yucatan, *Atmos. Chem. Phys*., 9, 5785–5812; DOI 10.5194/acp-9-5785-2009, 2009.

Ziese, M., Wex, H., Nilsson, E., Salma, I., Ocskay, R., Hennig, T., Massling, A., and Stratmann, F.: Hygroscopic growth and activation of HULIS particles: experimental data and a new iterative parameterization scheme for complex aerosol particles, *Atmos. Chem. Phys.*, 8, 1855-1866; DOI 10.5194/acp-8-1855-2008, 2008.

2.7 Figures

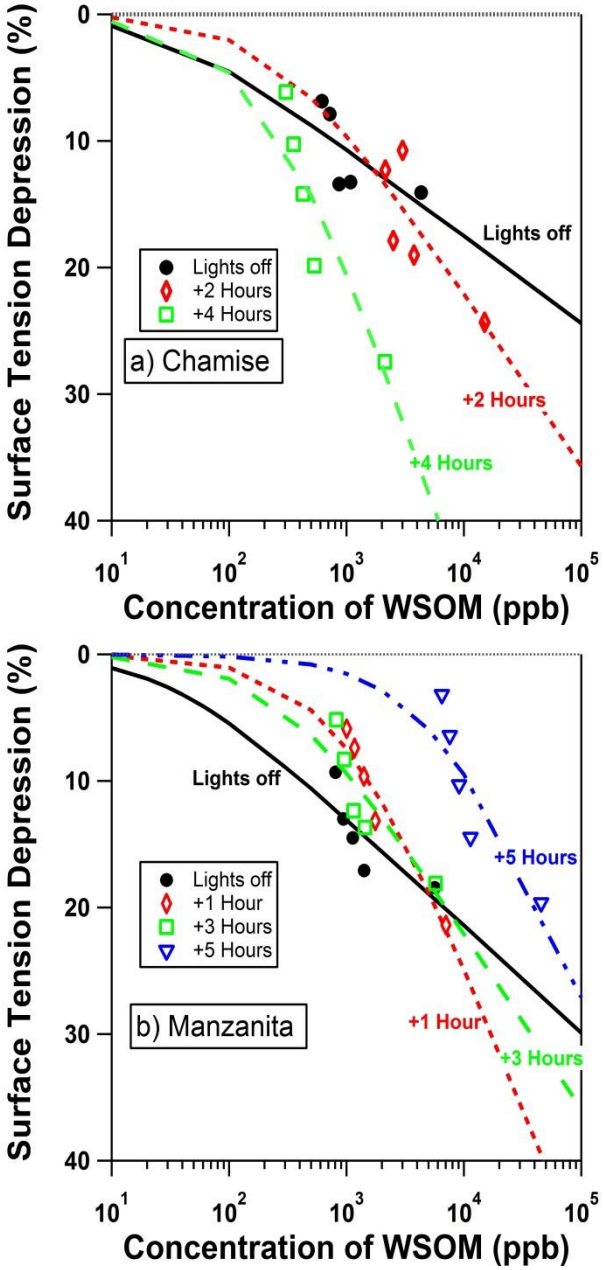

Figure 2.1: Szyskowski-Langmuir fits and data for chamise (a) and manzanita (b) biomass burning aerosol. Surface tension depression vs. water-soluble organic matter concentration is shown as a function of time of irradiation. The fit parameters α and β are given in Table 2S.1.

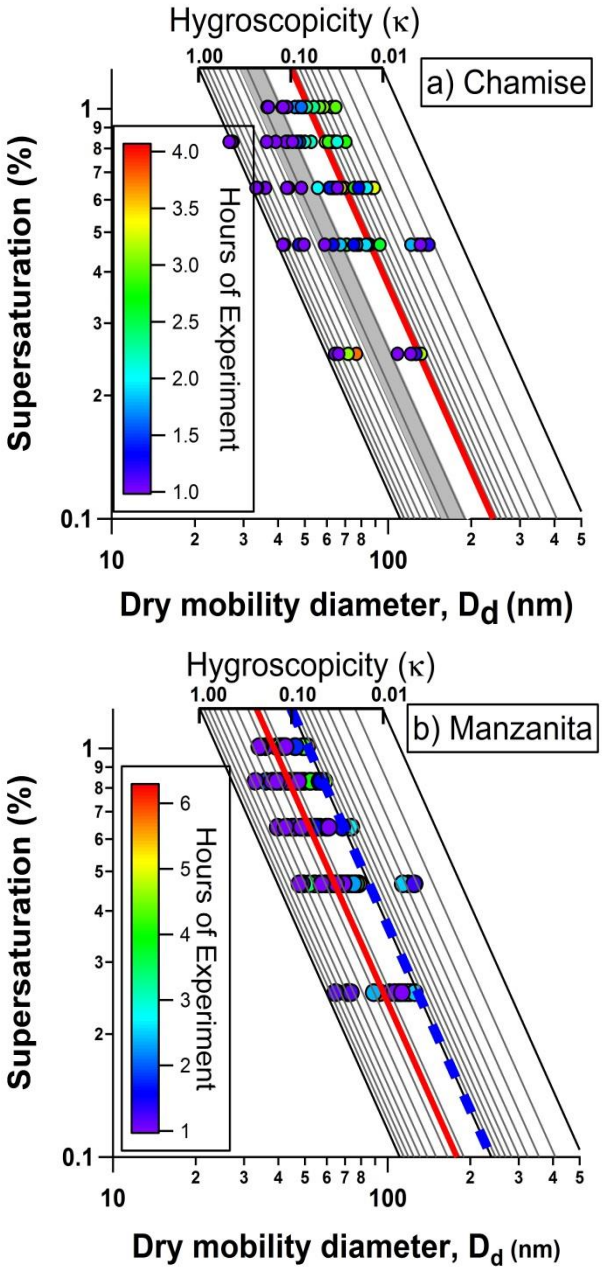

Figure 2.2: CCN activity of biomass burning aerosol from chamise (a) and manzanita (b). Data from a dark chamber are colored purple while irradiated data follows the color scale shown. The best-fit line of the data is represented in red for both graphs. The shaded

region in Fig. 2.2a is the reported average data from Engelhart et al. (2012). The blue line in Fig. 2.2b is the reported data from Petters et al. (2009).

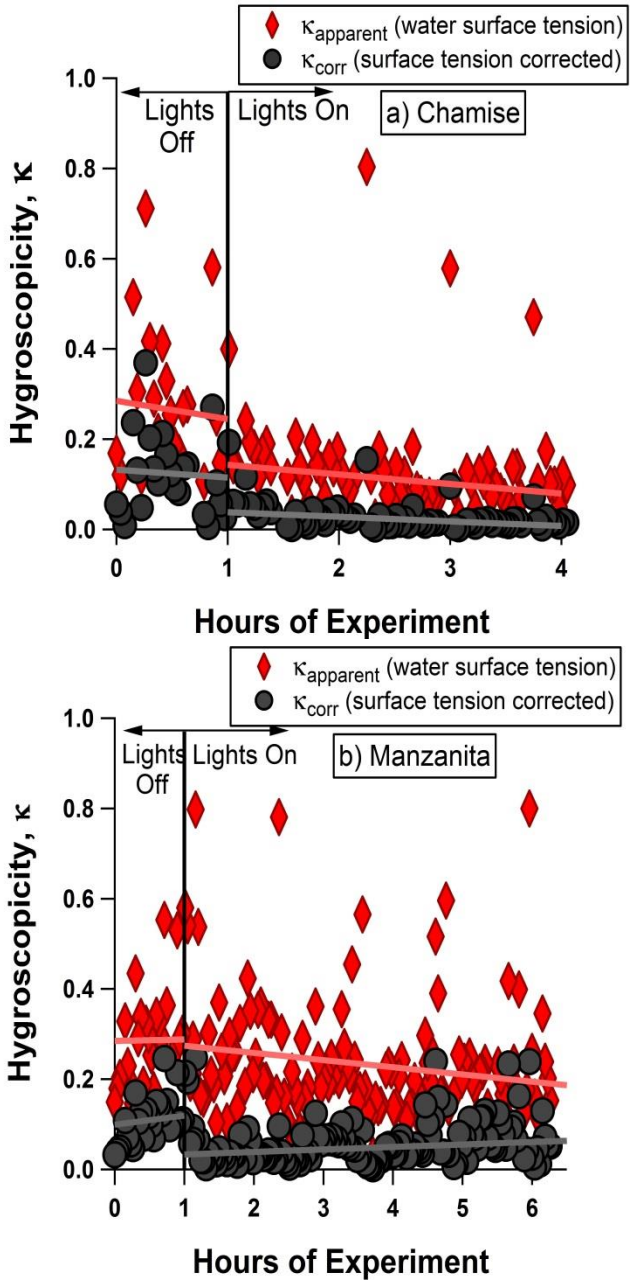

Figure 2.3: Single parameter hygroscopicity, κ, calculated without ($\kappa_{apparent}$) and with (κ_{corr}) surface tension correction for chamise (top, A) and manzanita (bottom, B). Solid vertical lines indicate when lights are turned on, 1 hour after injection. A 7-minute running average of the data before and after lights on is also provided.

2.8 Tables

Table 2.1: Sensitivity of A (Kelvin Term) and κ values using the data in Fig. 2.2 calculated with varying degrees of constant surface tension depression

	Surface tension depression					
	0%	5%	10%	15%	20%	25%
A, Kelvin Term	2.091	1.987	1.882	1.778	1.673	1.568
κ_{st} (Chamise)	.265	.227	.193	.162	.135	.112
κ_{st} (Manzanita)	.226	.194	.165	.139	.116	.095

2.9 Supplemental Figures

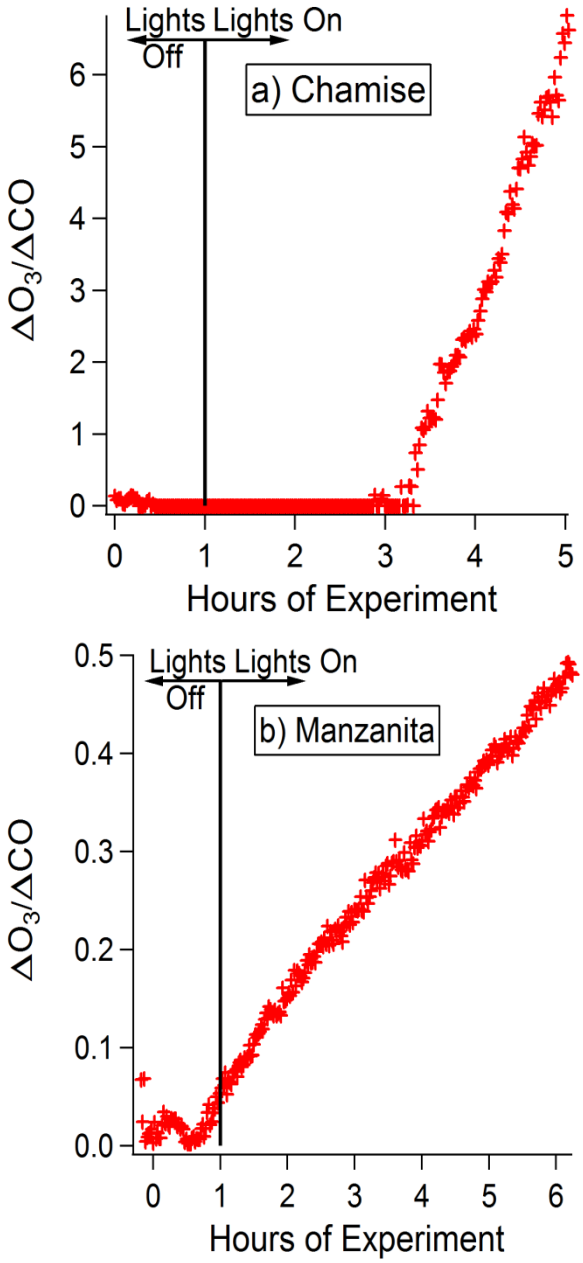

Figure 2S.1: $\Delta O_3/\Delta CO$ vs time for a) chamise and b) manzanita

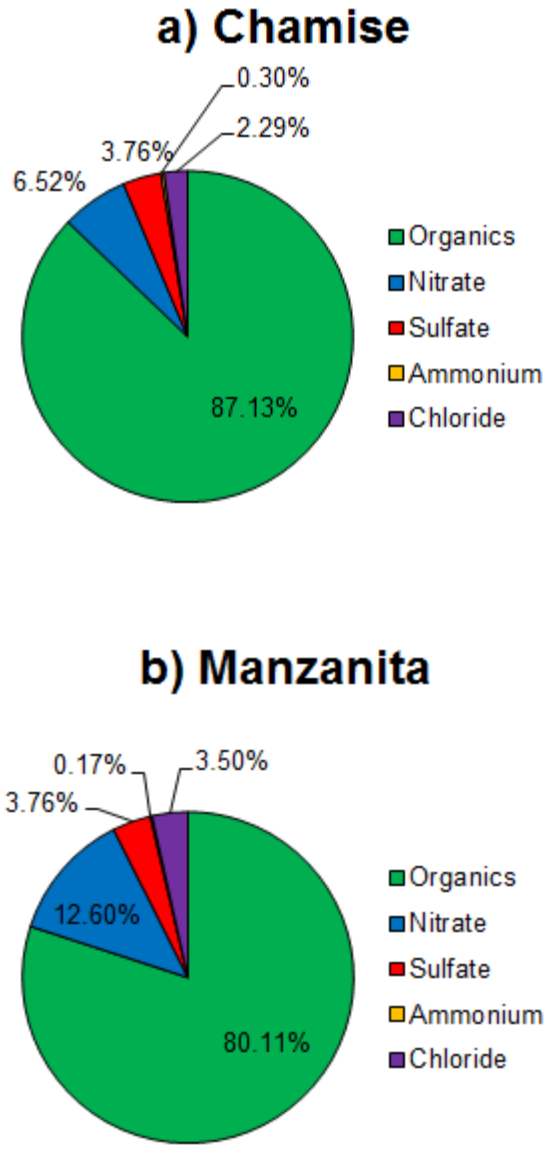

Figure 2S.2: Average species concentration from AMS measurements during a) chamise and b) manzanita experiments.

2.10 Supplemental Tables

Table 2S.1: α and β coefficients of Szykowski-Langmuir fits of surface tension vs. water-soluble organic matter (WSOM)

	Manzanita		Chamise	
	α (mN m^{-1} K^{-1})	β (ppm^{-1})	α (mN m^{-1} K^{-1})	β (ppm^{-1})
Lights Off	0.00887	0.034305	0.007204	0.03569
+1 hour of lights	0.024128	0.001111	-	-
+2 hours	-	-	0.01432	0.004091
+3 hours	0.01466	0.003713	-	-
+4 hours	-	-	0.028366	0.004786
+5 hours	0.022148	0.000181	-	-

Table 2S.2: $(NH_4)_2SO_4$ DMT CCN Calibration Information for a 0.5 L min^{-1} flowrate

Supersaturation Setting (%)	ΔT (°C)	D_d (nm)	*Supersaturation reported*
0.2	4.6	70.8	0.25%
0.4	7.6	47.21	0.46%
0.6	10.6	38.1	0.64%
0.8	13.6	32.1	0.83%
1.0	16.5	28.2	1.01%

3 Experimentally measured morphology of biomass burning aerosol and its impacts on CCN ability

3.1 Introduction

Aerosols have important health effects, affect regional visibility, are a key factor in the earth's climate via radiative forcing mechanisms, and play a vital role in atmospheric chemistry (Seaton et al., 1995; Haywood and Boucher, 2000; Ramanathan et al., 2001; Pöschl, 2005; Forster et al., 2007). For all impacts, particle composition and size are important. Particles are ubiquitous but can be non-uniform and non-spherical. As such, a number of instruments exist to measure these critical aerosol properties. One property that remains difficult to characterize through conventional techniques is particle morphology. Morphology is used here as a term to describe the shape of a 3-dimensional particle and has a direct impact on particle size measurements (DeCarlo et al., 2004). The true volume of a particle is difficult to accurately measure without knowledge of the particle morphology. Reducing uncertainties in particle morphology will increase the accuracy of characterizations and parameterizations that rely on knowing the true volume of a particle, e.g. particle density and hygroscopicity.

Biomass burning emissions are a major source of non-uniform and non-spherical complex aerosol emissions (2–5 petagrams of Carbon year^{-1}) to the atmosphere (Crutzen and Andreae, 1990; Andreae et al., 2004; Reid et al., 2005; van der Werf et al., 2006). Both the developed and developing world are subject to biomass burning events through agricultural burning, wildfires, and domestic burning applications (Forster

et al., 2007). Particles formed during the combustion process are non-uniform. The aerosol formed during biomass burning events is a complex mixture of volatile, semi-volatile, and non-volatile components that are able to seed clouds, modify cloud properties, and indirectly impact radiative forcing (Forster et al., 2007; Reutter et al., 2009; Liu and Wang, 2010). The impact of a potential wildfire or prescribed burn de pends on the fuel type, the burning regime (e.g. smoldering, flaming, or mixed), and the ageing time of the atmospheric emissions. This work further explores the role of biomass burning aerosol as Cloud Condensation Nuclei (CCN). We obtain information about the shape and true volume of biomass burning particles using a semi-continuous method to investigate the impact of particle size, changes in shape that occur during the evolution of photochemical ageing and changes in perceived hygroscopicity as a result of particle volume and sizing assumptions.

3.2 Theoretical Considerations

3.2.1 Biomass burning cloud condensation nuclei

Several recent works on biomass burning aerosol have focused on their ability to act as cloud condensation nuclei (CCN) (e.g.: Novakov and Corrigan, 1996; Martins et al., 2009; Petters et al., 2009; Carrico et al., 2010; Rose et al., 2010, 2011; Hennigan et al., 2011; Engelhart et al., 2012; Giordano et al., 2013; Lathem et al., 2013). The CCN ability of inorganic compounds can be described well by classical Köhler theory (Köhler, 1936). The theory has since been expanded to better model organic/inorganic mixed particles

with varying degrees of accuracy and complexity (e.g. Shulman et al., 1996; Raymond and Pandis, 2002). One extension, κ-Köhler theory, has become a common method for reporting CCN ability and estimating particle hygroscopicity. Its popularity is due to its empirical grounding, ease of understanding, ability to represent organic/inorganic mixed particles and translate to both the sub- and supersaturated regimes. This has led to a large body of published κ-Köhler theory values. The κ parameterization of hygroscopicity posits that particle diameter and the supersaturation at the point of activation effectively capture CCN ability (Petters and Kreidenweis, 2007):

$$\kappa = \frac{4A^3}{27D_d^3 ln^2 s_c} \text{ ; where } A = \frac{4\sigma_{s/a} M_w}{RT\rho_w} \qquad \text{Eq. 3.1}$$

where ρ_w is the density of water, M_w is the molecular weight of water, $\sigma_{s/a}$ is the surface tension of the solution/air interface, R is the universal gas constant, T is the temperature, D_d is the dry particle diameter, and s_c is the critical supersaturation required to activate a particle with size D_d. D_d is the measured mobility diameter and is calculated as the 50 % efficiency for which half of all particles activate at s_c, the instrument supersaturation. From Eq. 3.1, κ is interpolated using a linear regression of experimental D_d and calibrated s_c.

Thus, the CCN activity can be represented by a single hygroscopicity parameter, κ. A range of κ biomass burning literature values has been reported. Multiple factors affect this range. Different fuels can have a wide variability in CCN activity. The particles can be very non-hygroscopic (e.g. $\kappa < 0.1$ for various softwoods) to very hygroscopic (e.g. $\kappa >$ 0.5 for sage and sawgrass) (Petters et al., 2009; Carrico et al., 2010). Differences in

burning conditions contribute to the range of κ. Additionally, the oxidative aging of these emissions can affect the observed κ values (Hennigan et al., 2011; Engelhart et al., 2012). The presence of surface active compounds can also affect the range of κ (Giordano et al., 2013).

κ-Köhler theory applies a few assumptions. First, ideal droplet water activity conditions are assumed when the growing cloud droplet exists as an aqueous solution and all available solute is dissolved. Second, κ-Köhler theory applies the ideal surface tension of water, $\sigma_{s/a} = 0.072$ J m^{-2}. Third, and most important for application to biomass burning, the diameter of the particle cubed, D_d^3, is assumed to estimate the volume of a spherical particle. A number of studies have investigated the applicability of the first two assumptions and come to varying conclusions on their importance. However, the assumption of particle sphericity for hygroscopicity has only been theoretically manipulated and not experimentally measured, especially as a function of particle aging (Dusek et al., 2011). Here we provide simultaneous morphological and hygroscopicity measurements of fresh and aged biomass aerosol. These measurements together provide a more accurate parameterization of particle hygroscopicity.

3.2.2 Volume equivalent and electrical mobility diameters

CCN activity measurements require either mass or volume information in addition to droplet activation data. Particle diameter alone can introduce 84 to 96 % variation in CCN concentrations (Dusek et al., 2006). Particle volume information is commonly

obtained from mobility particle sizing instrumentation and is combined with a cloud condensation nuclei counter (CCNC). This experimental method selects the electrical mobility diameter of a particle. The mobility-selected particle then flows to the supersaturated column of the CCNC where, if above a critical size, it activates to form a cloud droplet. When combined with κ-Köhler theory, the method assumes that a particle's electrical mobility is equivalent to its volume equivalent diameter. For a spherical particle this is true: the mobility diameter equals the volume-equivalent diameter. However, for non-spherical particles, electrical mobility diameter deviates from the volume equivalent diameter. The phenomenon has also been observed in CCN experiments using mass-selected particles measured with a Kanomax APM (Kuwata and Kondo, 2009). The volume equivalent diameter (d_{ve}) is defined as the diameter of a spherical particle of the same volume as the particle of interest (Baron and Willeke, 2001). For a non-spherical particle, d_{ve} is the diameter of the particle if it were compacted or melted to form a sphere while preserving internal void spaces (empty regions of the particle that are isolated from the surrounding gas).

The electrical mobility diameter, d_m, can be measured with a differential mobility analyzer (DMA) and is defined as the diameter of a sphere with the same migration velocity in a constant electric field as the considered particle (Knutson and Whitby, 1975). A force balance occurs in the annular region of the DMA to mobility-select a certain "size" particle. The particle is first charged and flown into an annulus with a constant electric field being applied between the inner and outer walls. As the particle

moves in the electric field, the charge on the particle is attracted toward the inner annular wall. A drag force between the particle and gas is equal and opposite to the electrical force when the particle reaches a terminal migration velocity. Careful design of the annulus allows for a particle of a desired electrical mobility to exit the DMA in a monodisperse size stream.

Assuming a particle and its volume equivalent sphere have the same charge, the relationship between the two diameters is as follows:

$$\frac{d_m}{C_C(d_m)} = \frac{d_{ve}\chi}{C_C(d_{ve})} \qquad \text{Eq. 3.2}$$

where C_C is the Cunningham slip correction factor and χ is the dynamic shape factor. The dynamic shape factor is a correction to account for the increased drag on a non-spherical particle (Fuchs, 1964). The shape factor is equal to one for a sphere and can be greater than one for non-spherical particles. The flow regime of the suspending fluid relative to the particle dictates the nature of the forces acting on the particle. Hence, both C_C and χ are functions of the Knudsen number. The flow regime here is in the transition regime because both particle sizing and the CCNC commonly operate near standard ambient temperature and pressure (approx. 298 K, 1 atm) and the particles of interest as CCN are between 10–200 nm. This introduces an added level of complexity to volume calculations, as the dynamic shape factor behavior is more readily available in the continuum and free molecular regimes (Dahneke, 1973a, b; Kousaka et al., 1996; Baron et al., 2001). However, other work on non-spherical particles and their dynamic shape factors have assumed that the shape factor in the transition regime is approximately equal

to the shape factor in the free-molecular regime (DeCarlo et al., 2004). The analysis presented here also makes this assumption. Our analysis also neglects particle orientation effects on the shape factor. Because χ can be greater than one for non-spherical particles, the use of electrical mobility for volume measurement will likely over predict particle volume. An over prediction in particle volume in Eq. 3.1 will underestimate calculated κ-values thus misrepresenting the cloud forming ability of non-spherical aerosols.

3.2.3 Fractal and fractal-like dimensions

Combustion processes often generate aggregates of small (d < 10–30 nm) particles. The fractal dimension (D_f) is a semi-empirical relationship often used to describe aggregates. D_f is defined as the relationship between the number of primary particles in an aggregate to the aggregate's radius of gyration. The relation can be written as a power law expression (Mandelbrot, 1982):

$$N = C\left(\frac{R_g}{a}\right)^{D_f} \qquad \text{Eq. 3.3}$$

where N is the number of primary particles in the aggregate, R_g is the radius of gyration of the aggregate, a is the radius of the primary particles, and C is a constant. Park et al. (2003) use this relationship with the assumption that the primary particle diameters are approximately constant to show that N then varies proportionately to particle mass. Park et al. also assume that the radius of gyration is linearly proportional to the mobility diameter in the continuum and free-molecular regimes (Schmidt-Ott et al., 1990) to define a "fractal-like" dimension, here referred to as D_f':

$$m = C' D_{me}^{D_f'} \quad \text{Eq. 3.4}$$

where m is the mass of the aggregate. Here, a D_f' of 3 implies a spherical particle while D_f < 3 indicates a non-spherical particle. This relationship, and its analogue in density, is directly applicable to data obtained from the Kanomax Aerosol Particle Mass Analyzer (APM). Park et al. used to APM data to determine the fractal dimension of diesel exhaust particles. They obtained fractal dimensions of 2.33< D_f < 2.84 depending on engine load. Work done by Nakao et al. (2011) used this relationship to show SOA formation from diesel exhaust have similar D_f'. Zhang et al. (2008) exposed flame-generated soot to subsaturated sulfuric acid vapor and obtained a fresh (unexposed) D_f' of 2.1and an aged (exposed) D_f' of 2.8.

In this work, we obtain information about the shape and true volume of biomass burning particles using a semi-continuous method. We do this for both freshly emitted and photochemically aged emissions. We provide evidence to support the work of others that demonstrate that, (1) the particles emitted are non-spherical, (2) the degree of non-sphericity changes with photochemical aging, and (3) using the true volume equivalent diameter to calculate κ greatly shifts the predicted hygroscopicity. We also discuss how the limitations of the current methods for measuring particle volume affects CCN measurements.

3.3 Experimental methods and instrumentation

A series of biomass burning experiments were carried out at the University of California, Riverside College of Engineering – Center for Environmental Research and Technology (UCR CE-CERT) atmospheric processes lab from the spring to the summer of 2013. Two shrubs common to the California chaparral biome, chamise (*Adenostoma fasciculatum*) and manzanita (*Arctostaphylos glandulosa*), were burned in an outdoor wood-burning stove. Both fuels were collected on Bureau of Land Management land near the San Bernardino National Forest (approximately 33.84◦, −116.88◦ and the surrounding area). The collection site is approximately 3600–3900 feet in elevation. Chaparral species such as chamise, manzanita, scrub oak, and ceanothus surround the area. Both manzanita and chamise burned in the flaming regime. The flame integrated modified combustion efficiencies (MCE) of both fuels were greater than 0.97 (where $MCE \equiv \frac{\Delta CO_2}{(\Delta CO_2 + \Delta CO)}$) (Ward and Hao, 1991).

A sample line from the stack of the stove drew smoke from the fire and diluted it with a Venturi tube injection system. The diluted sample was then injected into a 12m^3 Teflon chamber to a final particle concentration ~ 100 μg m^{-3}. The chamber concentration is within range of ambient and plume-like concentrations also used in previous chamber studies (Hennigan et al., 2011). The sample was injected with a 10:1 total flow to sample flow ratio. As short of a copper transfer line as possible (approximately 7m in length) was used for the smoke injection. The enclosure is surrounded by 170 ultraviolet (UV) lights with peak intensity of 350 nm (350 BL, Sylvania®). UV lights were turned on one hour

after injection to promote photochemistry and remained on until the experiment concluded. The chamber was flushed and filled with filtered air prior to injection. The temperature of the chamber ranged approximately from 20-27°C during the experiments. The experiment was operated until the chamber was empty (up to 6 hours). This series of chamber burns produced data similar to that of ambient studies and previous biomass burning studies conducted at CE-CERT (Hennigan et al., 2011; Giordano et al., 2013).

Scanning Mobility CCN Analysis (SMCA) was used to obtain fast size-resolved CCN activity of the aging system (Moore et al., 2010). The sampled aerosol was size-classified using a Scanning Mobility Particle Sizer (SMPS, TSI 3080/3081). The monodisperse stream from the classifier was split and one stream entered a condensation particle counter (TSI 3772) while the other stream was sampled with a DMT Continuous Flow Streamwise Thermal Gradient Chamber CCN counter (CCNC) (Roberts and Nenes 2005; Rose et al., 2008). The CCNC instrument was operated at a 10:1 sheath-to-aerosol ratio with a sample flow of 0.5 L min^{-1}. The total concentration (CN) of sized particles measured by the CPC determined the ratio of CCN/CN. For each supersaturation, s_c, the activation diameter, $D_{d,}$ was defined as the diameter for which CCN/CN = 0.5. The experimental set-up was calibrated with ammonium sulfate ($(NH_4)_2SO_4$) aerosol. CCNC calibration information is provided in Table 3S.1.

A schematic of the experimental setup to measure particle mass and calculate particle effective density is shown in Fig. 3.1. Particles were selected by mass in the Kanomax

APM, then sized by electrical mobility in a downstream DMA column, and the DMA exit stream was split between the condensation particle counter (CPC, TSI 3084) and an electrostatic TEM precipitator (FHNW TEM sampler). The APM-DMA setup was used for improved time resolution over the DMA-APM setup (McMurry et al. 2002; Khalizov et al., 2009; Xue et al., 2009). The system is described in more detail in Malloy et al. (2009). Here, the APM selected 3 different particle masses between the (spherical, unit density equivalent) 50-100 nm particle size range. TEM grids were used to collect three masses of particles relevant to CCN activation, corresponding to approximately 50 nm, 75 nm, and 100 nm particles (assuming unit density). Using the effective density analogue of Eq. 3.4, the fractal-like dimension was obtained by fitting the power function (Park et al., 2003; Xue et al., 2009; Nakao et al., 2011):

$$\rho_{eff} = C d_m^{D_f'-3} \qquad \text{Eq. 3.5}$$

where ρ_{eff} is the effective density of particles, C a constant, d_m is the mobility diameter of the particles, and D_f' the fractal-like dimension. During the beginning and the end of the experiment, the TEM precipitator was turned on. The APM was operated in a single mass selection until the charge across the TEM grid was 60 pA, indicating a sufficient capture of particles. After an experiment, the TEM grids were stored in a grid holder away from heat and light. The grids were analyzed using a Philips Tecnai 12 Transmission Electron Microscope.

The pictures of the particles obtained from the TEM were further analyzed using the freeware image analysis program ImageJ (http://imagej.nih.gov/ij/). The shape factor, χ,

is determined from mobility diameter data and a volume calculation of each particle. The mean volume of the agglomerates for each APM mass selection was calculated as follows (Park et al., 2004):

$$\bar{V} = \frac{\sum_i N_i \frac{\pi}{6} \bar{d}_p^3}{n} \quad \text{Eq. 3.6}$$

where N is the number of primary particles in the agglomerate, d_p is the mean primary particle diameter, and n the number of agglomerates. By using two-dimensional projected images of three dimensional objects from the TEM, previous studies have demonstrated that the projected area can be used to calculate N or R_g in fractal agglomerates (e.g. Meakin et al., 1989; Koylu et al., 1995):

$$N = k_a \left(\frac{A_a}{A_p}\right)^{\alpha} \quad \text{Eq. 3.7}$$

where A_a is the projected area of the agglomerate, A_p is the mean projected area of primary particles, k_a is a constant, and α is a projected area exponent. Numerical simulations have been used to calculate the empirical factors of Eq. (7), k_a and α. In this study, we use the values of Oh and Sorensen (1997) who found that $\alpha = 1.19$ and $k_a = 1.81$ well described agglomerates whose primary particles were allowed to overlap. A_a, A_p, and d_p were determined through image analysis using ImageJ. Figure 3.2 shows how the three values were selected.

Once the mean volume of an aggregate at a certain mass was found with the above analysis, the diameter of the sphere with that volume was used as the volume-equivalent

diameter for that particle. The mean peak mobility diameter measured from the SMPS during the collection of the TEM grid was used as the mobility diameter for application in Eq. 3.2.

3.4. Results and Discussion

3.4.1 Morphology of Freshly Emitted Biomass Burning Aerosol

The APM-SMPS-TEM system (Fig. 3.1) measured the freshly emitted properties of biomass burning aerosol. The TEM grids were then photographed and analyzed as illustrated in Fig. 3.2. The primary particle diameter was both calculated from the projected area of the primary particles and measured directly. If the directly measured and calculated diameters deviated greater than 50 %, then the calculated value from the projected area was used and is reported here.

To measure the area and diameter of primary particles, only particles clearly distinguishable were selected for analysis. This usually meant that particles on the ends of fractal chains were selected as opposed to those in the center of the agglomerates. Previous work on flame-generated agglomerates has shown that the primary particle diameters follow a normal distribution with a mean between 28.5 to 34.4 nm (Koylu and Faeth, 1992; Lee et al., 2001). Figure 3.3 shows the primary particle diameter distribution from particles at the three selected masses from the APM-SMPS. The total number of individual primary particles analyzed is 475. The data is fit with a normal Gaussian

distribution whose mean lies at 25.7 ± 2.1 nm. This mean projected primary particle diameter, while slightly smaller than other reported values, is within the 25% standard deviation reported in the literature for primary particle size diameters (Koylu and Faeth, 1992). This value is smaller than China et al.'s (2013) projected primary particle diameters of 37–56 nm but a number of differences exist between these studies. Primarily, China et al. measured particles much larger than those examined here (aerodynamic diameters > 250 nm) through use of scanning electron microscopy (SEM). Their study was also an ambient study, conducted downstream of a fire plume. The China et al. fire likely had different fuel sources and different burning conditions than those presented here. The distribution here may also be shifted to the lower end from the abundance of 10–20 nm primary particles that appeared mostly in the 0.9 fg (50 nm) particles from the APM. Over 80% of the primary particle diameters below 20 nm were from these particles. Over 80% of the primary particles observed below 20 nm were from 0.9 fg agglomerates. However, primary particles below 20 nm only made up 40 % of counts for the total number of primary particles from the 0.9 fg agglomerates. When < 20 nm primary particles are omitted, the distribution of primary particle size shifts to a mean of 27 nm. When only the particles from the 0.9 fg agglomerates are considered, the distribution becomes a double-peaked normal distribution centered on 14 and 19 nm.

In this study, the mean primary particle projected area and diameter shown in Fig. 3.3 were used in the application of Eq. 3.7. The analysis was applied for each of the three selected agglomerate masses from the APM. The application of mean primary projected

area introduces a slight overestimation for the 50 nm agglomerates and a slight underestimation for the 75 and 100 nm agglomerates. However, the percent change on the calculated volume as a whole is small. For example, the bi-modal 50 nm primary particle distribution, if half of the total agglomerate projected area is assumed to be contributed by one peak, the calculated volume is forced upward by ~ 35 %. For the 75 and 100 nm particles, the calculated volume is forced downward by ~ 7 %.

Table 3.1 shows the calculated application of Eqs. 3.6 and 3.7 to the TEM images obtained for the 50 nm, 75 nm, and 100 nm equivalents selected from the APM-SMPS system. Figure 4 graphically demonstrates the size dependence of the shape factor to the mobility diameter. The shape factor for these particles ranges from 1.06 to 1.42 indicating a 6 % to 42 % overestimation of the true volume of a particle when using the electrical mobility diameter.

3.4.2 Morphology of aged biomass burning aerosol

To measure the effect of atmospheric aging on biomass burning aerosol's morphology, the APM-SMPS system was used as described in Nakao et al. (2011). The TEM was not used in this section because saturation of the TEM grids required extensive time, longer than that necessary to observe changing morphology that can occur with aging.

Figure 3.4 shows the evolution of the fractal-like dimension (D_f') as a function of experimental time. In this analysis a fractal-like dimension of 3 indicates a spherical

particle and $D_f' < 3$ indicates a non-spherical particle. Calibration with ammonium sulfate, an inorganic crystalline solute and not quite spherical particle ($D_f' = 2.7$), is included for comparison. The black line indicates the time the UV lights surrounding the chamber were turned on. The freshly emitted particles have a D_f' of 2.15 ± 0.05 indicating a non-spherical particle, similar to the D_f' of 2.20 of Xue et al. (2009) for freshly emitted diesel particles. After 4 hours of photochemical exposure, the D_f' rises nearly linearly to 2.60.

The D_f' analysis here is a bulk measurement of all the particles selected in the APM which increased from 50 nm to 250 nm equivalent sizes. While it should be theoretically possible to link the D_f' reported here to the dynamic shape factor, χ (Kaspar, 1982; DeCarlo et al., 2004), we do not do so here because of the limitations an ensemble method (the APM-SMPS system) has when expanded to a size-dependent individual particle analysis.

The APM-SMPS data set agrees with the TEM analysis of the previous section – that freshly emitted biomass burning aerosol are not spherical. Because the TEM operates at near-vacuum pressures, there is the possibility that volatile material may evaporate from the fractal backbone. This would skew the perceived importance of the particle's morphology. However, this second confirmation of morphology from the APM-SMPS indicates that volatile evaporation in the TEM is not completely the reason for shape

factors greater than one being reported.

As D_f' increases with time, the aerosol becomes more spherical with photochemical exposure. This is likely due to a coating of secondary organic aerosol (SOA) forming on the primary emissions (Nakao et al., 2011). The SOA fills in the void space inside the fractal agglomerates. This aged fractal-like dimension is smaller than the aged biomass burning plume aerosol measured by China et al. (2013) but the D_f' reported here is not directly comparable to their D_f. In addition to the different derivations, China et al. (2013) focused on larger particles than those investigated here, on a shorter period of atmospheric aging (1–2 h), and during the smoldering phase of the burn. However, both of these results confirm, through two different methods, that applying the electrical mobility diameter as the volume equivalent diameter will result in an overestimation of particle size and volume.

3.4.3 Applying a true volume equivalent diameter to the CCN analysis of biomass burning aerosol

The assumption that the electrical mobility diameter cubed is equal to the true volume of the particle will result in a skewed CCN prediction for aerosol from combustion sources. The previous work of Dusek et al. (2011) has investigated conceptually the importance of fractal-morphology in CCN analysis. We present experimental data for both the hygroscopicity and morphology of the particle and apply it to κ-Köhler analysis.

Figure 3.6 shows an example of the CCN to CN activation ratio as a function of mobility diameter for biomass burning at a supersaturation of 0.37%. Both the raw electrical mobility activation diameters and the volume equivalent diameters are shown on the figure. The volume equivalent diameters are determined on a point-by-point basis by using a logarithmic regression of the data in Fig. 3.4 and Eq. 3.2. The shape factor is assumed to be equal to unity for particles smaller than 30 nm where the regression falls below one. The activation ratio of ammonium sulfate at the same supersaturation is included for comparison. Figure 3.6 shows the shape factor of a particle affects its perceived mobility diameter. Since χ is greater than unity for particles larger than 30 nm, the activation curve shifts to smaller electrical mobility diameters. In this example, the diameter where half of all particles activate (D_{p50}) is measured at 75 nm electrical mobility but the true volume equivalent diameter for that particle is at 60 nm.

Figure 3.7 shows the total effect that accounting for the volume equivalent diameter can have on the calculation of κ. The data from a non-photochemically exposed chamise biomass burning injection into the chamber is presented. The markers in Fig. 3.7 are the activation diameters for each scan of the SMPS-CCNC at a supersaturation. The red line is the κ fit between the points as shown where the lines of constant κ are forced such that critical supersaturation scales with $d_d^{-3/2}$. The implications of this are discussed later. The black line is the fit of the points if the mobility diameter is converted to the volume equivalent diameter via the process described for Fig. 3.6. The hygroscopicity of manzanita biomass, without morphological corrections, has a κ of 0.38 ± 0.09. This value

agrees with Engelhart et al.'s (2012) hygroscopicity measurements of primary (non-aged) chamise emissions. When the shape factors of the particles is taken into account using the TEM data collected concurrently, the calculated κ increases to 0.52. Since the particles are not spherical, their volume equivalent diameters are smaller than their mobility diameters. Therefore, using only the mobility diameter when calculating κ can substantially underestimate hygroscopicity.

This analysis of particle morphology may help reconcile the difference in calculated hygroscopicity between filter reconstituted biomass burning aerosol and in-situ sampled aerosol. Carrico et al. (2008) reported HTDMA and CCN derived κ values for biomass burning filter samples extracted in water and methanol. The CCN derived κ from Carrico et al.'s study of Alaskan Duff core aerosol extracted in water was 0.148. This value is significantly higher than the on-line sampling of Alaskan Duff core done by both Petters et al. (2009) and Engelhart et al. (2012) which reported a CCN derived κ value of 0.09 and 0.07, respectively. The 50 % increase in filter reconstituted hygroscopicity may be due to the use of mobility diameter as the volume equivalent diameter for non-spherical aerosols. In filter reconstitution, the liquid solution is first atomized and dried before flowing into the downstream instruments. The process of drying may fill in void space in a non-spherical backbone thus producing a particle whose volume equivalent and electrical mobility diameters are identical. It is important to note that Carrico et al. (2008) reported a lower hygroscopicity value for reconstituted sagebrush than both Petters et al.'s (2009) and Engelhart et al.'s (2012) in-situ sampled aerosol. This discrepancy may

be due to different burning or feedstock conditions that may influence particle shape factor. However, since reconstitution of aerosols can increase measured hygroscopicity, this also suggests that cloud processing of fractal aerosols should be considered for biomass burning aerosol's climate impacts.

3.4.4 Sensitivity of κ to particle shape factor

Because the shape factor of particles derived from biomass burning can range from 1 to greater than 1.5, the importance of particle morphology can be negligible to substantial. While the current literature on the morphology of biomass burning aerosols is sparse, the work done on diesel particles suggests that burn conditions may play a part in particle morphology (Park et al., 2004; Nakao et al., 2011). Along with the affects that particle aging have on morphology shown in this study, it is prudent to analyze the potential range of hygroscopicities that biomass burning aerosols can have.

For any non-spherical, fractal particle generated from combustion, the larger the activation diameter in a CCNC, the greater the difference between the mobility diameter and volume equivalent diameter will be. Figure 3.8 shows how sensitive κ can be when applying a volume equivalent diameter calculation. In Fig. 3.8, hygroscopicity data from biomass burning tests by Petters et al. (2009) is used. The grey shaded area is the sensitivity of black spruce ($\kappa = 0.07$) when applying a dynamic shape factor of 1 (right-most boundary of the shaded area) and of 1.5 (left-most boundary of the shaded area). Here, black spruce ranges from a κ of 0.07 to 0.24. The blue shaded area is the same

treatment for sage brush ($\kappa = 0.33$ to 1.1 after applying χ). Douglas fir, oak, titi, and needlegrass, two relatively low-hygroscopic and two moderately hygroscopic biomass burning species, are included for comparison. In this analysis we apply a constant shape factor across all diameters as opposed to the mobility diameter-dependent treatment used earlier. This sensitivity analysis therefore shows the area that the true κ line falls in but not necessarily its slope. It is also a large range of χ which captures the effects that burn conditions and the species itself may have on particle morphology. This range is indicative of the effects that photochemical aging can have on morphology.

Figure 3.9 shows the sensitivity of the slope of the κ-Köhler isolines (heretofore referred to as the experimental exponent or exponent) to two different methods of applying shape factor to CCN analysis. Shown in the figure are an application of a constant shape factor ($\chi \neq f(d_{dry})$) and a variable shape factor ($\chi = f(d_{dry})$). The data shown is data from the chamise experiments shown in Fig. 3.7. The constant application of χ does not exhibit any change in the experimental exponent of the κ lines. S_c scales with $d_d^{-3/2}$ as predicted by Köhler theory. This suggests that the solute dissolution process is thermodynamically ideal, the particle completely dissolves and surface tension effects are negligible. When a variable shape factor is applied, s_c then scales with $d_d^{-1.8}$. Kumar et al. (2011) observed a similar effect on the κ exponent in wet processed soil and dust samples. Their study observed an unusually low experimental exponent of −2.16 for the wet processed mineral sample, Arizona Test Dust (ATD). This deviation from Köh ler theory could be caused by sparingly soluble species, an externally mixed sample (composition as a function of

particle size), or activation physics. The presence of black carbon (BC) in biomass burning may act as the sparingly soluble species for biomass burning generated aerosol. The presence of BC could explain the deviation from Köhler theory for the corrected data set from combustion aerosol and further investigation into this phenomenon is required. The complexity and non-ideal behavior of the aerosol solute can be masked if electrical mobility diameter is used in CCN analysis.

3.5 Conclusions

This work investigated the morphology and hygroscopicity of biomass burning aerosol. We show, through two independent measurements that particles emitted from biomass combustion are not spherical and that the degree of non-sphericity can change with photochemical exposure. Thus, for biomass burning aerosol sampled near source with electrical mobility techniques, size and volume measurements are likely overestimated. As the ageing process occurs, SOA condenses on the fractal particle and the volume changes (measured through electrical mobility) are small compared to changes in particle mass. We also measure the dynamic shape factor of freshly emitted particles and apply it to κ-Köhler theory to ensure a mobility diameter derived volume. We find that particle morphology is a function of a particle's electrical mobility diameter, which is consistent with literature, and a particle's dynamic shape factor can range from 1.06 to 1.42 for electrical mobility equivalent diameters of 50 to 100 nm. These mobility diameters are relevant for CCN activation and therefore represent an underestimation of κ since the volume of particle that is being activated is smaller than assumed. Alone, this suggests an

underestimation of up to almost 50 %. The uncertainty induced by excluding particle morphology in CCN data sets is consistent with the range of biomass burning κ values presented in literature data. The issue is further complicated by changes in particle morphology that occur with photochemical aging and time. Biomass burning derived aerosols experience a decrease in hygroscopicity with aging. The results presented here suggest that morphological changes as well as chemical compositional changes may contribute to that phenomenon. A number of questions still remain to be investigated about the true nature of biomass hygroscopicity. Since shape factor, χ, is a function of particle size, in practice this means that the κ-isolines do not follow those of an ideal solution, where critical supersaturation scales with $d_d^{-3/2}$. Scaling with ideal theory suggests that critical solubility and surface tension limits are negligible and thus non-ideal effects are partially hidden from electrical mobility-CCNC observation. The corrected data suggests that s_c scales with $d_d^{-1.8}$ and does not follow ideal thermodynamic behavior. Non-ideal behavior is observed because the process of chemical transformation (secondary aerosol formation) occurs concurrently with physical rounding (decrease in the fractal nature) of the particles. The importance of timescales for chemical vs. physical evolution of ambient biomass burning aerosols needs to be further explored.

3.6 Acknowledgements

Many thanks to David Weise and Joey Chong of the USDA Forest Service, Pacific Southwest Research Station in Riverside, CA, for their advice and pivotal role in the acquisition of fuels. The authors would also like to thank David

Cocker and the Keck Foundation for use of the environmental chamber. MG would also like to thank Bibiana Lopez for her work supporting this paper. MG would like to thank California NASA Space Grant Consortium for partially supporting this work. MG and AA would also like to thank the U.S Environmental Protection Agency for funding this work made possible by EPA grant number 83504001. Any opinions, findings, and conclusions expressed in this material are those of the authors and do not necessarily reflect the views of NSF, NASA, or EPA.

3.7 References

Andreae, M. O., Rosenfeld, D., Artaxo, P., Costa, A. A., Frank, G. P., Longo, K. M., and Silva-Dias, M. A. F.: Smoking rain clouds over the Amazon, *Science*, 303, 1337–1342, doi:10.1126/science.1092779, 2004.

Baron, P. A., Sorensen, C. M., and Brockmann. J. E.: Nonspherical particle measurements: Shape factors, fractals, and fibers. In Aerosol Measurement: Principles. Techniques. and Applications, edited by P. A. Baron and K. Willeke. John Wiley. New York , pp. 705-749, 2001.

Carrico, C. M., M. D. Petters, S. M. Kreidenweis, J. L. Collett Jr., G. Engling, and W. C. Malm: Aerosol hygroscopicity and cloud droplet activation of extracts of filters from biomass burning experiments, J. Geophys. Res., 113, D08206, doi:10.1029/2007JD009274, 2008.

China, S., Mazzoleni, C., Gorkowski, K., Aiken, A. C., and Dubey, M. K.: Morphology and mixing state of individual freshly emitted wildfire carbonaceous particles, *Nature Communications* **4**, Article number: 2122, doi:10.1038/ncomms3122, 2013.

Crutzen, P. J. and Andreae, M. O.: Biomass burning in the tropics: Impact on atmospheric chemistry and biogeochemical cycles, *Science*, 250, 1669–1678, doi:10.1126/science.250.4988.1669, 1990.

Dahneke, B.: Slip correction factors for nonspherical bodies-I Introduction and continuum flow, J. Aerosol Sci., 4, 139-145, 1973a.

Dahneke, B.: Slip correction factors for nonspherical bodies-II Free molecule flow, J. Aerosol Sci., 4,147-161, l973b.

Dusek, U., Frank, G. P., Massling, A., Zeromskiene, K., Iinuma, Y., Schmid, O., Helas, G., Hennig, T., Wiedensohler, A., and Andreae, M. O.: Water uptake by biomass burning aerosol at sub- and supersaturated conditions: closure studies and implications for the role of organics, *Atmos. Chem. Phys*., 11, 9519-9532, doi:10.5194/acp-11-9519-2011, 2011.

Engelhart, G. J., Hennigan, C. J., Miracolo, M. A., Robinson, A. L., and Pandis, S. N.: Cloud condensation nuclei activity of fresh primary and aged biomass burning aerosol, *Atmospheric Chemistry and Physics*, *12*(15), 7285-7293, 2012.

Forster, P., Ramaswamy, V., Artaxo, P., Berntsen, T., Betts, R., Fa hey, D. W., Haywood, J., Lean, J., Lowe, D. C., Myhre, G., Nganga, J., Prinn, R., Raga, G., Schulz, M., and Van Dorland, R.: Changes in Atmospheric Constituents and in Radiative Forcing, in: Climate Change 2007: The Physical Science Basis. Con tribution of Working Group I to the Fourth Assessment Report of the Intergovernmental Panel on Climate Change, edited by: Solomon, S., Qin, D., Manning, M., Chen, Z., Marquis, M., Averyt, K. B., Tignor, M.,

and Miller, H. L., Cambridge University Press, Cambridge, United Kingdom and New York, NY, USA, 2007.

Fuchs, N. A.: The Mechanics of aerosols, Pergamon, New York, 1964.

Giordano, M.R., Short, D.Z., Hosseini, S., Lichtenberg, W., and Asa-Awuku, A.: Changes in droplet surface tension affect the observed hygroscopicity of photochemically aged biomass burning aerosol, Env. Sci. & Tech., 47(19), 10980–10986, doi:10.1021/es401867j, 2013.

Haywood, J. and Boucher, O.: Estimates of the direct and indirect radiative forcing due to tropospheric aerosols: A review, *Reviews of Geophysics*, *38*(4), 513-543, 2000.

Hennigan, C. J., Miracolo, M. A., Engelhart, G. J., May, A. A., Presto, A. A., Lee, T., Sullivan, A. P., McMeeking, G. R., Coe, H., Wold, C. E., Hao, W.-M., Gilman, J. B., Kuster, W. C., de Gouw, J., Schichtel, B. A., J. L. Collett Jr., Kreidenweis, S. M., and Robinson, A. L.: Chemical and physical transformations of organic aerosol from the photo-oxidation of open biomass burning emissions in an environmental chamber, *Atmos. Chem. Phys.*, 11, 7669-7686; doi:10.5194/acp-11-7669-2011, 2011.

Kaspar. G.: Dynamics and measurement of smokes. I. Size characterization of non-spherical particles, Aerosol Sci. Technol. 1(2), 187-199, 1982.

Khalizov, A. F., Zhang, R., Zhang, D., Xue, H., Pagels, J., and McMurry, P. H.: Formation of highly hygroscopic soot aerosols upon internal mixing with sulfuric acid vapor, J. Geophys. Res., 114:D05208, doi:10.1029/2008JD010595, 2009.

Knutson, E.O. and Whitby, K.T.: Aerosol classification by electric mobility: apparatus, theory, and applications, J. Aerosol Sci., 6(6), 443-451, doi: 10.1016/0021-8502(75)90060-9, 1975.

Kohler, H.: The nucleus in and the growth of hygroscopic droplets, Trans Farad Soc, 32, 1152–1161, 1936.

Kousaka, Y., Endo, Y., Ichitsubo, H., and Alonso, M.: Orientation-specific dynamic shape factors for doublets and triplets of spheres in the transition regime, Aerosol Sci. Technol., 24(1), 36-44, 1996.

Koylu, U. O., and Faeth, G. M.: Structure of overfire soot in buoyant turbulent diffusion flames at long residence times, Comb. Flame, 89,140-156, 1992.

Koylu, U. O., Faeth, G. M., Farias, T. L., and Carvalho, M. G.: Fractal and projected structure properties of soot aggregates, Comb. Flame, 100, 621-633, 1995.

Kumar, P., Sokolik, I. N., and Nenes, A.: Cloud condensation nuclei activity and droplet activation kinetics of wet processed regional dust samples and minerals, Atmos. Chem. Phys., 11, 8661-8676, doi:10.5194/acp-11-8661-2011, 2011.

Kuwata, M. and Kondo, Y.: Measurements of particle masses of inorganic salt particles for calibration of cloud condensation nuclei counters, Atmos. Chem. Phys., 9, 5921-5932, doi:10.5194/acp-9-5921-2009, 2009.

Lathem, T. L., Beyersdorf, A. J., Thornhill, K. L., Winstead, E. L., Cubison, M. J., Hecobian, A., and Nenes, A.: Analysis of CCN activity of Arctic aerosol and Canadian biomass burning during summer 2008, *Atmos. Chem. Phys.*, *13*(5), 2735-2756, 2013.

Lee, K. O., Cole, R., Sekar, R., Choi, M. Y., Zhu, J., Kang J., and Bae, C.: Detailed characterization of morphology and dimensions of diesel particulates via thermophoretic sampling, SAE Technical Paper Series 2001-01-3572, 2001.

Liu, X. and Wang, J.: How important is organic aerosol hygroscopicity to aerosol indirect forcing?, *Environmental Research Letters*, 5(4); doi:10.1088/1748-9326/5/4/044010, 2010.

Malloy, Q.G.J., Nakao, S., Qi, L., Austin, R., Stothers, C., Hagino, H., and Cocker, D.R. III: Real-time aerosol density determination utilizing a modified scanning mobility

particle sizer—aerosol particle mass analyzer system, Aerosol Science and Technology, 43:7, 673-678, DOI: 10.1080/02786820902832960, 2009.

Martins, J. A., Gonçalves, F. L. T., Morales, C. A., Fisch, G. F., Pinheiro, F. G. M., Júnior, J. B. V. L., and Dias, M. A. F. S.: Cloud condensation nuclei from biomass burning during the Amazonian dry-to-wet transition season, *Meteorology and Atmospheric Physics*, *104*(1-2), 83-93, 2009.

McMurry. P. H., Wang. X., Park. K., and Ebara, K.: The relationship between mass and mobility for atmospheric particles: A new technique for measuring particle density. Aerosol Sci. Technol.. 36(2), 227-238, 2002.

Meakin, P., Donn, B., and Mulholland, G. W.: Collisions between point masses and fractal aggregates, Langmuir, 5, 510-518, 1989.

Moore, R. H., Nenes, A., and Medina, J.: Scanning mobility CCN analysis—a method for fast measurements of size-resolved CCN distributions and activation kinetics, *Aerosol Science & Tech.*, 44(10), 861-871, doi:10.1080/02786826.2010.498715, 2010.

Nakao, S., Shrivastava, M., Nguyen, A., Jung, H., and Cocker, D. III: Interpretation of secondary organic aerosol formation from diesel exhaust photooxidation in an

environmental chamber, Aerosol Science and Technology, 45:8, 964-972, doi:10.1080/02786826.2011.573510, 2011.

Novakov, T. and Corrigan, C. E.: Cloud condensation nucleus activity of the organic component of biomass smoke particles, *Geophysical Research Letters*, *23*(16), 2141-2144, 1996.

Oh, C., and Sorensen, C. M. The Effect of overlap between monomers on the determination of fractal cluster morphology, J. Colloid Interface Sci., 193, 17-25, 1997.

Park. K., Cao, F., Kittelson, D. B., and McMurry. P. H.: Relationship between particle mass and mobility for diesel exhaust particles, Environ. Sci. Technol. 37(3), 577-583, 2003.

Park, K., Kittelson, D.B., and McMurry, P.H.: Structural properties of diesel exhaust particles measured by transmission electron microscopy (TEM): Relationships to particle mass and mobility, Aerosol Science and Technology, 38:9, 881-889, doi:10.1080/027868290505189, 2004.

Petters, M. D. and Kreidenweis, S. M.: A single parameter representation of hygroscopic growth and cloud condensation nucleus activity, *Atmos. Chem. Phys*., 7, 1961–1971; doi:10.5194/acp-7- 1961-2007, 2007.

Petters, M. D., Carrico, C. M., Kreidenweis, S. M., Prenni, A. J., DeMott, P. J., Collett, J. L., and Moosmüller, H.: Cloud condensation nucleation activity of biomass burning aerosol, *J. Geophys. Res.*, 114, D22205, doi:10.1029/2009JD012353, 2009.

Pöschl, U.: Atmospheric aerosols: Composition, transformation, climate and health effects, *Angewandte Chemie International Edition*, *44*(46), 7520-7540, 2005.

Ramanathan, V., Crutzen, P. J., Kiehl, J. T., & Rosenfeld, D.: Aerosols, climate, and the hydrological cycle, *Science*, *294*(5549), 2119-2124, 2001.

Raymond, T. M. and Pandis, S. N.: Cloud activation ofsingle-component organic aerosol particles, J. Geophys. Res.,107(D24), 4787, doi:10.1029/2002JD002159, 2002.

Reid, J. S., Koppmann, R., Eck, T. F., and Eleuterio, D. P.: A review of biomass burning emissions part II: intensive physical properties of biomass burning particles, *Atmos. Chem. Phys.*, 5, 799– 825, doi:10.5194/acp-5-799-2005, 2005.

Reutter, P., Su, H., Trentmann, J., Simmel, M., Rose, D., Gunthe, S. S., Wernli, H., Andreae, M. O., and Pöschl, U.: Aerosol- and updraft-limited regimes of cloud droplet formation: influence of particle number, size and hygroscopicity on the activation of cloud condensation nuclei (CCN), *Atmos. Chem. Phys.*, 9, 7067– 7080, doi:10.5194/acp-9-7067-2009, 2009.

Roberts, G. C. and Nenes, A.: A continuous-flow streamwise thermal-gradient CCN chamber for atmospheric measurements, *Aerosol Sci. Tech*., 39(3), 206–221, doi:10.1080/027868290913988, 2005.

Rose, D., Gunthe, S. S., Mikhailov, E., Frank, G. P., Dusek, U., Andreae, M. O., and Pöschl, U.: Calibration and measurement uncertainties of a continuous-flow cloud condensation nuclei counter (DMT-CCNC): CCN activation of ammonium sulfate and sodium chloride aerosol particles in theory and experiment, Atmos. Chem. Phys., 8, 1153–1179, doi:10.5194/acp-8-1153-2008, 2008.

Rose, D., Nowak, A., Achtert, P., Wiedensohler, A., Hu, M., Shao, M., and Pöschl, U.: Cloud condensation nuclei in polluted air and biomass burning smoke near the mega-city Guangzhou, China–Part 1: Size-resolved measurements and implications for the modeling of aerosol particle hygroscopicity and CCN activity, *Atmospheric Chemistry and Physics*, *10*(7), 3365-3383, 2010.

Rose, D., Gunthe, S. S., Su, H., Garland, R. M., Yang, H., Berghof, M., and Pöschl, U.: Cloud condensation nuclei in polluted air and biomass burning smoke near the mega-city Guangzhou, China–Part 2: Size-resolved aerosol chemical composition, diurnal cycles, and externally mixed weakly CCN-active soot particles, *Atmospheric Chemistry and Physics*, *11*(6), 2817-2836, 2011.

Schmidt-Ott. A., Baltensperger. U., Gaggeler, H. W., and Jost, D. T.: Scaling behavior of physical parameters describing agglomerates, J.Aerosol Sci., 21(6), 711-717, 1990.

Seaton, A., Godden, D., MacNee, W., and Donaldson, K.: Particulate air pollution and acute health effects, *The Lancet*, *345*(8943), 176-178, 1995.

Shulman, M. L., Jacobson, M. C., Carlson, R. J., Synovec, R. E., and Young, T. E.: Dissolution behavior and surface tension effects of organic compounds in nucleating cloud droplets, Geophys. Res. Lett., 23(3), 277–280, 1996.

van der Werf, G. R., Randerson, J. T., Giglio, L., Collatz, G. J., Kasibhatla, P. S., and Arellano Jr., A. F.: Interannual variability in global biomass burning emissions from 1997 to 2004, *Atmos. Chem. Phys*., 6, 3423-3441, doi:10.5194/acp-6-3423-2006, 2006.

Ward, D.E. and Hao, W.M.: Projections of emissions from burning of biomass for use in studies of global climate and atmospheric chemistry, Proceedings of the 84th Annual Meeting and Exhibition Air & Waste Management Association, Volume 19, 16-21 June 1991, Vancouver, British Colombia, Canada.

Xue, H., Khalizov, A. F., Wang, L., Zheng, J., and Zhang, R.: Effects of coating of dicarboxylic acids on the mass-mobility relationship of soot particles, Environ. Sci. Technol., 43:2787–2792, 2009.

Yokelson, R. J., Crounse, J. D., DeCarlo, P. F., Karl, T., Urbanski, S., Atlas, E., Campos, T., Shinozuka, Y., Kapustin, V., Clarke, A. D., Weinheimer, A., Knapp, D. J., Montzka, D. D., Holloway, J., Weibring, P., Flocke, F., Zheng, W., Toohey, D., Wennberg, P. O., Wiedinmyer, C., Mauldin, L., Fried, A., Richter, D., Walega, J., Jimenez, J. L., Adachi, K., Buseck, P. R., Hall, S. R., and Shetter, R.: Emissions from biomass burning in the Yucatan, *Atmos. Chem. Phys*., 9, 5785–5812, doi:10.5194/acp-9-5785-2009, 2009.

Zhang, R., Khalizov, A.F., Pagels, J., Zhang, D., Xue, H., and McMurry, P.H.: Variability in morphology, hygroscopicity, and optical properties of soot aerosols during atmospheric processing, PNAS, 105(30), 10291-10296, doi:10.1073/pnas.0804860105, 2008.

3.8 Figures

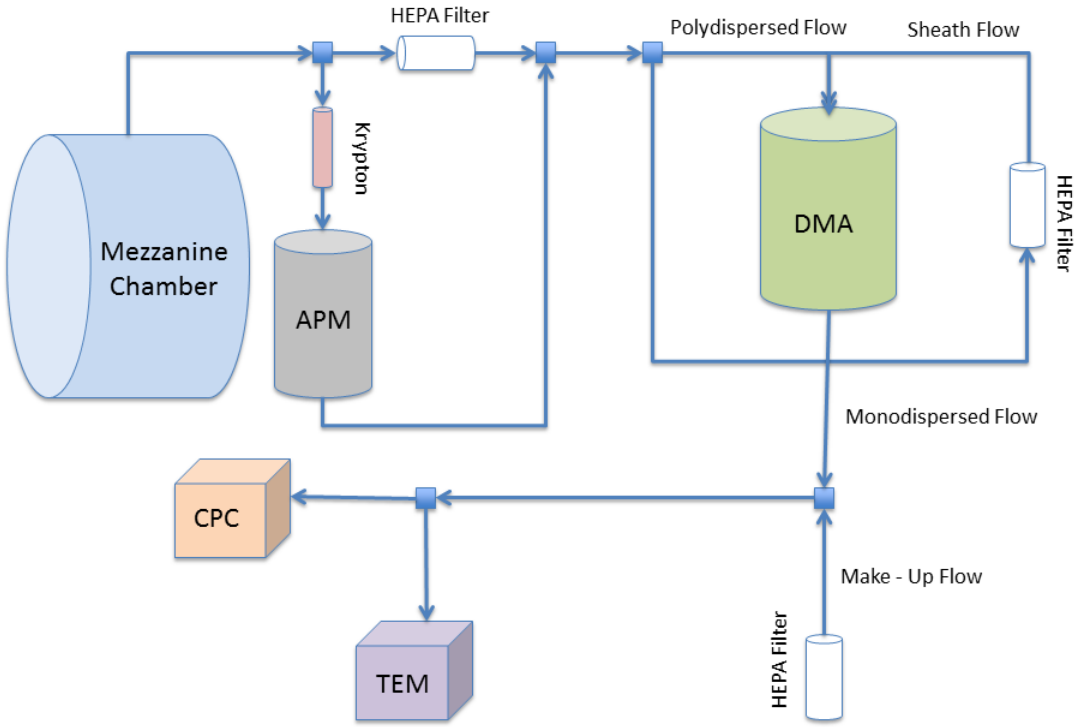

Figure 3.1: Schematic of the APM-DMA-TEM setup.

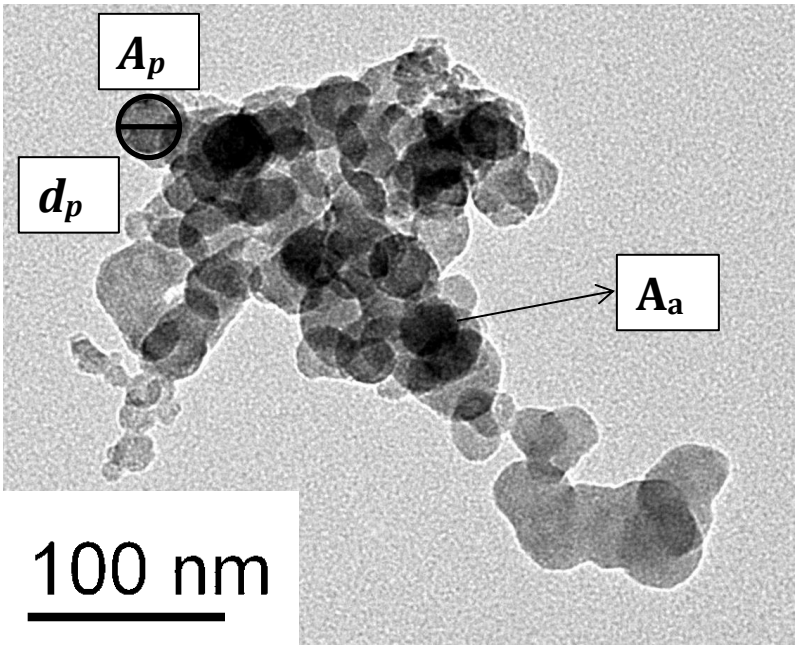

Figure 3.2: The three measured parameters from the TEM pictures used in this study: the primary particle projected area (A_p), primary particle diameter (d_p), and the projected area of the particle (A_a).

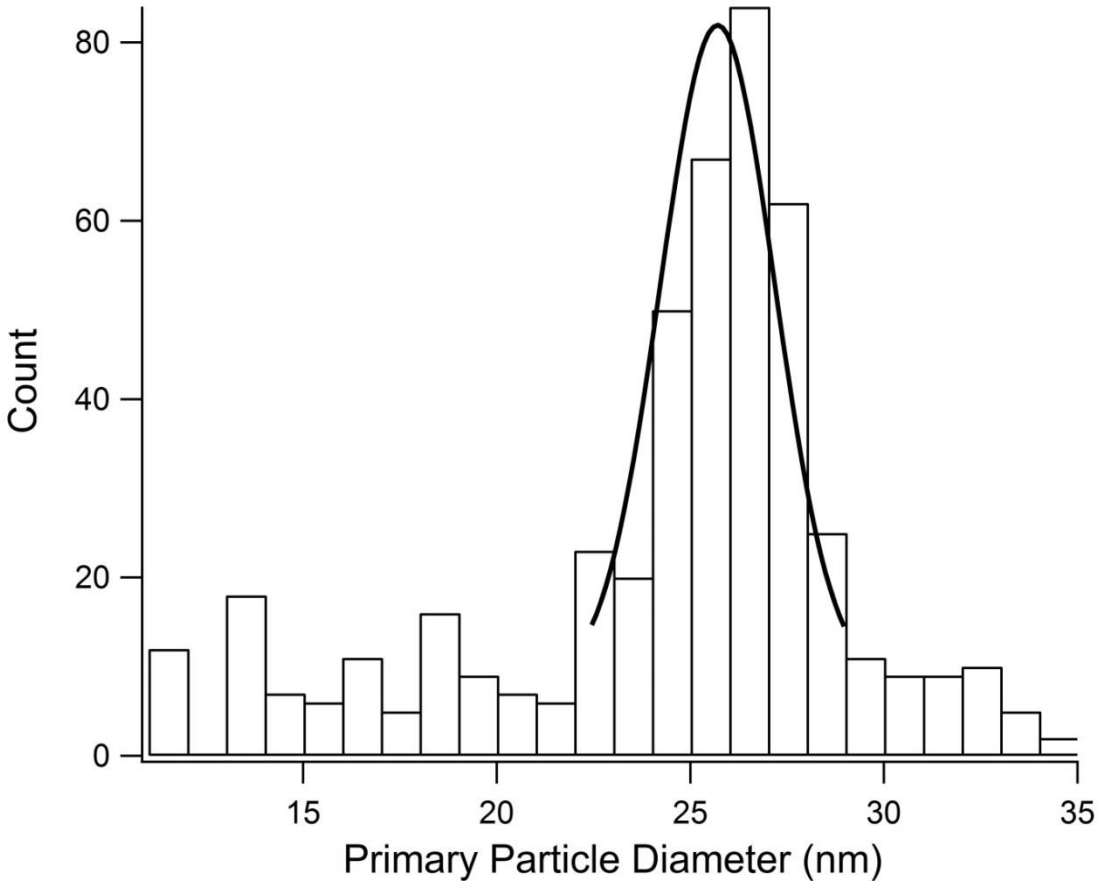

Figure 3.3: TEM analysis of primary particle diameters of agglomerates generated from biomass burning of chamise. Data is fit with a normal Gaussian distribution. The mean of the distribution is 25.7 ± 2.1 nm.

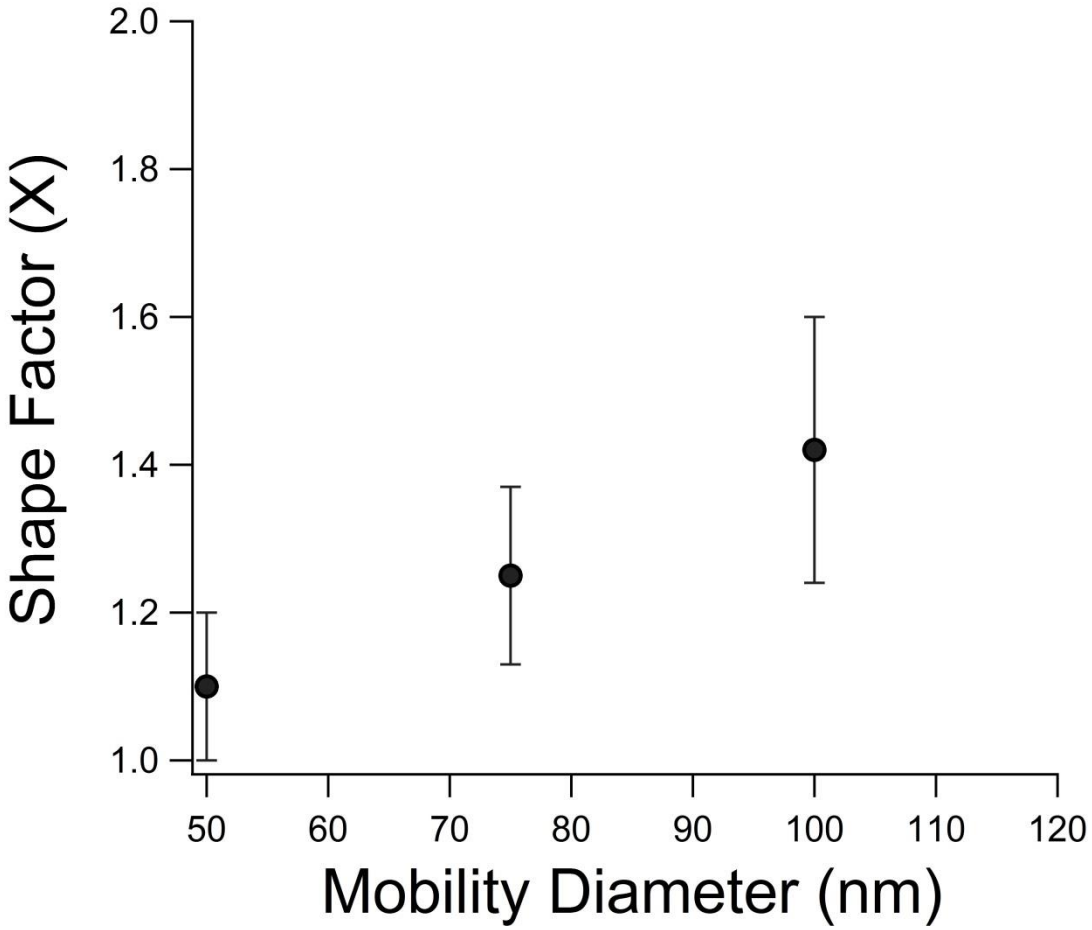

Figure 3.4: Shape factor (χ) vs. the APM selected mobility diameter equivalent for freshly emitted biomass burning aerosol.

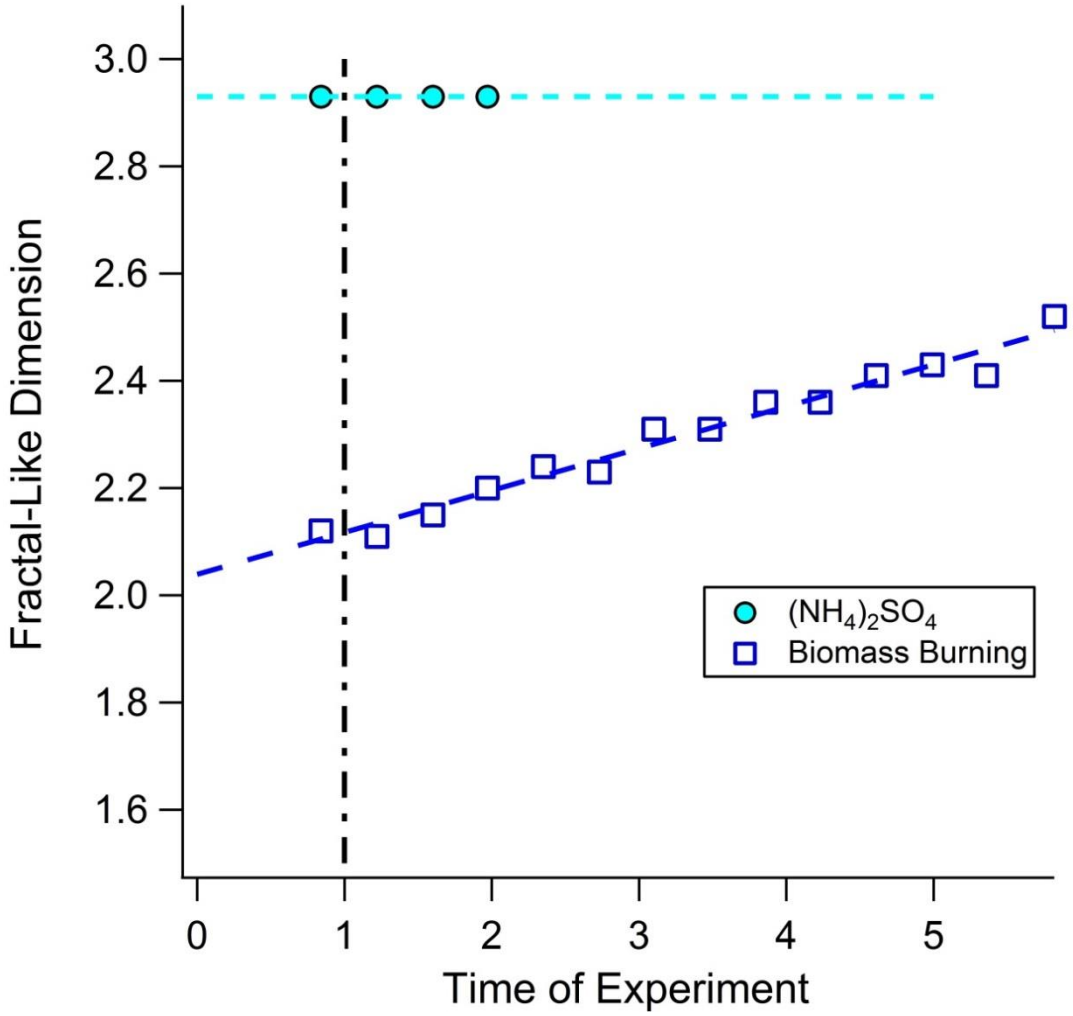

Figure 3.5: APM-SMPS derived fractal-like dimension data vs. time of experiment. A fractal-like dimension of 3 indicates a spherical particle while $D_f < 3$ is non-spherical. Black line indicates time of UV lights being turned on. Ammonium sulfate calibration data is included for comparison.

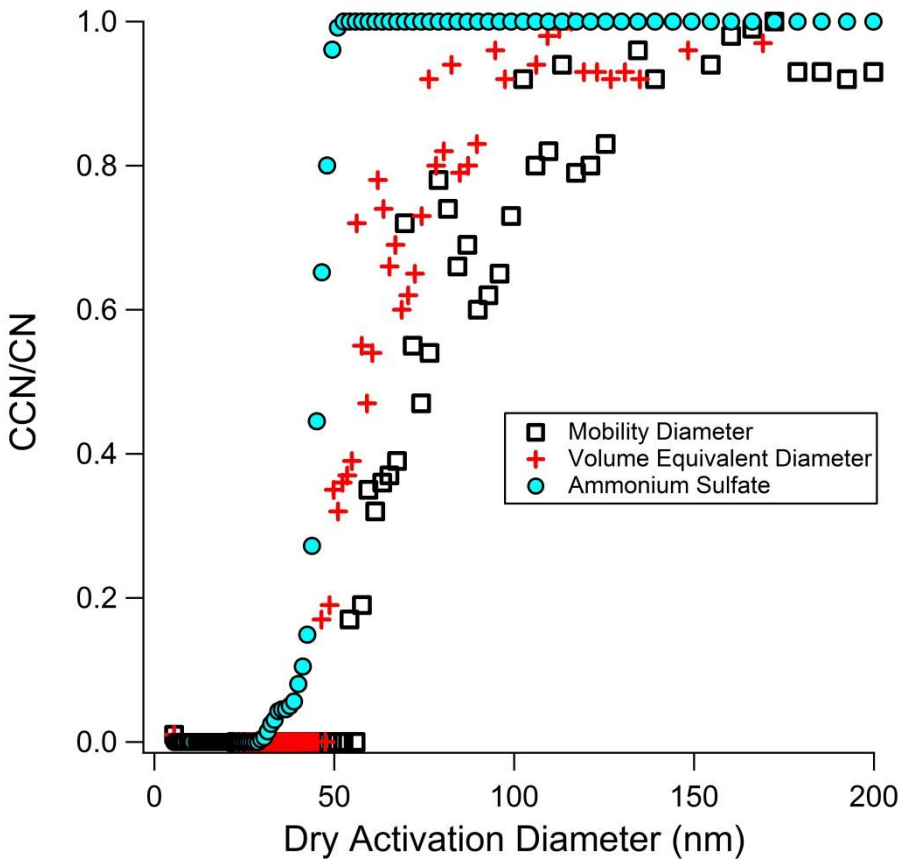

Figure 3.6: Activation curves for manzanita using the mobility diameter and the volume equivalent diameter calculated using the shape factor data from Fig.3. 4. The activation curve of ammonium sulfate is included for comparison. The black squares represent the raw electrical mobility activation diameters and the red crosses are the volume equivalent diameters.

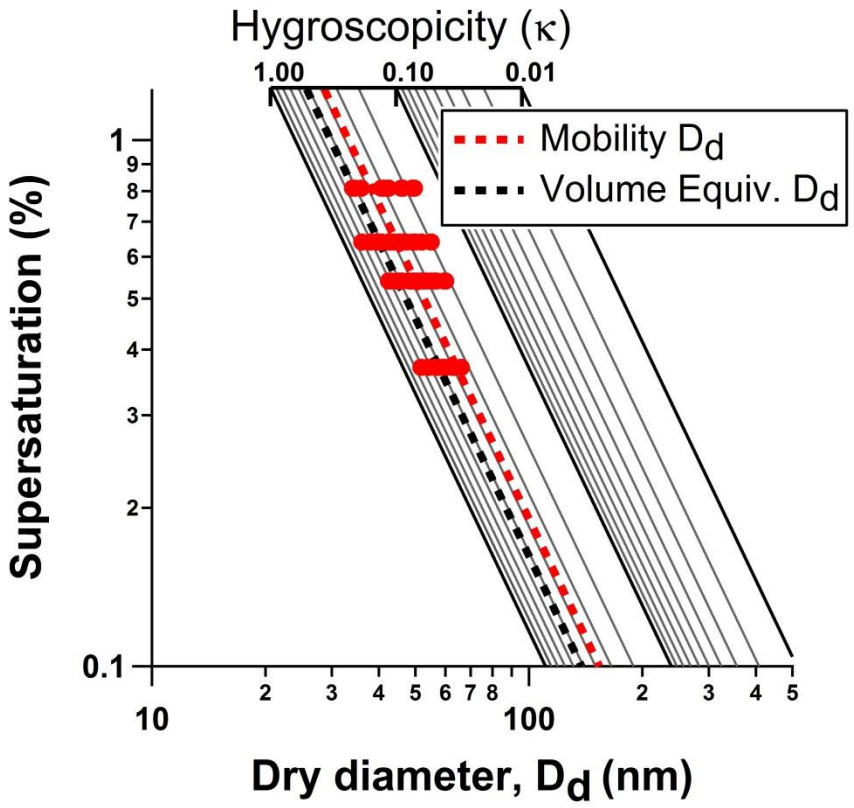

Figure 3.7: Supersaturation vs. the dry activation diameter for one chamise experiment. Markers indicate the data from the SMPS-CCNC and the red line is the best-fit κ between the points. The black line indicates the κ when the volume equivalent diameter is used instead of the mobility diameter.

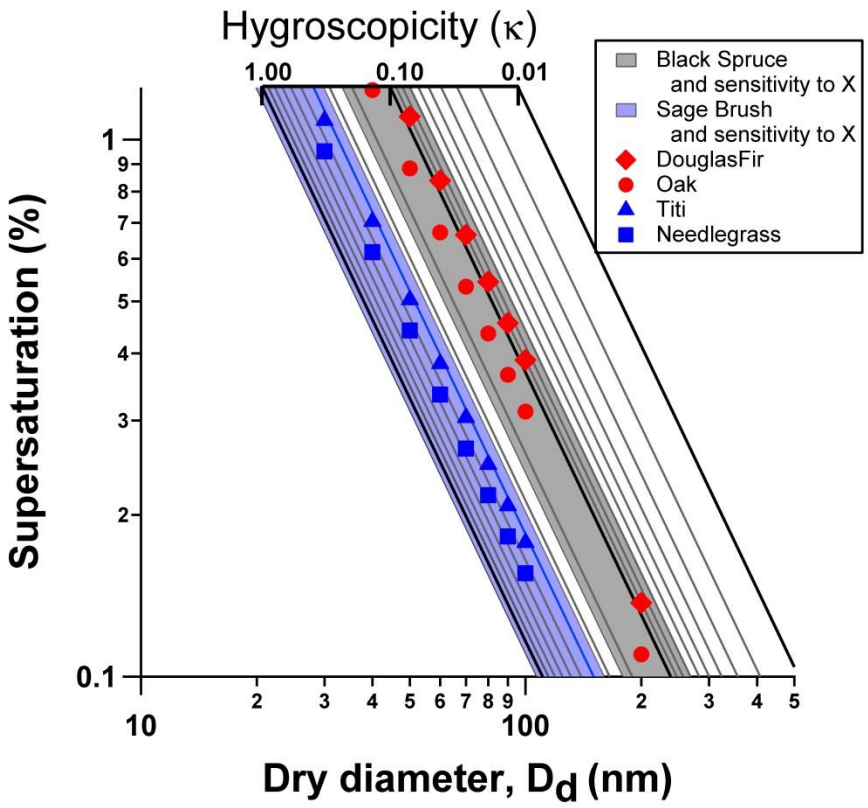

Figure 3.8: Sensitivity analysis of κ to χ. κ data for each biomass burning species is taken from Petters et al. 2009. The sensitivity of κ to χ is analyzed using two constant dynamic shape factors of 1 to 1.5. The region between the two χ values is shaded in grey for black spruce and blue for sage brush. The κ lines for Douglas fir, oak, titi, and needlegrass rush are shown for comparison.

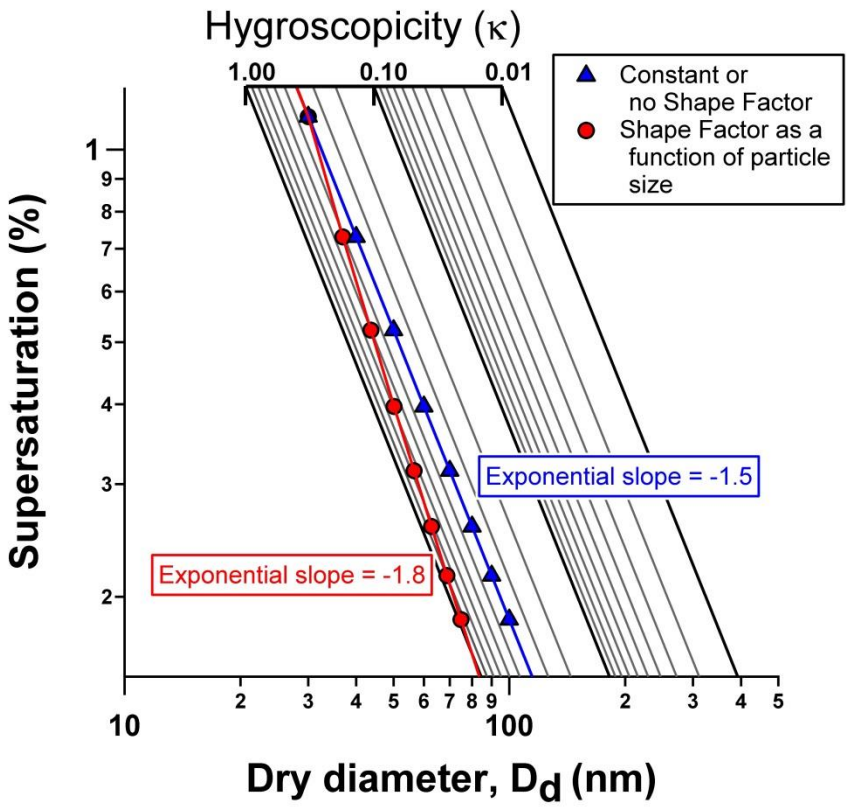

Figure 3.9: Variation of κ-Köhler isolines when applying a constant or no shape factor and applying a shape factor as a function of particle size. The blue triangles have a critical supersaturation that scales with $d_d^{-3/2}$ due to a constant shape factor being applied while the red circles scale with $d_d^{-1.8}$ due to the χ-$d_{mobility}$ relationship from Fig. 3.4 being applied.

3.9 Tables

$D_{mobility}$ (nm)	Number of particles analyzed	Number of primary particles [calculated]	Volume of the total agglomerate [calculated] (nm^3)	D_{VE} (nm)	χ
50	42	6 ± 1	5.5E+04	47 ± 3	1.06 ± 0.1
75	197	12 ± 1	1.1E+05	60 ± 4	1.25 ± 0.1
100	153	20 ± 2	1.8E+05	70 ± 8	1.42 ± 0.18

Table 3.1. The number of particles analyzed from TEM images of the mobility diameters ($D_{mobility}$) of particles selected with the APM-SMPS-TEM system for freshly emitted biomass burning. Eq. 3.6 and 3.7 are used to calculate the volume equivalent diameter (D_{VE}) and shape factor (χ).

3.10 Supplemental Tables

Supersaturation Setting (%)	ΔT (°C)	D_d (nm)	*Supersaturation reported*
0.2	4.6	81.0	0.20%
0.4	7.6	54.81	0.37%
0.6	10.6	42.2	0.54%
0.8	13.6	37.3	0.64%
1.0	16.5	32.05	0.81%

Table 3S.1: $(NH_4)_2SO_4$ DMT CCN Calibration Information for a 0.5 L min^{-1} flowrate

4 Combining surface tension and morphology effects for a holistic view of biomass burning aerosol

4.1 Motivation

The previous two chapters of this dissertation have focused on two of the major assumptions made when using the κ-Köhler hygroscopicity parameterization. Chapter two discusses the assumption that cloud condensation nuclei active aerosols can be parameterized by assuming the droplet has the surface tension of water and that surface tension does not evolve with photochemical aging (Giordano et al., 2013). Chapter three discusses the assumption that the electrical mobility diameter is equivalent to the volume equivalent diameter and is relevant over the atmospheric lifetime of the aerosol (Giordano et al., 2014). The previous chapters have examined these assumptions and their implications separately. This chapter will evaluate what happens when the results from the previous chapters are brought together.

4.2 Theoretical Framework and Methodology

The theoretical framework of CCN ability can be described by classical Köhler theory. An extension of Köhler theory, κ-Köhler, has become a popular method of reporting CCN ability and estimating particle hygroscopicity. The κ-Köhler parameterization of hygroscopicity has an empirical grounding and translates to both the sub- and super-saturated regimes (Petters and Kreidenweis, 2007):

$$\kappa = \frac{4A^3}{27D_d^3 ln^2 s_c} \text{ ; where } A = \frac{4\sigma_{s/a}M_w}{RT\rho_w} \quad (1)$$

where ρ_w is the density of water, M_w is the molecular weight of water, $\sigma_{s/a}$ is the surface tension of the solution/air interface, R is the universal gas constant, T is the temperature, D_d is the dry particle diameter of a volume equivalent sphere, and s_c is the critical supersaturation required to activate a particle with size D_d. D_d usually takes as the measured mobility diameter that is calculated as the 50% efficiency for which half of all particles activate at s_c. κ is interpolated using a linear regression of experimental D_d and calibrated s_c.

Two large assumptions in κ-Köhler theory is that the surface tension of the forming droplet is equal to the surface tension of water and that the diameter term cubed is the volume of the particle. As demonstrated in Chapter 2, the assumption that $\sigma_{s/a}$ is equal to the surface tension of water, 0.072 N m^{-1}, and is treated as a constant is not always valid. Similarly, as discussed in Chapter 3, the assumption that the electrical mobility diameter cubed is a surrogate for the volume of the particle is also not always valid.

The analysis of the data for this Chapter is a combination of the previous two Chapters. First, the dry volume equivalent diameter of an activated particle is calculated via the shape factor/mobility diameter from Figure 3.4 (Fuchs, 1964; Knutson and Whitby, 1975; Baron and Willeke, 2001). The calculated diameter is then applied in Equations 2.3, 2.4, and 2.5 to calculate the surface tension depression at activation of the particle (Szyskowski, 1908; Padró et al., 2007; Petters and Kreidenweis, 2008). Finally, the

volume equivalent diameter and the surface tension are applied in the κ-Köhler equation (Petters and Kreidenweis, 2007).

4.3 Results and Discussion

Figure 4.1 shows the results of applying a constant shape factor correction and a surface tension correction to experimentally observed data. A constant shape factor of 1.2 is applied in the analysis (black line). By applying a constant shape factor, d_d still scales with $d^{3/2}$. The surface tension data (green line) is taken directly from the chamise data of Chapter 2. The shape factor correction changes the activation diameters to smaller sizes than those observed from the DMA/SMPS system and causes κ to shift higher. The surface tension correction forces the κ values to shift lower because of the changes in droplet properties upon activation. The observed κ for this data is 0.3 which shifts to 0.4 when both corrections are taken into account. Taken together, the surface tension decreases the magnitude of impact of the shape factor correction but not enough to imply that the observed κ (red line in the figure) is the "true" κ. The implication here is that current literature still underestimates the hygroscopicity of biomass burning aerosols and thus their importance in the indirect effect. We are still left with a hygroscopicity that falls within the sensitivity range shown in Figure 3.8. As in Figure 3.8, though we are now correcting for two competing effects, there is still a large range that hygroscopicity can fall into.

However, the application of a constant shape factor still does not capture the total picture of the cloud nucleating properties of biomass burning aerosol. Figure 4.2 shows the same analysis as Figure 4.1 but now applying the shape factor/mobility diameter relationship from Figure 3.4. Shown in the figure is the observed κ, a shape factor only corrected κ with the shape factor applied as a function of particle size, and a surface tension and shape factor corrected κ. Because of the shape factor relationship, the exponential factor of κ scales with $d^{-1.8}$ as opposed to $d^{3/2}$. Here, the surface tension correction again decreases the κ by the same amount as in Chapter 2 and Figure 4.1. The implication of these findings is that while the observed hygroscopicity is still underestimating the true hygroscopicity, the estimation may not be that off.

The conclusion that the estimation of the true hygroscopicity may not be too far off is especially true for the photochemically aged system. Figure 4.3 shows how κ is subject to changes with time when both surface tension and morphology are taken into account. The figure includes the observed κ, a surface tension corrected κ, a shape factor corrected κ, and a combination of both corrections. As before, the surface tension correction lowers κ. Here the analysis is applying chamise surface tension data where surface active material increases with photochemical aging. Also as before, the shape factor correction raises κ. The analysis presented here assumes that the shape factor decreases to a value of 1.0 at the same rate as the fractal-like dimension increases to 3.0. When both corrections are applied, the resulting freshly emitted κ is almost 0.1 higher than the observed fresh emission κ. Since 0.1 is a significant change in κ, the analysis confirms that the observed

hygroscopicity is under predicting biomass burning aerosol's cloud forming abilities. However, when both correction are applied, the result is an aged κ value that is only 0.025 higher than the observed aged κ. In terms of hygroscopicity, a difference of 0.025 is negligible. The implication here is that for aged biomass burning aerosol, it is relatively unimportant to take into account either surface tension or morphology effects on hygroscopicity. As long as sufficient time has elapsed for the void space in the aerosol to fill in and create a spherical aerosol, observations of hygroscopicity with a CCNC system will be accurate.

4.4 Conclusions

The analysis presented in this section continues to build on the theme that current estimates for the hygroscopicity of biomass burning ignore crucial components of the system. The combination of the analyses from previous chapters, however, changes the magnitude of the error of current estimation, especially for freshly emitted aerosol. For photochemically aged aerosol, it becomes obvious that the observed hygroscopicity is approximately the true hygroscopicity. The conclusions on the change of the exponential slope are identical to those in Chapter 3 and must be a continued source of inquiry for future biomass burning studies. An important point of this dissertation has been that the observed hygroscopicity may not be an accurate representation of the true hygroscopicity of biomass burning aerosol. The analysis presented here confirms this finding but suggests that for photochemically aged aerosol, the observed hygroscopicity is close enough to the true hygroscopicity that any associated error is negligible. For the error to

be negligible, however, sufficient time in the atmosphere must be allowed so that the aerosol particles can become spherical. The work presented in this dissertation suggests that time period is on the order of more than 4 hours, under realistic atmospheric conditions. The results suggest that biomass burning aerosol is more likely to form a cloud droplet, given that enough water vapor is present, upon being freshly emitted, and less likely with increasing photochemical aging. More observational field studies on when biomass burning plumes form clouds should be conducted to confirm this.

4.5 References

Baron, P. A., Sorensen, C. M., and Brockmann. J. E.: Nonspherical particle measurements: Shape factors, fractals, and fibers. In Aerosol Measurement: Principles. Techniques. and Applications, edited by P. A. Baron and K. Willeke. John Wiley. New York , pp. 705-749, 2001.

Fuchs, N. A.: The Mechanics of aerosols, Pergamon, New York, 1964.

Giordano, M.R., Short, D.Z., Hosseini, S., Lichtenberg, W., and Asa-Awuku, A.: Changes in droplet surface tension affect the observed hygroscopicity of photochemically aged biomass burning aerosol, Env. Sci. & Tech., 47(19), 10980–10986, doi:10.1021/es401867j, 2013.

Giordano, M. R., Espinoza, C., Asa-Awuku, A.: Experimentally measured morphology of biomass burning aerosol and its impacts on CCN ability, Atmos. Chem. Phys. Discuss., 14, 12555-12589, 2014.

Knutson, E.O. and Whitby, K.T.: Aerosol classification by electric mobility: apparatus, theory, and applications, J. Aerosol Sci., 6(6), 443-451, doi: 10.1016/0021-8502(75)90060-9, 1975.

Padró, L. T., Asa-Awuku, A., Morisson, R., and Nenes, A.: Inferring Thermodynamic Properties from CCN Activation Experiments: Single-component and Binary Aerosols, *Atmos. Chem. Phys.*, 7, 5263–5274; DOI 10.5194/acp-7-5263-2007, 2007.

Petters, M. D. and Kreidenweis, S. M.: A single parameter representation of hygroscopic growth and cloud condensation nucleus activity, *Atmos. Chem. Phys.*, 7, 1961–1971, DOI 10.5194/acp-7-1961-2007, 2007.

Petters, M. D. and Kreidenweis, S. M.: A single parameter representation of hygroscopic growth and cloud condensation nucleus activity – part 2: including solubility, *Atmos. Chem. Phys.*, 8, 6273-6279, DOI 10.5194/acp-8-6273-2008, 2008.

Szyskowski, B. V.: Experimentelle studien über kapillare eigenschaften der wässerigen lösungen von fettsauren, *Zeitschrift für Physikalische Chemie*, 64, 385–414, 1908.

4.6 Figures

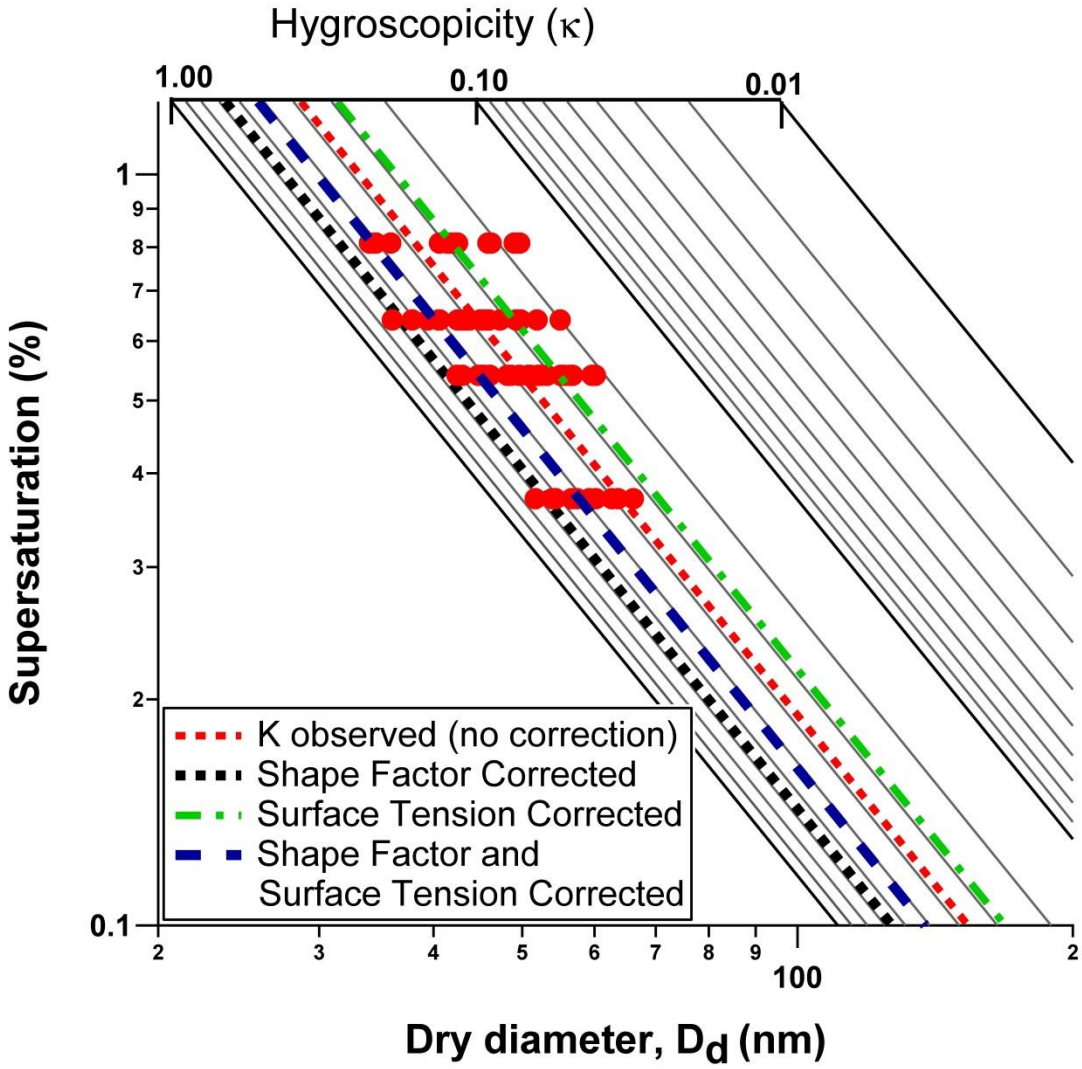

Figure 4.1: Supersaturation versus dry diameter of one set of biomass burning experiments. Shown are the observed activation points (red dots), the observed κ- from those activation points (red line), the results of including surface tension corrections (green line), including a shape factor correction (black line) and combining both corrections (blue line).

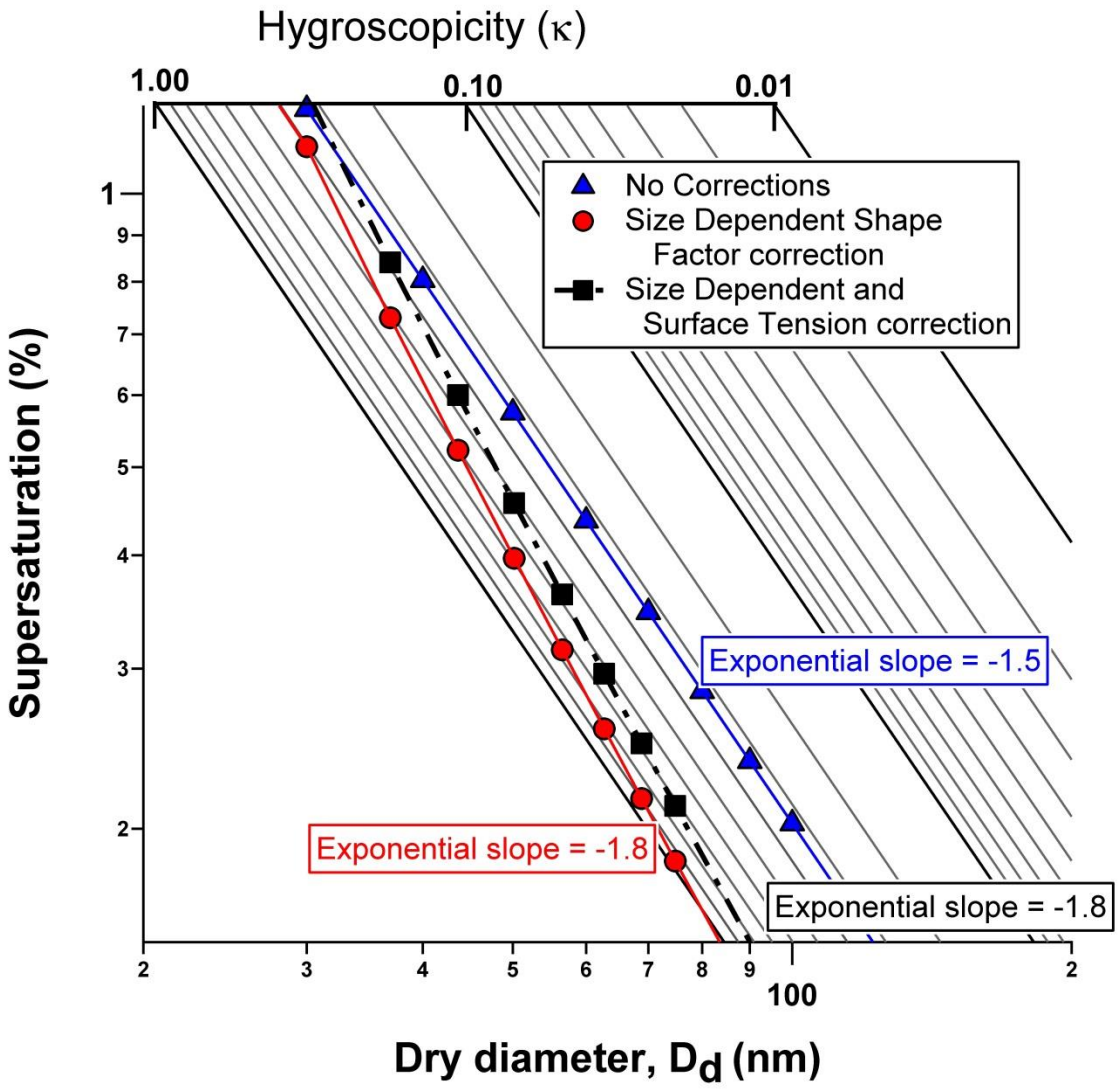

Figure 4.2: Supersaturation versus dry diameter of biomass burning. Shown are the average observed activation points and κ line (blue), the results of applying a shape factor that is a function of particle size (red) and the results of applying surface tension results to size dependent shape factor results (black).

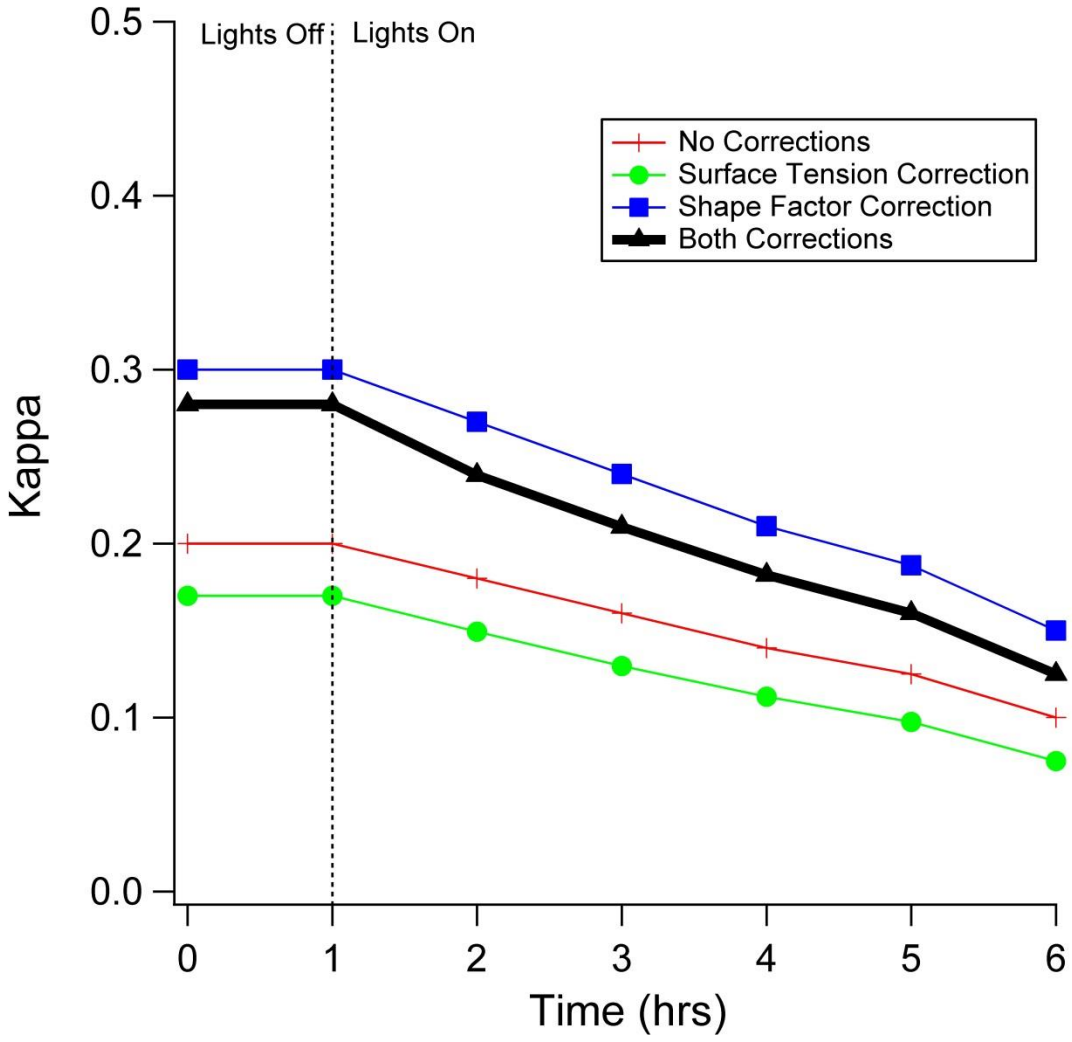

Figure 4.3: Kappa versus photochemical aging. Shown are the observed average κ values (red), surface tension corrected κ values (green), shape factor as a function of time corrected values (blue), and results when both corrections are applied (black).

5 Photochemistry driven light absorbance changes in biomass burning aerosol

5.1 Introduction

The "direct effect" of aerosols, scattering and absorption of shortwave radiation, is one of the largest contributors to the global radiative forcing budget (Forster et al., 2007). Both natural and anthropogenic aerosols can contribute to the direct effect. Aerosol's effects on modulating the radiation budget have been a subject of investigation for a number of years (Charlson et al., 1992; Hansen et al., 1997; Bergstrom and Russel, 1999; Abel et al., 2005; Yu et al., 2006 and references therein). Despite the interest though, absorption and scattering of solar radiation remains the largest source of uncertainty in the overall radiative forcing budget (Forster et al., 2007). Particle scattering and absorption of radiation can result in cooling or warming of the planet since an aerosol's interaction with light is highly dependent on its composition, size distribution, and mixing state. The direct effect of aerosols is thus subject to significant uncertainty (Horvath, 1993; Jacobson, 2001; Yu et al., 2006). The uncertainty is compounded by the fact that aerosol composition can change due to photochemical and mechanical aging in the atmosphere.

One of the largest contributors to the global aerosol budget is biomass burning emissions. Hallquist et al. (2009) estimated that 69% of POA and 23% of SOA, globally, are contributed from biomass burning. With such a high contribution to the total global aerosol load, biomass burning aerosol plays a major role in the atmospheric radiative balance (Penner et al., 1998; Ramanathan et al., 2001). However, the total effect of biomass burning aerosol on the global radiative balance is difficult to constrain. Difficulty constraining the emissions arises from the variability in the properties of the

aerosol, both chemical and physical, between burning events. Biomass burning emissions are sensitive to the species of biomass being burned, the burning conditions upon emission, and the amount of oxidative aging the particles are exposed to (Petters et al, 2009; Carrico et al., 2010; Hennigan et al., 2011; Engelhart et al., 2012; Giordano et al., 2013).

In addition to the wide range of chemical and physical properties biomass burning aerosol can have at emission, these properties can change with the aerosol's lifetime in the atmosphere. Previous work has shown that biomass burning aerosols are highly reactive to photochemical aging and that the timescale for aging is rapid (e.g. Hennigan et al., 2011; Engelhart et al., 2012; Giordano et al., 2013).

Biomass burning aerosol can be primarily separated into two major components: organic carbon (OC) and elemental carbon (EC). EC is characterized as nonvolatile, refractory, and strongly light absorbing (Medalia and Rivin, 1982; Hoffer et al., 2005; Decesari et al., 2006). OC is generally semivolatile and soluble or partially-soluble (Saxena and Hildemann, 1996 and references therein; Bond and Bergstrom, 2006). OC's light absorption characteristics are poorly understood due to the broad composition and concentration regimes that make up OC in ambient aerosols (Jimenez et al., 2009).

With a high global emissions inventory and a variable carbonaceous composition, biomass burning aerosol has been suggested as a nonnegligible contributor to the aerosol

direct effect. The light absorption of biomass burning is pronounced in the ultraviolet (UV) and near-ultraviolet visible wavelengths. 49% of total aerosol light absorption between 300 and 400 nm has been attributed to biomass burning aerosol, as measured by filter-based ambient sampling (Kirchstetter and Thatcher, 2012). The light absorption of BC in biomass burning is proportional to the wavelength of incoming light and is highly absorptive in the near-UV to near-infrared regions of radiation (Moosmuller et al., 2011). The main light-absorbing component of atmospheric aerosols is attributed to BC but the OC component is nonnegligable (Forster et al., 2007).

The OC component of biomass burning is composed of humic-like substances (HULIS), also termed "brown carbon" for the light-absorbing properties of the aerosol (Andreae and Gelenscer, 2006). Hoffer et al. (2006) measured the optical properties of HULIS derived from filter-reconstituted biomass burning aerosol. Hoffer et al.'s work showed that the absorbance of HULIS has a high wavelength dependency. Hoffer et al. calculated that HULIS causes up to 50% of the total light absorption in biomass burning aerosol at 300 nm. Photo-acoustic techniques have estimated that the OC from biomass burning aerosol contributes 27% of the total aerosol absorption at 404 nm (Lack et al., 2012). Chen and Bond (2010) demonstrated that the OC from biomass pyrolysis is more absorptive when pyrolyzed at higher temperatures. In addition to ambient and laboratory measurements of biomass burning aerosol, the optical properties of HULIS have also been measured using HULIS mimics. Dinar et al. (2008) used ambient particles and showed that the HULIS from smoke particles are more absorptive than HULIS from rural

particles. Dinar et al. (2008) also confirmed that HULIS is most absorptive in the UV wavelengths. Del Vecchio and Blough (2004) used Suwanee River Fulvic Acid (SRFA) and Suwanee River Humic Acid (SRHA) which showed high UV absorptivity and demonstrated that the absorption spectra of HULIS cannot be easily parameterized. Despite being primarily responsible for the absorption of OC in the UV wavelengths, HULIS has been shown to be highly effective at scattering light in the visible range (Hoffer et al., 2006).

Recent work by Zhong and Jang (2014) looked at the dynamic light absorption of the total biomass burning aerosol. Their study focused on hickory hardwood logs burned in a wood grill stove. Zhong and Jang attributed the observed changes in biomass burning light absorption to chromophore formation (increasing absorption in the short term) and sunlight bleaching (decreasing absorption in the long term).

Some work has been done regarding the volatility of biomass burning aerosol but the results vary. Maruf Hossain et al. (2012) burned rice straw and reported a VFR (at 100°C) of 0.9 and 0.4 for freshly emitted 49 nm and 116 nm particles from flaming combustion. Leskinen et al. (2007) reported an increase of the volatile fraction (at 360°C) of wood chip combustion aerosol with 24 hours of outdoor chamber aging. Grieshop et al. (2009) reported the opposite trend, using flaming hard- and soft-wood fires, with aging decreasing the volatile fraction. Grieshop et al. reported average mass fractions remaining (at 70°C) of fresh and aged of 0.2 and 0.5, respectively.

This work investigates the photochemical aging of biomass burning aerosol through UV-Visible light absorption and volatility. With limited chemical speciation information, volatility can be used to characterize changes in the semi-volatile aerosol composition. This work demonstrates that changes in the semi-volatile composition can also lead to changes in the organic carbonaceous UV-Vis absorption spectrum.

5.2 Methodology

This series of biomass burning experiments was performed at the University of California, Riverside College of Engineering-Center for Environmental Research and Technology (UCR CE-CERT) Atmospheric Processes Lab (APL). The $12m^3$ Teflon environmental chamber at APL was used for the experiments. Prior to the start of the experiments, the chamber was flushed and filled with filtered air and all instruments were turned on to establish a clean chamber baseline. Two plants common to the California chaparral biome, chamise (*Adenostoma fasciculatum*) and manzanita (*Arctostaphylos glandulosa*), were collected on Bureau of Land Management land near the San Bernardino National Forest (approx. 33.84°, -116.88°) and used as feedstocks. The site is 3600-3900 feet in elevation and chamise, manzanita, scrub oak, and ceanothus surround the area. The feedstocks were burned separately for each experiment in a wood-burning stove. The emissions were drawn from the stack of the wood stove, diluted, and injected into the environmental chamber using an injection system. A flame-integrated modified

combustion efficiency (MCE ≡ $(\Delta CO_2)/(\Delta CO_2+\Delta CO)$) of 0.94-0.99 was obtained for this series of experiments, indicating the burns were conducted in the flaming fire regime (Ward and Hao, 1991). Each experiment reached a targeted 50-100 μg m^{-3} particle concentration to simulate ambient to plume-like concentrations. The concentration was chosen to remain consistent with previous chamber studies (Hennigan et al., 2011; Giordano et al., 2013). The chamber is surrounded by 170 UV lights with peak intensity of 350nm (350 BL, Sylvania). The lights were turned on one hour after injection to promote photochemistry and remained on until the experiment was concluded (Giordano et al., 2013, 2014). This series of experiments lasted 4-5 hours. Seven chamise and five manzanita experiments were conducted.

The Particle-into-Liquid-Sampler - water-soluble organic carbon (PILS-WSOC) system (Weber et al., 2001; Orsini et al., 2003) used in this work is similar to that described in Sullivan et al. (2004). Two additions set apart the setup used here, the use of an SMPS and a UV/Vis spectrophotometer. A schematic of the experimental setup is shown in Figure 5.1. First, an activated carbon denuder strips particles and the sample stream from the chamber of volatile gases. The stripped particles are then flowed into a TSI Differential Mobility Analyzer (DMA) for size selection. The DMA was operated with a 2 lpm mono-disperse flowrate at a total to sheath flowrate ratio of 15:2. A clean air make-up stream provided additional air into the PILS at a flowrate of 14 lpm. The DMA was set to select 100 nm particles for 30 minutes and 200 nm particles for another 30 minutes. 100 and 200 nm were chosen to explore the potential of size-specific absorbance

differences. The size-selected particles are then flown into the PILS which collects the particles into a liquid medium. The PILS uses Millipore water (18.2 mΩ, <5 ppb total organic carbon) as the collection medium. After sample collection by the PILS, the sample is sent through a Waveguide inline UV-Vis spectrophotometer. The spectrophotometer non-destructively measures the absorbance of the liquid stream. UVVis spectroscopy does have limitations such as displacement due to conjugation, substitution, and solvent which can limit the quantitative conclusions that can be drawn from the technique (Lund Myhre and Neilsen, 2004). Concentration is of course also an important factor when considering these spectra.

The liquid stream is then flown into a Sievers WSOC analyzer. The spectrophotometer was blanked with the same Millipore water used in the PILS. The UVVis-WSOC portion of the system was operated first in the on-line method similar to that described in Sullivan et al. (2004) but when clogs were evident in the spectrophotometer, samples were collected from the PILS and stored in photo-chemical resistant HDPE bottles for off-line analysis.

Prior to injection of smoke into the chamber, the PILS system was run for one hour (30 minutes at 100 and 200 nm each) to establish a background of UVVis absorbance and WSOC in the chamber. The established baseline was subtracted from the data for each respective run.

In addition to the PILS-WSOC system, particle measurements were conducted with a homebuilt SMPS and Volatility-Tandem Differential Mobility Analyzer (V-TDMA) (Orsini et al., 1999). The SMPS system measures the total aerosol population and was used to determine the collection efficiency of the DMA-PILS system. Collection efficiency of the PILS system was approx. 60% at both particle diameters. The V-TDMA thermodenuder was set to a temperature of 100°. The V-TDMA was set to select 50, 100, 150, and 200 nm particles for the first DMA and a volume fraction remaining (VFR) calculated from the second DMA (operated in scanning mode). Gas phase emissions were monitored using Teledyne carbon monoxide (CO) and ozone (O_3) analyzers.

5.3 Results

In both fuels, photochemical aging modifies the light-absorbing properties of biomass burning aerosol. Consistent with other work, this study shows that the UV-Vis absorbance of biomass burning aerosol is dependent on particle lifetime in the atmosphere.

An example of the UV-Vis absorption spectra for 100 nm freshly emitted chamise and manzanita are shown in Fig. 5.2. Though only one mobility diameter is shown, both 100 and 200 nm particle mobility diameters exhibit similar absorption spectra. The absorbance for both fuels peaks between 240-250 nm. The absorption trails off at 350-400 nm which is consistent with previous work (Del Vecchio and Blough, 2004; Hoffer

et al., 2006; Chen and Bond, 2010; Kirchstetter and Thatcher, 2012; Zhong and Jang, 2014). Results for all the experimental runs of both fuels are remarkably consistent in both absorption peak shape and peak locations.

Due to the complex nature of biomass burning emissions, multiple explanations for the absorption spectra exist. Work by Hawkins and Russel (2010) showed that the carbonyl and carboxyl functional groups are present in biomass burning aerosol and make up the majority of the FTIR spectra. Fig. 5.2 includes examples of the functional groups responsible for absorption in the UV range of interest here which matches previous work. The weak $n \rightarrow \pi^*$ transition of the carboxylic group has been shown to start at 300nm and exhibit its maximum around 260 nm (Maria and McGlynn, 1972; Back, 1984). Carbonyl groups are known to absorb at ~280nm for the $n \rightarrow \pi^*$ transition. The $\pi \rightarrow \pi^*$ absorption of aromatic compounds occurs between ~230-330 nm depending on the substituents of the benzene rings.

The spectra in Fig. 5.2 show similarities to the various aliphatic dicarboxylic acids (e.g. oxalic acid) UVVis spectra investigated in Lund Myhre and Nielsen (2004). Dicarboxylic acids have previously been identified as a major component in biomass burning emissions through various field campaigns (Narukawa et al., 1999; Falkovitch et al., 2005; Kundu et al., 2010). How influential the primary emission or secondary production of dicarboxylic acids (from species such as ethene, isoprene, methylglyoxal, etc.) is to overall concentrations remains unclear (Warneck, 2003; Ervans et al., 2004; Lim et al.,

2005; Carlton et al., 2007). However, Salo et al.'s (2010) work on the volatility of dicarboxylic acids does not match the volatility of the aerosol measured here as is discussed later. With a difference in volatility, the absorbance similarities indicate biomass burning light absorption is due to a similarity in functional groups in the OC portion of the as opposed to the OC portion being composed of primarily dicarboxylic acids.

It is worth noting that although glyoxal has been found to be a component in the pyrolysis of biomass and has been identified in field measurements of biomass burning influenced air masses, the spectra reported here do not resemble those for glyoxal or methylglyoxal or their secondary organic material (Thamburaj, 2000; Kundu et al., 2010; Shapiro et al., 2009; Sareen et al., 2010). The lack of α-dicarbonyl absorption resemblance may indicate a larger relative concentration of the dicarboxylic acids to the α-dicarbonyls.

Similar to the consistency of freshly emitted UVVis absorption spectra, photochemical aging of the aerosol was also remarkably consistent. Figure 5.3 shows two spectra of chamise aerosol comparing the freshly emitted spectrum versus a 3-hour aged spectrum. The major peak shape and absorbance wavelengths do not change with photochemical aging. Static peak location and shape indicates that the functional groups responsible for the UVVis absorption remain consistent with photochemical aging. Evident in Fig. 3 though, and characteristic of all of the experiments conducted, is an increase in the absolute magnitude of absorbance with photochemical aging. Because absorption is a

function of concentration, an increase in absorption indicates that one of two things is happening: either the concentration of the OC portion of the aerosol is increasing with photochemical aging or the absorbance characteristics of the OC portion are changing with aging. SMPS results (not presented here) do not show any new particle formation events so SOA is likely forming a coating on existing particles.

To elucidate if the concentration or the composition is changing the magnitude of absorbance, Fig. 5.3 includes an inset graph of the scaled absorption coefficient versus time. The inset shows the results from one experiment but results are similar across all experiments conducted. The scaled absorption coefficient is presented as the difference between the absorbance at 365 nm and 700 nm, scaled by the amount of water soluble organic carbon. 365 nm was chosen to avoid interference from non-organic compounds and to be consistent with previously published work (Lukacs et al., 2007; Hecobian et al., 2010). The difference between 365 nm and 700 nm is used to correct for instrument drift and provide a baseline to compare results across an experiment with since no absorption is evident at 700 nm. By scaling the results by the amount of WSOC, the figure removes the possibility that increased concentration of OC is altering the absorption spectra of biomass burning aerosol. Therefore, the OC composition of the aerosol must be evolving with photochemical aging. The result obtained in this work is consistent with Hecobian et al.'s (2010) work on ambient biomass burning aerosol in magnitude of the scaled absorbance coefficient.

To confirm compositional changes in the aerosol, the V-TDMA system was used to monitor the volatility of the particles as they aged. Average VFR results across the conducted chamise experiments (manzanita is similar) are shown in Fig. 5.4 along with the standard deviation. At 100°C, the VFR of the aerosol was always constant when the lights surrounding the chamber were off and always rose when the lights were turned on. The absolute changes in the VFR for each experiment differed due to the complex nature of biomass burning but the VFR generally started at approx. 0.5 and increased to approx. 0.7-0.8 after approx. 4 hours of photochemical aging. Since BC cannot be formed in the chamber, volatility changes must be due to compositional changes in the aerosol OC fraction. The results here are similar to those of Grieshop et al. (2009), at least qualitatively. A quantitative comparison would require an assumption of the densities of the fresh and aged aerosol and is beyond the scope of this text.

Interestingly, the results of our study are remarkably consistent with the volatility results of SOA formation (Kalberer et al., 2004; Baltensperger et al., 2005; Alfarra et al., 2006; An et al., 2007; Qi et al., 2010). VFR data for fresh and aged α-pinene (VFR = 0.5 and 0.65, respectively) and aged trimethylbenzene (VFR = 0.75) at 100°C are included in Fig. 4 for comparison (Baltensperger et al., 2005; Salo et al., 2011).

Figure 5.5 shows how the absorbance coefficient changes with time for two sizes of chamise biomass burning aerosol selected from the SMPS. Results are shown from three different experiments though again results are generally consistent for all experiments

conducted. To place the particle volatility on a comparable scale, the graph is plotted as a percent change of the non-volatile fraction of the aerosol. Since particle volatility started at different VFR's upon emission and ended up at various elevated VFR's, plotting the data using this dimensionless number provides an easy way to compare the general changes in the system. Again, the absorption data is presented as the difference between the absorbance at 365 nm and 700 nm, scaled by the amount of water-soluble organic carbon. Displayed in this manner, the results for separate experiments, despite having varying volatility start and end points, collapse onto each other. This result is significant since it suggests that the UVVis absorbance of biomass burning aerosols is reproducible and internally consistent. Consistency for biomass burning aerosol properties is generally not the case (e.g. hygroscopicity).

Fig. 5.5 shows that as particle volatility decreases, absorbance increases. As can also be seen in the inset of Fig. 5.3, an order of magnitude change in the scaled absorbance is evident for both the 100 nm and 200 nm particles selected by the SMPS. Again, the data suggests that the composition of the biomass burning aerosol is becoming more absorbent with photochemical aging. Becoming more absorbent while simultaneously becoming less volatile suggests that aerosol-phase reactions and kinetics dominate the UVVis absorbance of biomass burning aerosols.

Figure 5.5 implies the formation of chromophores and colored products from the photooxidation of semivolatile organic compounds is occurring with photochemical

aging. Kalberer et al. (2004) proposed that decreasing volatility is due to oligimerization of organic species inside the aerosol. If oligimerization is occurring in our work, then the implication is that the formed polymers enhance the UVVis absorption. Shapiro et al. (2009) observed exactly this increasing absorption with oligimerization of glyoxal products in ammonium sulfate solutions. The volatility and absorption evidence here suggests that the same may occur in biomass burning aerosols that are photochemically aged. The chromophore formation of aging biomass burning aerosol was also seen by Zhong and Jang (2014). However, Zhong and Jang's (2014) observed photobleaching was not seen in this study. This may be due to this experiment not aging the aerosols as long as their study or may be due to above UV wavelengths in ambient sunlight.

5.4 Summary

The photochemical evolution of the light absorbing OC of biomass burning aerosol is presented here. The UVVis light absorbance coefficient is shown to increase with photochemical aging and that the increase is due to compositional changes as opposed to concentration increases. Compositional evolution is shown using a VTDMA, which indicates a rapid decrease in volatility of the aerosol with aging. The work presented here offers a unique insight into the effects of photochemical aging on light absorbance by showing that an aged, nonvolatile biomass burning aerosol is more absorbent than freshly emitted, volatile emission.

5.5 Acknowledgements

Many thanks to David Weise and Joey Chong of the USDA Forest Service for their advice and pivotal role in the acquisition of fuels. Additional thanks go to Dr. Lelia Hawkins and her students at Harvey Mudd College for the use of their instrument. The authors would also like to thank David Cocker and the Keck Foundation for use of the environmental chamber.

5.6 References

Abel, S. J., Highwood, E. J., Haywood, J. M., and Stringer, M.A.: The direct radiative effect of biomass burning aerosols over southern Africa, Atmos. Chem. Phys., 5, 1999–2018, 2005.

Alfarra, M. R., Paulsen, D., Gysel, M., Garforth, A. A., Dommen, J., Prévôt, A. S. H., Worsnop, D. R., Baltensperger, U., and Coe, H.: A mass spectrometric study of secondary organic aerosols formed from the photooxidation of anthropogenic and biogenic precursors in a reaction chamber, Atmos. Chem. Phys., 6, 5279-5293, doi:10.5194/acp-6-5279-2006, 2006.

An, W. J., Pathak, R. K., Lee, B. H., and Pandis, S. N.: Aerosol volatility measurement using an improved thermodenuder: Application to secondary organic aerosol, *Journal of Aerosol Science*, *38*(3), 305-314, 2007.

Andreae, M. O. and Gelencsér, A.: Black carbon or brown carbon? The nature of light-absorbing carbonaceous aerosols, Atmos. Chem. Phys., 6, 3131-3148, doi:10.5194/acp-6-3131-2006, 2006.

Back, R. A.: The ultraviolet absorption spectrum of oxalic acid vapor, Can. J. Chem., 62, 8, 1414–1428, 1984.

Baltensperger, U., Kalberer, M., Dommen, J., Paulsen, D., Alfarra, M. R., Coe, H., Fisseha, R., Gascho, A., Gysel, M., Nyeki, S., Sax, M., Steinbacher, M., Prevot, A.S.H., Sjogren, S., Weingartner, E., and Zenobi, R.: Secondary organic aerosols from anthropogenic and biogenic precursors, *Faraday Discussions*, *130*, 265-278, 2005.

Bergstrom R. W. and Russell, P. B.: Estimation of aerosol direct radiative effects over the mid-latitude North Atlantic from satellite and in-situ measurements, Geophys. Res. Lett., 26, 1731–1734, 1999.

Carlton, A. G., Turpin, B. J., Altieri, K. E., Seitzinger, S., Reff, A., Lim, H.-J., and Erven, B.: Atmospheric oxalic acid and SOA production from glyoxal: Results of aqueous photooxidation experiments, Atmos. Environ., 41, 7588–7602, 2007.

Charlson, R. J., S. E. Schwartz, J. M. Hales, R. D. Cess, J. A. Coakley Jr., J. E. Hansen, and D. J. Hofmann (1992), Climate forcing by anthropogenic aerosols, Science, 255, 423 – 430.

Chen, Y. and Bond, T. C.: Light absorption by organic carbon from wood combustion, Atmos. Chem. Phys., 10, 1773-1787, doi:10.5194/acp-10-1773-2010, 2010.

Hoffer, A., Gelencsér, A., Guyon, P., Kiss, G., Schmid, O., Frank, G. P., Artaxo, P., and Andreae, M. O.: Optical properties of humic-like substances (HULIS) in biomass-burning aerosols, Atmos. Chem. Phys., 6, 3563-3570, doi:10.5194/acp-6-3563-2006, 2006.

Crutzen, P.J. and Andreae, M.O.: Biomass burning in the tropics: impact on atmospheric chemistry and biogeochemical cycles, Science, 250(4988), 1669-1678, 1990.

Decesari, S., Fuzzi, S., Facchini, M. C., et al.: Characterization of the organic composition of aerosols from Rondonia, Brazil, during the LBA-SMOCC 2002 experiment and its representation through model compounds, Atmos. Chem. Phys., 6, 375–402, 2006.

Del Vecchio, R. and Blough, N.V.: On the Origin of the Optical Properties of Humic Substances, *Environmental Science & Technology* , *38* (14), 3885-3891, 2004.

Dinar, E., Rizig, A. A., Spindler, C., Erlick, C., Kiss, G., and Rudich, Y.: The complex refractive index of atmospheric and model humic-like substances (HULIS) retrieved by a cavity ring down aerosol spectrometer (CRD-AS), *Faraday Discussions,* 137, 279-295, 2008.

Ervens, B., Feingold, G., Frost, G, J., and Kreidenweis, S. M.: A modeling study of aqueous production of dicarboxylic acids: 1. Chemical pathways and speciated organic mass production, J. Geophys. Res., 109, D15205, doi:10.1029/2003JD004387, 2004.

Falkovitch, A. H., Graber, E. R., Schkolnik, G., Rudich, Y., Maenhaut,W., and Artaxo, P.: Low molecular weight organic acids in aerosol particles from Rondˆonia, Brazil, during the biomassburning, transition and wet periods, Atmos. Chem. Phys., 5, 781–797, 2005.

Faust, B. C.: Photochemistry of Clouds, Fogs, and Aerosols, *Environmental Science & Technology, 28* (5), 216A-222A, 1994.

Giordano, M.R., Short, D.Z., Hosseini, S., Lichtenberg, W., and Asa-Awuku, A.A. Changes in droplet surface tension affect the observed hygroscopicity of photochemically aged biomass burning aerosol. Env. Sci. & Tech., 47(19), 10980-10986, DOI:10.1021/es401867j. 2013

Giordano, M.R., Espinoza, C., and Asa-Awuku, A.: Experimentally measured morphology of biomass burning aerosol and its impacts on CCN ability, Atmos. Chem. Phys. Discuss., acp-2014-293, 2014.

Grieshop, A. P., Logue, J. M., Donahue, N. M., and Robinson, A. L.: Laboratory investigation of photochemical oxidation of organic aerosol from wood fires 1: measurement and simulation of organic aerosol evolution, Atmos. Chem. Phys., 9, 1263-1277, doi:10.5194/acp-9-1263-2009, 2009.

Hallquist, M., Wenger, J. C., Baltensperger, U., Rudich, Y., Simpson, D., Claeys, M., Dommen, J., Donahue, N. M., George, C., Goldstein, A. H., Hamilton, J. F., Herrmann, H., Hoffmann, T., Iinuma, Y., Jang, M., Jenkin, M. E., Jimenez, J. L., Kiendler-Scharr, A., Maenhaut, W., McFiggans, G., Mentel, Th. F., Monod, A.,

Prévôt, A. S. H., Seinfeld, J. H., Surratt, J. D., Szmigielski, R., and Wildt, J.: The formation, properties and impact of secondary organic aerosol: current and emerging issues, Atmos. Chem. Phys., 9, 5155-5236, doi:10.5194/acp-9-5155-2009, 2009.

Hansen, J.E., Sato, M., and Ruedy, R.: Radiative forcing and climate response, J. Geophys. Res., 102(D6), 6831 – 6864, 1997.

Hecobian, A., Zhang, X., Zheng, M., Frank, N., Edgerton, E. S., & Weber, R. J. (2010). Water-Soluble Organic Aerosol material and the light-absorption characteristics of aqueous extracts measured over the Southeastern United States. *Atmospheric Chemistry and Physics*, *10*(13), 5965-5977.

Hennigan, C. J., Miracolo, M. A., Engelhart, G. J., May, A. A., Presto, A. A., Lee, T., Sullivan, A. P., McMeeking, G. R.; Coe, H., Wold, C. E., Hao, W.-M., Gilman, J. B., Kuster, W. C., de Gouw, J., Schichtel, B. A., Collett, J. L., Kreidenweis, S. M., and Robinson, A. L.: Chemical and physical transformations of organic aerosol from the photo-oxidation of open biomass burning emissions in an environmental chamber. Atmos. Chem. Phys., 11, 7669−7686, DOI: 10.5194/acp-11-7669-2011, 2011.

Horvath, H.: Atmospheric light absorption – A review, Atmos. Environ., 27A, 293–317, 1993.

Jacobson, M. Z.: Strong radiative heating due to the mixing state of black carbon in atmospheric aerosols, Nature, 409, 695–697, 2001.

Jimenez, J. L., Canagaratna, M. R., Donahue, N. M., Prevot, A. S. H., Zhang, Q., Kroll, J. H., DeCarlo, P. F., Allan, J. D., Coe, H., Ng, N. L., Aiken, A. C., Docherty, K. S., Ulbrich, I. M., Grieshop, A. P., Robinson, A. L., Duplissy, J., Smith, J. D., Wilson, K. R., Lanz, V. A., Hueglin, C., Sun, Y. L., Tian, J., Laaksonen, A., Raatikainen, T., Rautiainen, J., Vaattovaara, P., Ehn, M., Kulmala, M., Tomlinson, J. M., Collins, D. R., Cubison, M. J., E., Dunlea, J., Huffman, J. A., Onasch, T. B., Alfarra, M. R., Williams, P. I., Bower, K., Kondo, Y., Schneider, J., Drewnick, F., Borrmann, S., Weimer, S., Demerjian, K., Salcedo, D., Cottrell, L., Griffin, R., Takami, A., Miyoshi, T., Hatakeyama, S., Shimono, A., Sun, J. Y., Zhang, Y. M., Dzepina, K., Kimmel, J. R., Sueper, D., Jayne, J. T., Herndon, S. C., Trimborn, A. M., Williams, L. R., Wood, E. C., Middlebrook, A. M., Kolb, C. E., Baltensperger, U., and Worsnop, D. R.: Evolution of Organic Aerosols in the Atmosphere, Science, 326, 1525–1529, doi:10.1126/science.1180353, 2009.

Kalberer, M., Paulsen, D., Sax, M., Steinbacher, M., Dommen, J., Prevot, A. S. H., Fisseha, R., Weingartner, E., Frankevish, V., Zenobi, R., and Baltensperger, U.: Identification of polymers as major components of atmospheric organic aerosols. *Science*, *303*(5664), 1659-1662, 2004.

Kirchstetter, T. W. and Thatcher, T. L.: Contribution of organic carbon to wood smoke particulate matter absorption of solar radiation, Atmos. Chem. Phys., 12, 6067-6072, doi:10.5194/acp-12-6067-2012, 2012.

Kundu, S., Kawamura, K., Andreae, T. W., Hoffer, A., and Andreae, M. O.: Molecular distributions of dicarboxylic acids, ketocarboxylic acids and α-dicarbonyls in biomass burning aerosols: implications for photochemical production and degradation in smoke layers, Atmos. Chem. Phys., 10, 2209-2225, doi:10.5194/acp-10-2209-2010, 2010.

Lack, D. A., Langridge, J. M., Bahreini, R., Cappa, C. D., Mid dlebrook,A. M., and Schwarz, J. P.: Brown carbon and internal mixing in biomass burning particles, P. Natl. Acad. Sci., 109,14802–14807, doi:10.1073/pnas.1206575109, 2012.

Leskinen, A. P., Jokiniemi, J. K., and Lehtinen, K. E.: Characterization of aging wood chip combustion aerosol in an environmental chamber, *Atmospheric Environment*, *41*(17), 3713-3721, 2007.

Lim, H.-J., Carlton, A. G., and Turpin, B. J.: Isoprene Forms Secondary Organic Aerosol through Cloud Processing: Model Simulations, Environ. Sci. Technol., 39, 4441–4446, doi:10.1021/es048039h, 2005.

Lund Myhre, C.E. & Nielsen, C.J. Optical properties in the UV and visible spectral region of organic acids relevant to tropospheric aerosols. Atmos. Chem. Phys., 4, 1759-1769, 2004.

Maria, H. J. and McGlynn, S. P.: Electronic states of oxalic acid and dimethyloxalate. Absorption studies, J. Mol. Spectr., 42, 1, 177–196, 1972.

Maruf Hossain, A. M. M., Park, S., Kim, J. S., and Park, K.: Volatility and mixing states of ultrafine particles from biomass burning, *Journal of Hazardous materials*, *205*, 189-197, 2012.

Medalia, A. I. and Rivin, D.: Particulate carbon and other components of soot and carbon black, Carbon, 20, 481–492, 1982.

Moosmüller, H., Chakrabarty, R. K., Ehlers, K. M., and Arnott, W. P.: Absorption Ångström coefficient, brown carbon, and aerosols: basic concepts, bulk matter, and spherical particles, Atmos. Chem. Phys., 11, 1217-1225, doi:10.5194/acp-11-1217-2011, 2011.

Narukawa, M., Kawamura, K., Takeuchi, N., and Nakajima, T.: Distribution of dicarboxylic acids and carbon isotopic compositions in aerosols from 1997 Indonesian forest fires, Geophys. Res. Lett., 26(20), 3101–3104, 1999.

Orsini, D. A., A. Wiedensohler, F. Stratmann, D. S. Covert: A New Volatility Tandem Differential Mobility Analyzer to Measure the Volatile Sulfuric Acid Aerosol Fraction. *J.*

Atmos. Oceanic Technol., 16, 760–772, doi: http://dx.doi.org/10.1175/1520-0426(1999)016<0760:ANVTDM>2.0.CO;2, 1999.

Penner, J.E., Chuang, C.C., Grant, K. Climate forcing by carbonaceous and sulfate aerosols. Climate Dynamics, 1998, 14(12), 839-851.

Ramanathan, V., Crutzen, P.J., Kiehl, J.T., Rosenfeld, D. Aerosols, Climate, and the Hydrological Cycle, Science, 294 (5549), 2119-2124, 2001.

Reid, J. S., Eck, T. F., Christopher, S. A., Koppmann, R., Dubovik, O., Eleuterio, D. P., and Zhang, J.: A review of biomass burning emissions part III: intensive optical properties of biomass burning particles. *Atmospheric Chemistry and Physics*, *5*(3), 827-849, 2005.

Salo, K., Hallquist, M., Jonsson, Å. M., Saathoff, H., Naumann, K.-H., Spindler, C., Tillmann, R., Fuchs, H., Bohn, B., Rubach, F., Mentel, Th. F., Müller, L., Reinnig, M., Hoffmann, T., and Donahue, N. M.: Volatility of secondary organic aerosol during OH radical induced ageing, Atmos. Chem. Phys., 11, 11055-11067, doi:10.5194/acp-11-11055-2011, 2011.

Sareen, N., Schwier, A. N., Shapiro, E. L., Mitroo, D., and McNeill, V. F.: Secondary organic material formed by methylglyoxal in aqueous aerosol mimics. *Atmospheric Chemistry and Physics*, *10*(3), 997-1016, 2010.

Saxena, P. and Hildemann, L. M.: Water-soluble organics in atmospheric particles: a critical review of the literature and application of thermodynamics to identify candidate compounds, J. Atmos. Chem., 24, 1, 57–109, 1996.

Shapiro, E. L., Szprengiel, J., Sareen, N., Jen, C. N., Giordano, M. R., and McNeill, V. F.: Light-absorbing secondary organic material formed by glyoxal in aqueous aerosol mimics. *Atmospheric Chemistry and Physics*, *9*(7), 2289-2300, 2009.

Sullivan, A. P., R. J. Weber, A. L. Clements, J. R. Turner, M. S. Bae, and J. J. Schauer (2004), A method for on-line measurement of water-soluble organic carbon in ambient aerosol particles: Results from an urban site, Geophys. Res. Lett., 31, L13105, doi:10.1029/ 2004GL019681.

Thamburaj, R.: Fast pyrolysis of biomass for green power generation, paper presented at First World Conference on Biomass for Energy and Industry, Energia TA, Seville, Spain, 2000.

Ward, D. E.; Hao, W. M. Projections of emissions from burning of biomass for use in studies of global climate and atmospheric chemistry. Proceedings of the 84th Annual Meeting and Exhibition Air and Waste Management Association, Vancouver, British Colombia, Canada, June 16−21, 1991; Vol. 19.

Warneck, P.: In-cloud chemistry opens pathway to the formation of oxalic acid in the marine atmosphere, Atmos. Environ., 37, 2423–2427, 2003.

Watson, J.G., Chow, J.C., and Antony Chen, L.-W.: Summary of organic and elemental carbon/black carbon analysis methods and intercomparisons, Aerosol and Air Quality Research, 5(1), 65-102, 2005.

Yu, H., Kaufman, Y. J., Chin, M., Feingold, G., Remer, L. A., Anderson, T. L., Balkanski, Y., Bellouin, N., Boucher, O., Christopher, S., DeCola, P., Kahn, R., Koch, D., Loeb, N., Reddy, M. S., Schulz, M., Takemura, T., and Zhou, M.: A review of measurement-based assessments of the aerosol direct radiative effect and forcing, Atmos. Chem. Phys., 6, 613-666, doi:10.5194/acp-6-613-2006, 2006.

5.7 Figures

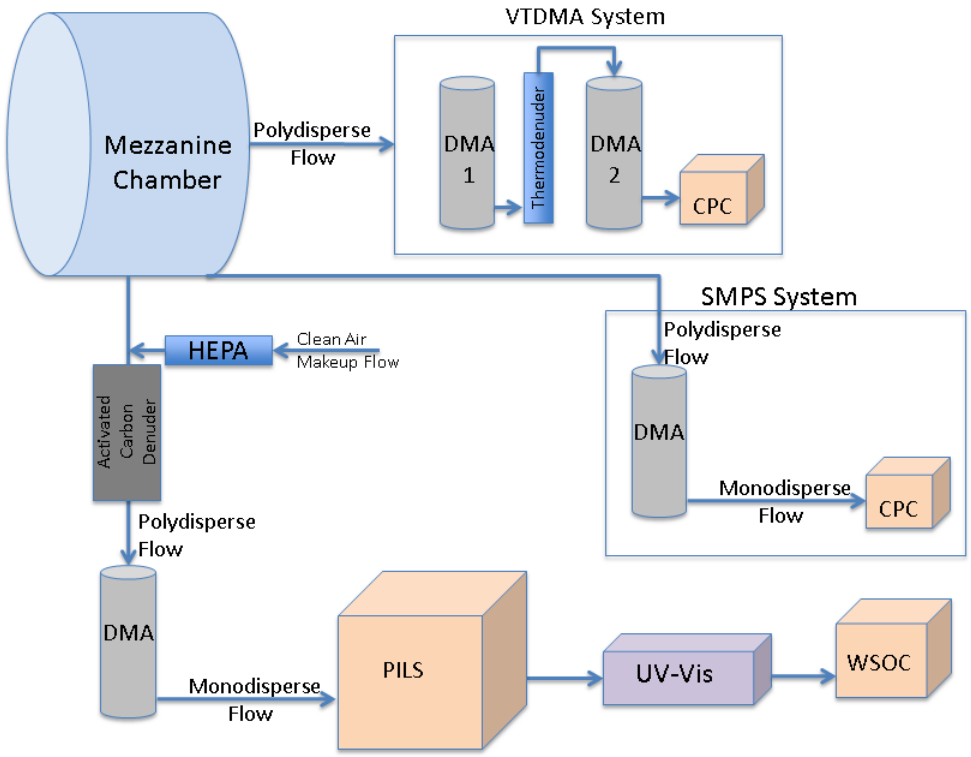

Figure 5.1: Schematic of the experimental setup.

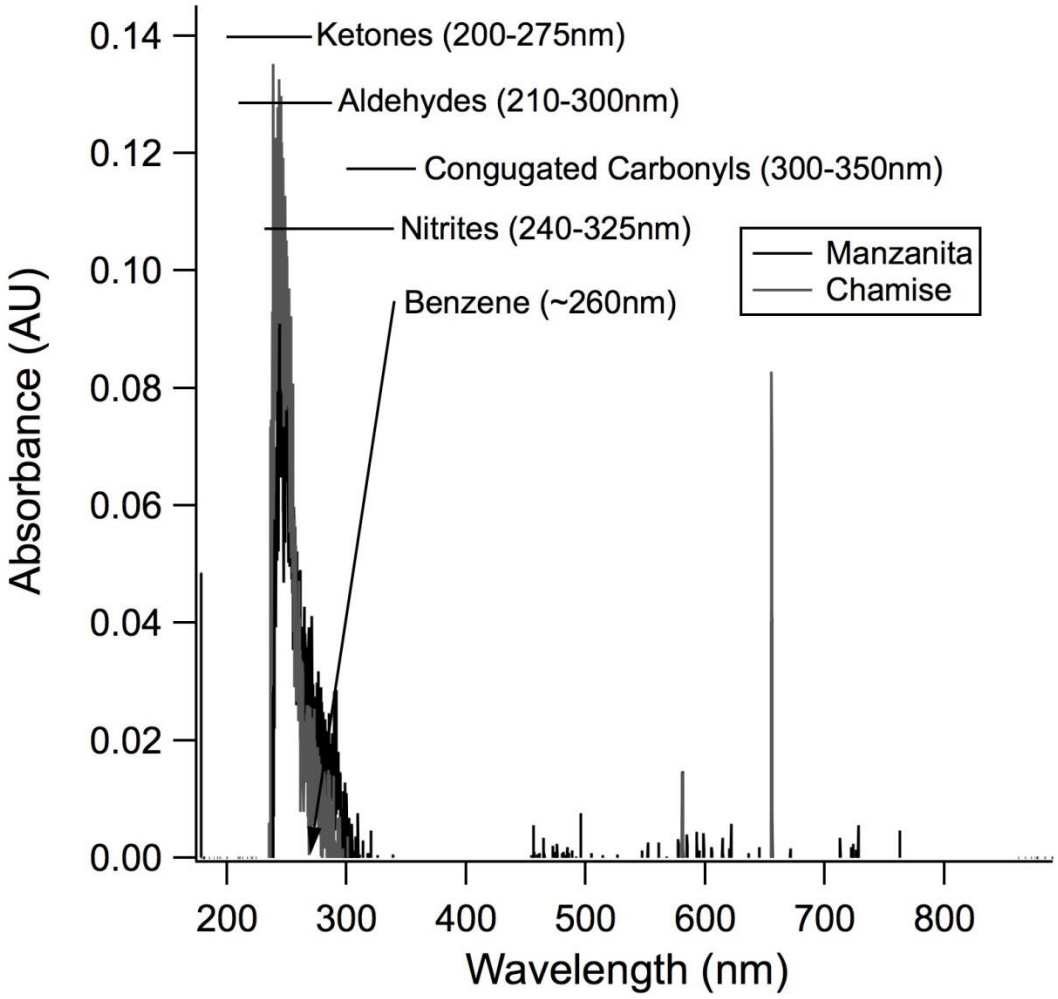

Figure 5.2: Characteristic absorbance spectra for freshly emitted manzanita and chamise biomass burning aerosol. Manzanita (black) and chamise (grey) show similar absorbance peaks and shapes. Characteristic absorbance bands for various functional groups are included for comparison.

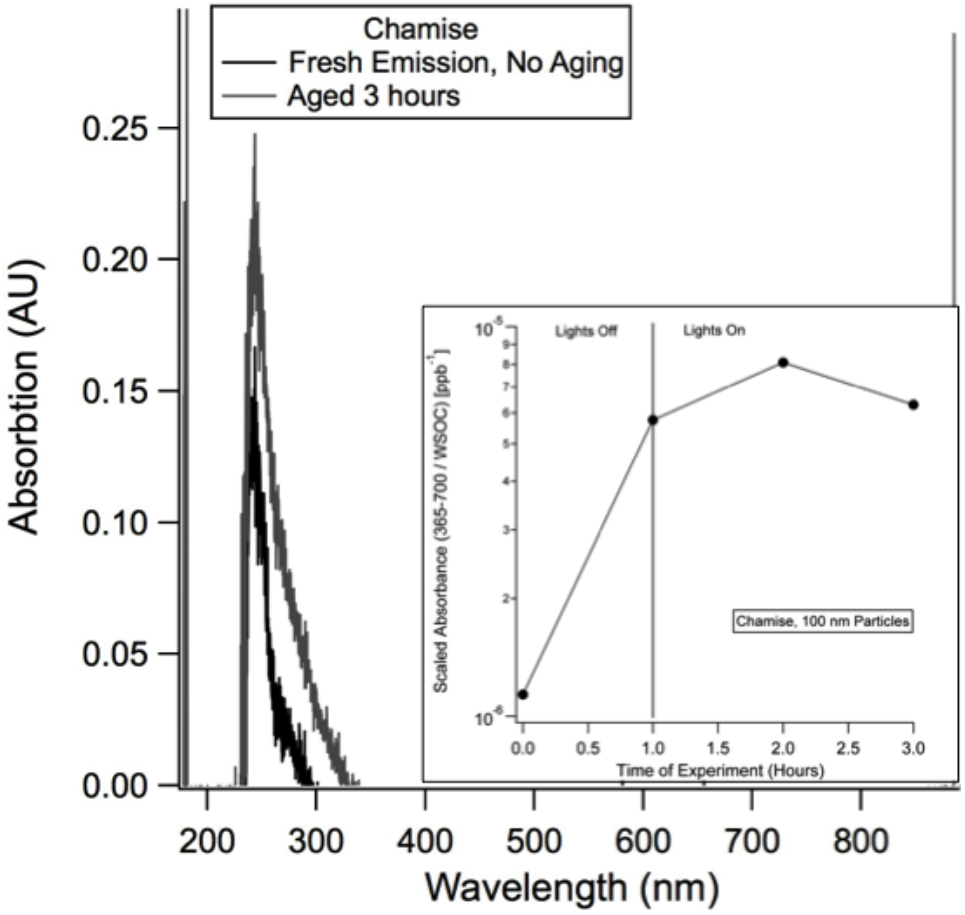

Figure 5.3: Example of changes of the UVVis absorbance of biomass burning aerosol with photochemical aging. 100 nm particles of chamise is shown in the figure. The inset graph shows how the scaled absorbance coefficient changes with photochemical aging of the same aerosol in the main part of the figure.

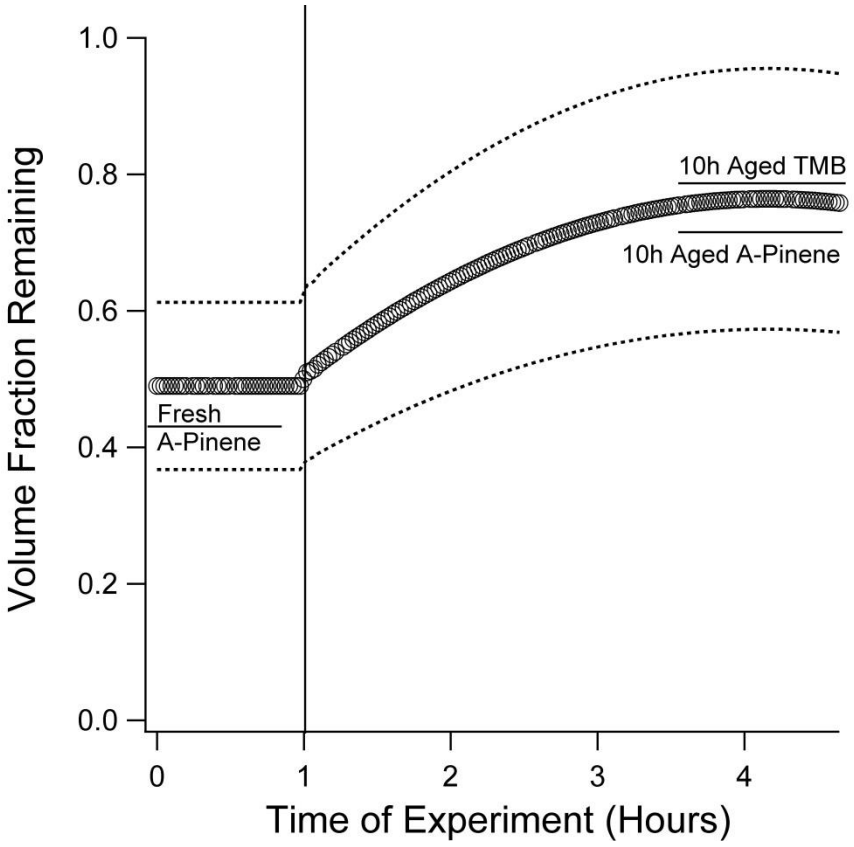

Figure 5.4: Average Volume Fraction Remaining as a function of time of the biomass burning experiments conducted. Dotted lines represent the standard deviation of the data. Lights surrounding the chamber were turned on at 1 hour as indicated by the line in the figure. SOA from Trimethylbenzene (TMB) and α-pinene at 100°C are shown for comparison (Baltensperger et al., 2005; Salo et al., 2011).

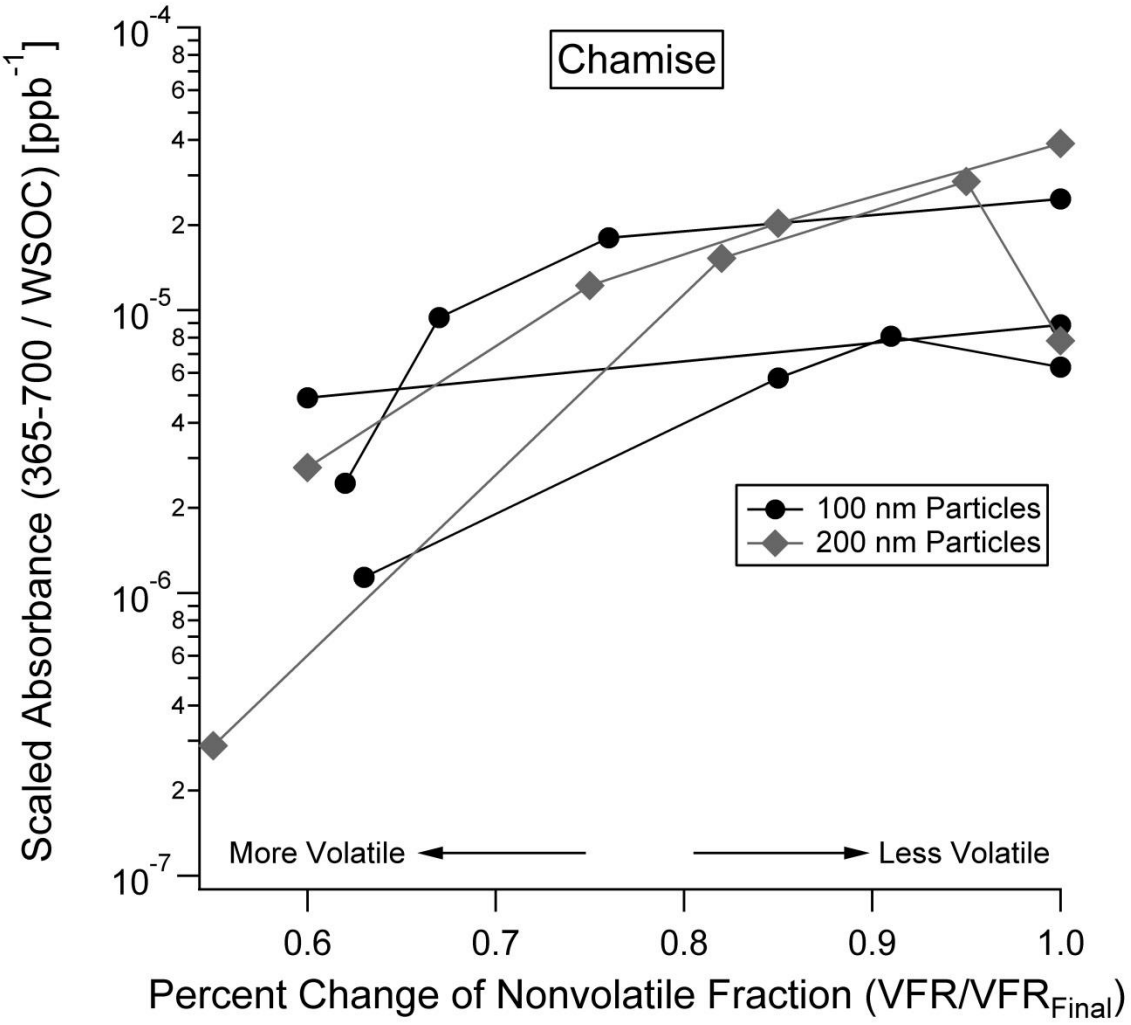

Figure 5.5: Scaled absorbance of chamise biomass burning aerosol against the percent change of the non-volatile fraction of the aerosol for two different aerosol particle sizes. The absorbance is shown as the difference between 365 nm and 700 nm to correct for instrument drift and scaled by the total amount of water soluble organic carbon in the aerosol sample. The percent change of the non-volatile fraction is written as a dimensionless number to allow comparison between experiments. Each line connecting points represents one experiment.

6 How growing conditions effect biomass burning emissions: the effects of chronic nitrogen deposition on combustion aerosol emissions

6.1 Introduction

Aerosols play a major role in the earth's climate system. Aerosols can have health effects on humans and local ecosystems, can affect regional visibility, and have a large impact on the earth's radiative forcing balance (Forster et al., 2007). One major source of aerosol and trace gases to the atmosphere is biomass burning (Crutzen and Andreae, 1990; Ramanathan et al., 2001; van der Werf, 2006; Akagi 2011). Biomass burning emits a complex mixture of gases and aerosol. Emissions can vary in both composition and amount depending on a number of factors. Previous work has shown that the biomass species being burned, composition and moisture of the fuel, packing ratio of the fire, and the fire regime (e.g. flaming, smoldering, or mixed phase) all affect the emissions properties of biomass burning (Andreae and Merlet, 2001; Petters et al., 2009; Thonicke et al., 2010; Hosseini et al., 2013). Additionally, photochemical aging of biomass burning emissions has been shown to effect aerosol properties such as hygroscopicity, light absorption, surface activity, and morphology (Hennigan et al., 2011; Engelhart et al., 2012; Giordano et al., 2013; Giordano et al., 2014; Zhong and Jang, 2014). Because of the sheer number of factors that can affect emissions, constraining the climate impact of biomass burning remains difficult.

One factor that has not been studied with regards to biomass burning emissions is the local air quality of biomass growth sites. The San Bernardino Mountains, located east of

Los Angeles, California, are situated on a gradient of elevated ozone and nitrogenous pollutants and offer an opportunity for such a study. The area is subject to oxidant and particulate air pollution from the Los Angeles air basin and has been of particular interest to plant and forest health researchers for over 50 years (Cobb and Stark, 1970; Miller 1973; Fenn and Bytnerowicz, 1993; Grulke et al., 1998). The pollution gradients over the mountains decrease from west to east (as the distance from Los Angeles increases) and have been well characterized (Miller et al., 1986; Grulke et al., 1998). Increased air pollution, oxidant exposure, and nitrogen deposition rates in the area have been shown to negatively affect the health of the mixed conifer forest that covers the area (McBride et al., 1975; Pronos et al., 1978; Fenn et al., 1996; Miller et al., 1996; Grulke et al., 1998).

When considering biomass burning events in forested areas, the forest floor is a crucial component of the events. On the forest floor, plant detritus collects and forms the basis for nutrient cycles within the forest. Soil science generally classifies the detritus in various layers based on the decomposition and depth of the organic material. The topmost layer is referred to as the L-layer and is characterized by relatively undecomposed material (Schaetzl and Anderson, 2005). Due to the limited decomposition, this layer is still able to play a large role in burning events (Kauffman et al., 1995).

The objective of this study is to determine what, if any, effect local air quality has on the emissions from biomass burning events. Recently fallen plant material from a polluted and a clean site is burned and injected into an environmental chamber. Aerosol and gas-

phase properties are monitored both at fresh emission and during photochemical aging and the impacts of local air quality on the emissions is discussed.

6.2 Experimental Methods

6.2.1 Fuel collection locations

Biomass samples were collected from two sites in southern California. Both sites are located in the San Bernardino National Forest. The San Bernardino National Forest vegetation is composed primarily of mixed conifer forest. Pine, fir, incense cedar, and black oak dominate the landscape. Two sites along a known pollution gradient were chosen for biomass collection: a polluted site and a clean site. The polluted site is located on the western edge of the mountains, closer to Los Angeles. The clean site is situated east of the polluted site in the heart of the mountain range. The pollution gradient exists due to local topography and prevailing air mass movement patterns.

The polluted site, with a high nitrogen deposition rate, is located near Camp Paivika at N34 14.477 W117 19.570 (WGS84 datum). Previous work has estimated the nitrogen deposition rate of the site to be 45 kg N ha^{-1} and an average ozone concentration of 0.09 ppm-h (Allen et al., 1998; Grulke et al., 1998). The clean site is located near Jenks Lake and Camp Osceola at N34 09.573 W116 52.699 (WGS84 datum). The total nitrogen deposition rate is unavailable for the Camp Osceola but literature supports the site being cleaner than Camp Paivika. Lower average ozone concentration (0.07 ppm-h) and lower

deposition rates and atmospheric concentrations of species such as NH_4^+, SO_4^{2-}, NO_3^-, and HNO_3 have been observed at Camp Osceola (Fenn and Bytnerowicz, 1993; Grulke et al., 1998).

6.2.2 Fuel type description

Samples of vegetation from the topmost litter-layer, the L-layer, were collected from both collection sites with assistance from USDA Forest Service employees. The forest litter was collected from locations away from main roads and a minimum of 5 m away from secondary roads to avoid pollution from vehicles that use the roads. The samples were collected by hand and stored in clean plastic containers. Due to the vegetation in both collection areas, the samples were primarily composed of conifer needles. Special attention was paid to exclude materials such as conifer cones and branches. The fuels were then delivered to CE-CERT and stored in their containers at ambient conditions until burned. The time from collection to conducting the burns was less than 3 weeks.

6.2.3 Environmental Chamber and Experimental Setup

A series of six total experiments, three on polluted and three on clean fuels, were conducted at the Atmospheric Processes Lab at the University of California, Riverside College of Engineering – Center for Environmental Research and Technology (UCR CE-CERT). Prior to an experiment, the chamber was flushed and filled with filtered air. 100 grams of a fuel were measured and burned in the wood-burning stove outside of the lab.

Smoke from the burns was diluted and injected into the $12m^3$ Teflon chamber through a Venturi tube injection system. The smoke was injected with a 10:1 total flow to sample flow ratio through as short of a copper transfer line as possible (approximately 7m in length). The injection was completed when the fuel had burned itself out and the remaining ash was collected and weighed. 100 grams was chosen because it yielded a final particle concentration into the chamber of 50-100 $\mu g\ m^{-3}$ which is within range of ambient and plume-like biomass burning conditions (Hennigan et al., 2011). The Teflon chamber is surrounded by ultraviolet lights with peak intensity of 350 nm (350 BL, Sylvania) which were turned on approximately 1 hour after the injection was completed. Each experiment was operated until the chamber was empty (generally 5-6 hours). A flame-integrated modified combustion efficiency ($MCE \equiv (\Delta CO_2)/(\Delta CO_2+\Delta CO)$) of 0.85-0.91 was obtained for this series of experiments, indicating the burns were conducted in the smoldering and mixed phase fire regimes (Ward and Radke, 1993). Due to instrument limitations, flame temperature was not monitored or controlled for during these experiments.

Instrumentation used for this set of experiments included both gas-phase and aerosol phase measurements. Gas-phase monitoring included Teledyne carbon monoxide (CO), ozone (O_3), and NO_x/NO analyzers as well as a Licor carbon dioxide (CO_2) analyzer. Aerosol-phase measurements included particle size distributions with a scanning mobility particle sizer (SMPS, TSI 3080/3081), particle mass measurements with an aerosol particle mass analyzer (APM, Kanomax), and particle volatility with a homebuilt

volatility-tandem differential mobility (V-TDMA) analyzer (Wang and Flagan, 1990; Orsini et al., 1999; McMurry et al. 2002). The V-TDMA thermodenuder was set to a temperature of 100°C. The V-TDMA was set to select 50, 100, 150, and 200 nm particles for the first DMA and a volume fraction remaining (VFR) calculated from the second DMA operated in scanning mode.

The APM system used here is the AMP-DMA system described in Malloy et al. (2009). The system selected 5 different particle masses in the 50-200 nm particle size range. The effective density of the aerosol was obtained by fitting the power-law function (Park et al., 2003; Xue et al., 2009; Nakao et al., 2011):

$$\rho_{eff} = C d_m^{D_f'-3} \quad \text{Eq. 6.1}$$

where ρ_{eff} is the effective density of particles, C a constant, d_m is the mobility diameter of the particles, and D_f' is the fractal-like dimension. Here, the fractal-like dimension is a measure of the deviation from sphericity of the particle where $D_f' < 3$ indicates a non-spherical particle.

6.3 Results and Discussion

Both gas-phase and aerosol-phase measurements confirm that chronic local air pollution during biomass growth will measurably alter the emissions of biomass burning events.

Figure 6.1 shows the average NO_x emissions for both the polluted and clean fuels, written as a mass emission-like factor: concentration emitted scaled by the amount of fuel burned (ppb g^{-1}). The amount of fuel burned in all of the analysis in this paper refers to the difference between the mass of the burned fuel before and after the fire. The shaded areas of the figure represent the standard deviation of the averages and the time the lights are turned on is indicated on the figure. Unfortunately, CHNS analysis was unavailable for this series of experiments and calculation of a true emission factor, mass of emitted compound per mass of biomass burned, is unavailable. However, our measure is still useful for placing all of the experiments on the same basis. The polluted fuels exhibit higher initial NO_x emissions (1.7 ppb/g) than the clean fuels (1.3 ppb/g) for the same amount of mass burned. The results for NO are similar with polluted fuels having a higher mass emission-like factor than clean fuels (1.2 ppb/g compared to 1 ppb/g). Work has shown that plants grown in areas of high nitrogen deposition rates have higher nitrogen content than plants grown in cleaner areas (Baddeley et al., 1994) so it may well be expected that polluted area fuels would release more NO_x and NO than fuels from clean areas. The climatic impacts of releasing more NO_x and NO from biomass burning are far reaching. An increase of tropospheric nitrogen oxides would have substantial impacts on regional OH concentrations. Up to a sixfold increase in OH has been predicted solely from biomass burning and deforestation in the tropics (Crutzen and Andreae, 1990). If biomass from heavily polluted urban areas, such as Mexico City, releases 50% more NO_x as we show here, then current models may be under predicting

the impact of biomass burning if only clean fuels are used for emission factor values in the models.

Figure 6.2 shows how the average particle size distributions released from polluted and clean fuels change with 6 hours of photochemical aging, based on a per gram of fuel burned basis. Like with NO_x and NO, the polluted fuels emit more particles on a scaled basis. It is interesting to note that the peak size in the distributions for the fresh and 6 hour aged emissions are similar. When considering both fuels, the freshly emitted particle size distribution peaks at 85 ± 5 nm while the photochemical aging process shifts the peak to 110 ± 6 nm. This study therefore agrees with previous work that shows the particle size distributions from biomass burning are much more sensitive to the fire properties (MCE) of the burns than the species being burned (Hosseini et al., 2010). A key result of this study shows that particle size distributions from polluted fuels have higher particle emission rates than clean fuels. As with NO_x and NO, utilizing a single emission factor for biomass burning may not capture the reality of particulate emissions if considering, for example, locations close to and far away from polluted megacities.

The common theme so far with polluted and clean fuels is that there is a measureable difference in multiple gas and particulate-phase properties of the biomass burning emissions. The particle volatility results are support these findings. Figure 6.3 shows the average VFR at 100°C of both the polluted and clean fuels as a function of aging in the chamber. As in Fig. 6.1, the standard deviation is represented with a shaded area and the

time the lights are turned on is shown as a dotted line at 1 hour. Both fuels exhibit an increasing VFR with photochemical aging indicating a change in the composition of the aerosol, consistent with literature (Kalberer et al., 2004). Both fuels even increase their VFR at approximately the same rate throughout the photochemical aging. The polluted fuels start more nonvolatile (VFR = 0.38) than the clean fuels (VFR = 0.27) and end much more nonvolatile (VFR = 0.7 as compared to VFR = 0.5). This indicates that polluted fuels have a much different aerosol composition than the clean fuels both before and after oxidative aging. It is possible that the decreased volatility of polluted fuels is related to an increased starting concentration of particulate nitrogen and gas-particle partitioning of NO/NO_x with photochemical aging. Additional aerosol chemical speciation techniques, not available during this study, are needed in the future.

Figure 6.4 shows the average calculated effective density from the APM system for the clean and polluted fuels. The same conventions as in previous figures for shading and marking are used again. The difference between the two values is smaller than some of the previous figures and may indeed not be statistically significant. The data presented here agrees with the literature that exists on biomass burning aerosol physical morphology characteristics (Giordano et al., 2014). The measured effective density ranges from 0.3 to 0.8 g cm^{-3} and the fresh aerosol emission is likely fractal in nature. The results do generally agree with previous work done on the photochemical exposure of biomass burning aerosol and diesel exhaust as well (Nakao et al., 2011; Giordano et al., 2014). The particles do not become denser until photochemical aging is initiated. The

freshly emitted particles are likely made up of a backbone of some black carbon agglomerate. As the particles age, a covering of low-volatility secondary organic aerosol is likely forming on the backbone which would fill the void spaces in the agglomerate giving a higher effective density. The fact that there is little difference between the clean and polluted fuels here indicates that the bulk effective density of a combustion particle may be like particle size distribution where the physical fire processes are more important than fuel properties.

It is possible that the differences in the emissions between the polluted and clean biomass could be due to circumstances other than their growing conditions. For most combustion fuels (e.g. biomass, coal, and natural gas) higher flame temperature has been shown to correlate with higher NO_x emissions (Levine, 1990; Reid and Hobbs, 1998; Flynn et al., 2000; Glaude et al., 2010). In this study, we use the MCE of the individual burns to compare burning conditions though MCE and the completeness of combustion may not effectively capture flame intensity or temperature (Reid and Hobbs, 1998). If the polluted fuels are emitting more NO_x due to higher flame temperatures, then there may be a connection between biomass growth area air pollution and combustion flame temperature. Future work on this topic should examine if there is a flame temperature and pollution connection. However, despite the uncertainty of the cause of the differences between the emissions of the two fuels, this work presents an interesting path of study that should be examined in more detail in the future.

6.4 Conclusions

This work demonstrates that local air quality during the growth of biomass has a measurable effect on the emissions when that biomass is burned. By conducting environmental chamber experiments on biomass collected from a polluted site and a clean site, this work has showed significant differences in the per mass emission rates of gaseous nitrogen species, total particle number, and the volatility of the aerosol emitted. The photochemical evolutions of polluted and clean fuels are shown to be remarkably similar though. The implications of the observed photochemical evolution are good for models, since it means that only a difference in emission factors need to be considered for clean and polluted fuels.

The work presented here is a preliminary study on a factor that may influence biomass burning emissions. In future studies, fire properties such as flame temperature should be better controlled or accounted for but this work represents a first step towards identifying another factor that can affect biomass burning emissions.

6.5 References

Akagi, S. K., Yokelson, R. J., Wiedinmyer, C., Alvarado, M. J., Reid, J. S., Karl, T., Crounse, J. D., and Wennberg, P. O.: Emission factors for open and domestic biomass burning for use in atmospheric models, Atmos. Chem. Phys., 11, 4039-4072, doi:10.5194/acp-11-4039-2011, 2011.

Allen, E. B., Padgett, P. E., Bytnerowicz, A., & Minnich, R. A. (1996, February). Nitrogen deposition effects on coastal sage vegetation of southern California. In *Bytnerowicz A, Arbaugh MJ, Schilling S, tech. coords. Proceedings of the international symposium on air pollution and climate change effects on forest ecosystems, Riverside, California. General Technical Report PSW-GTR* (Vol. 164).

Baddeley, J. A., Thompson, D. B. A., & Lee, J. A.: Regional and historical variation in the nitrogen content of Racomitrium lanuginosum in Britain in relation to atmospheric nitrogen deposition. *Environmental pollution*,*84* (2), 189-196, 1994.

Cobb, F. W., Jr. & Stark, R. W.: Decline and mortality of smog-injured ponderosa pine. J. For., 68, 147-9, 1970.

Engelhart, G. J., Hennigan, C. J., Miracolo, M. A., Robinson, A. L., and Pandis, S. N.: Cloud condensation nuclei activity of fresh primary and aged biomass burning aerosol, *Atmospheric Chemistry and Physics*, *12*(15), 7285-7293, 2012.

Fenn, M.E. and Bytnerowicz, A.: Dry deposition of nitrogen and sulfur to ponderosa and Jeffrey pine in the San Bernardino National Forest in southern California, Environmental Pollution, 81, 277-285, 1993.

Fenn, M.E., Poth, M.A., and Johnson, D.W.: Evidence for nitrogen saturation in the San Bernardino Mountains in southern California, Forest Ecol. Manag., 82, 211-230, 1996.

Flynn, P. F., Hunter, G. L., Durrett, R. P., Farrell, L. A., and Akinyemi, W. C.: Minimum engine flame temperature impacts on diesel and spark-ignition engine NOx production, No. 2000-01-1177, SAE Technical Paper, 2000.

Giordano, M.R., Short, D.Z., Hosseini, S., Lichtenberg, W., and Asa-Awuku, A.: Changes in droplet surface tension affect the observed hygroscopicity of photochemically aged biomass burning aerosol, Env. Sci. & Tech., 47(19), 10980–10986, doi:10.1021/es401867j, 2013.

Giordano, M.R., Espinoza, C., and Asa-Awuku, A.: Experimentally measured morphology of biomass burning aerosol and its impacts on CCN ability, Atmos. Chem. Phys. Discuss., acp-2014-293, 2014.

Glaude, P., Fournet, R., Bounaceur, R., and Moliere, M.: Adiabatic flame temperature from biofuels and fossil fuels and derived effect on NO*x* emissions, Fuel Processing Technology, 91(2), 229-235, 2010.

Grulke, N.E., Andersen, C.P., Fenn, M.E., and Miller, P.R.: Ozone exposure and nitrogen deposition lowers root biomass of ponderosa pine in the San Bernardino Mountains, California, Environmental Pollution, 103(1), 63-73, 1998.

Hennigan, C. J., Miracolo, M. A., Engelhart, G. J., May, A. A., Presto, A. A., Lee, T., Sullivan, A. P., McMeeking, G. R., Coe, H., Wold, C. E., Hao, W.-M., Gilman, J. B., Kuster, W. C., de Gouw, J., Schichtel, B. A., J. L. Collett Jr., Kreidenweis, S. M., and Robinson, A. L.: Chemical and physical transformations of organic aerosol from the photo-oxidation of open biomass burning emissions in an environmental chamber, *Atmos. Chem. Phys.*, 11, 7669-7686; doi:10.5194/acp-11-7669-2011, 2011.

Hosseini, S., Li, Q., Cocker, D., Weise, D., Miller, A., Shrivastava, M., Miller, J.W., Mahalingam, S., Princevac, M., and Jung, H.: Particle size distributions from laboratory-scale biomass fires using fast response instruments. Atmos. Chem. & Phys., 10, 8065-9076, 2010.

Hosseini, S., Urbanski, S.P., Dixit, P., Qi, L., Burling, I., Yokelson, R., Shrivastava, M., Jung, H., Weise, D. R., Miller, W., and Cocker, D.: Laboratory characterization of PM

emissions from combustion of wildland biomass fuels. *J. Geophys. Res.* 2013,DOI:10.1002/jgrd.50481

Kalberer, M., Paulsen, D., Sax, M., Steinbacher, M., Dommen, J., Prevot, A. S. H., and Baltensperger, U.: Identification of polymers as major components of atmospheric organic aerosols. *Science*, *303*(5664), 1659-1662, 2004.

Kauffman, J.B., Cummings, D.L., Ward, D.E., and Babbitt, R.: Fire in the Brazilian Amazon: 1. Biomass, nutrient pools, and losses in slashed primary forests, Oecologia, 104(4), 397-408, 1995.

Kroll, J.H. and Seinfeld, J.H.: Chemistry of secondary organic aerosol: Formation and evolution of low-volatility organics in the atmosphere, Atmos. Environ., 42(16), 3593-3624, 2008.

Levine, J. S.: Global biomass burning: atmospheric, climatic and biospheric implications. *Eos, Transactions American Geophysical Union*,*71*(37), 1075-1077, 1990.

Malloy, Q.G.J., Nakao, S., Qi, L., Austin, R., Stothers, C., Hagino, H., and Cocker, D.R. III: Real-time aerosol density determination utilizing a modified scanning mobility particle sizer—aerosol particle mass analyzer system, Aerosol Science and Technology, 43:7, 673-678, DOI: 10.1080/02786820902832960, 2009.

McBride, J.R., Semion, V.P., and Miller, P.R.: Impact of air pollution on the growth of ponderosa pine, Calif. Agric., 29(12), 8-9, 1975.

McMurry. P. H., Wang. X., Park. K., and Ebara, K.: The relationship between mass and mobility for atmospheric particles: A new technique for measuring particle density. Aerosol Sci. Technol.. 36(2), 227-238, 2002.

Miller, P. R.: Oxidant-induced community change in a mixed conifer forest. Advan. Chem. Ser., 122, 101-17, 1973.

Miller, P. R., Taylor, O. C. & Poe, M. P.: Spatial variation of summer ozone concentrations in the San Bernardino Mountains. In Proceedings of the Air Pollution Control Association Annual Meeting, Minneapolis, MN, 22-27 June 1986. Air Pollution Control Association, Pittsburgh, PA, Vol. 3, pp. 86-39.2, 1986.

Miller, P.R., Stolte, K.W., Duriscoe, E., Pronos, J. (tech coor), 1996. Monitoring ozone air pollution effects on western pine forests. USDA Forest Service, Pacific Southwest Region, GTR-155, Albany, CA, USA.

Nakao, S., Shrivastava, M., Nguyen, A., Jung, H., and Cocker, D. III: Interpretation of secondary organic aerosol formation from diesel exhaust photooxidation in an

environmental chamber, Aerosol Science and Technology, 45:8, 964-972, doi:10.1080/02786826.2011.573510, 2011.

Orsini, D. A., A. Wiedensohler, F. Stratmann, D. S. Covert, 1999: A New Volatility Tandem Differential Mobility Analyzer to Measure the Volatile Sulfuric Acid Aerosol Fraction. *J. Atmos. Oceanic Technol.*, 16, 760–772.

Park. K., Cao, F., Kittelson, D. B., and McMurry. P. H.: Relationship between particle mass and mobility for diesel exhaust particles, Environ. Sci. Technol. 37(3), 577-583, 2003.

Petters, M. D., Carrico, C. M., Kreidenweis, S. M., Prenni, A. J., DeMott, P. J., Collett, J. L., and Moosmüller, H.: Cloud condensation nucleation activity of biomass burning aerosol, *J. Geophys. Res.*, 114, D22205, doi:10.1029/2009JD012353, 2009.

Pronos, J., Vogler, D.R., and Smith, R.S., : An evaluation of ozone injury to pines in the southern Sierra Nevada. USDA Forest Service, Pacific Southwest Region, Forest Pest Management Report 78-1, 1-13. Albany, CA, USA, 1978.

Ramanathan, V., Crutzen, P. J., Kiehl, J. T., and Rosenfeld, D.: Aerosols, climate, and the hydrological cycle, *Science*, *294*(5549), 2119-2124, 2001.

Reid, J. S. and Hobbs, P. V.: Physical and optical properties of young smoke from individual biomass fires in Brazil, Journal of Geophysical Research: Atmospheres (1984–2012), 103(D24), 32013-32030, 1998.

Sato, K., Nakao, S., Clark, C. H., Qi, L., and Cocker III, D. R.: Secondary organic aerosol formation from the photooxidation of isoprene, 1,3-butadiene, and 2,3-dimethyl-1,3-butadiene under high NO_x conditions, Atmos. Chem. Phys., 11, 7301-7317, doi:10.5194/acp-11-7301-2011, 2011.

Schaetzl, R. J. and Anderson, S.: Basic Concepts: soil horizon...the alphabet of soils. *Soils: Genesis and Geomorphology* . Cambridge: Cambridge University Press, 2005.

Thonicke, K., Spessa, A., Prentice, I.C., Harrison, S.P., Dong, L., and Carmona-Moreno, C.: The influence of vegetation, fire spread and fire behaviour on biomass burning and trace gas emissions: results from a process-based model." *Biogeosciences* 7(6), 2010.

van der Werf, G. R., Randerson, J. T., Giglio, L., Collatz, G. J., Kasibhatla, P. S., and Arellano Jr., A. F.: Interannual variability in global biomass burning emissions from 1997 to 2004, *Atmos. Chem. Phys*., 6, 3423-3441, doi:10.5194/acp-6-3423-2006, 2006.

Wang, S. C., Flagan, R. C.: Scanning Electrical Mobility Spectrometer, Aerosol Science and Technology, 13, 230–240, 1990.

Ward, D. E. and Radke, L. E.: Emission measurements from vegetation fires: a comparative evaluation of methods and results, in: Fire in Environment. The Ecological, Atmospheric and Climatic Importance of Vegetation Fires, edited by: Crutzen, P. J. and Goldammer, J. G.,John Wiley and Sons, New York, pp. 53–76, 1993.

Xue, H., Khalizov, A. F., Wang, L., Zheng, J., and Zhang, R.: Effects of coating of dicarboxylic acids on the mass-mobility relationship of soot particles, Environ. Sci. Technol., 43:2787–2792, 2009.

6.6 Figures

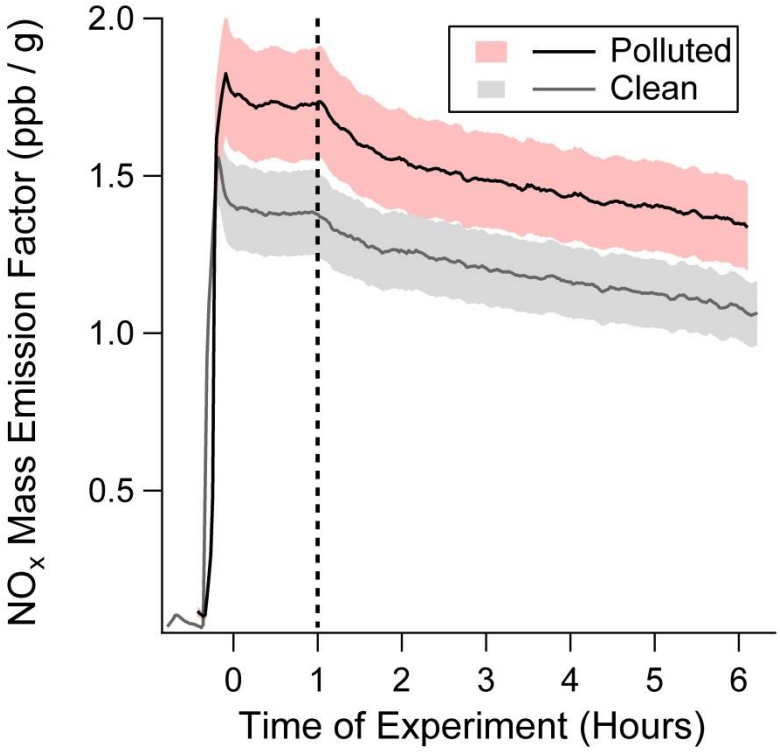

Figure 6.1: Average NO_x mass emission rate versus time in the chamber for polluted and clean fuels. Shaded areas represent the standard deviation of the average. The dotted line at one hour indicates the time the lights were turned on.

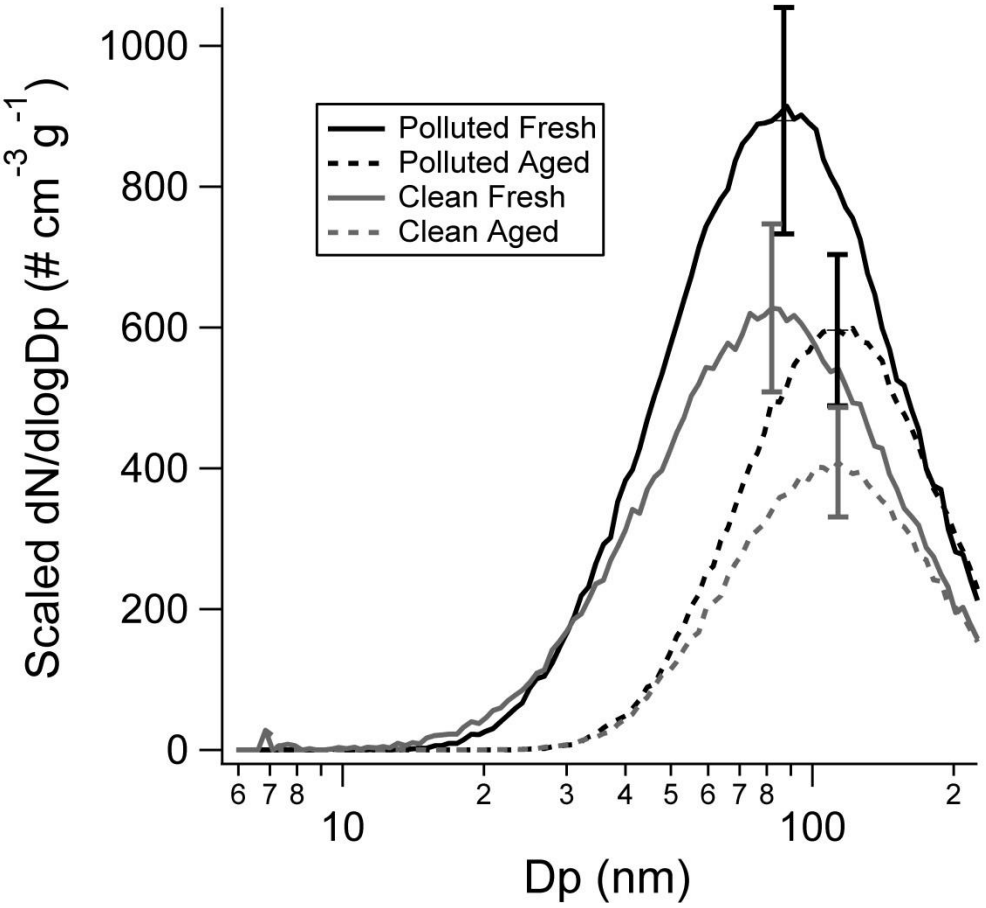

Figure 6.2: Average particle size distribution, on a per gram of fuel burned basis, for freshly emitted (solid lines) and 6 hour photochemically aged (dotted lines) emissions of clean (grey lines) and polluted (black lines) fuels. Included are the standard deviations of the data.

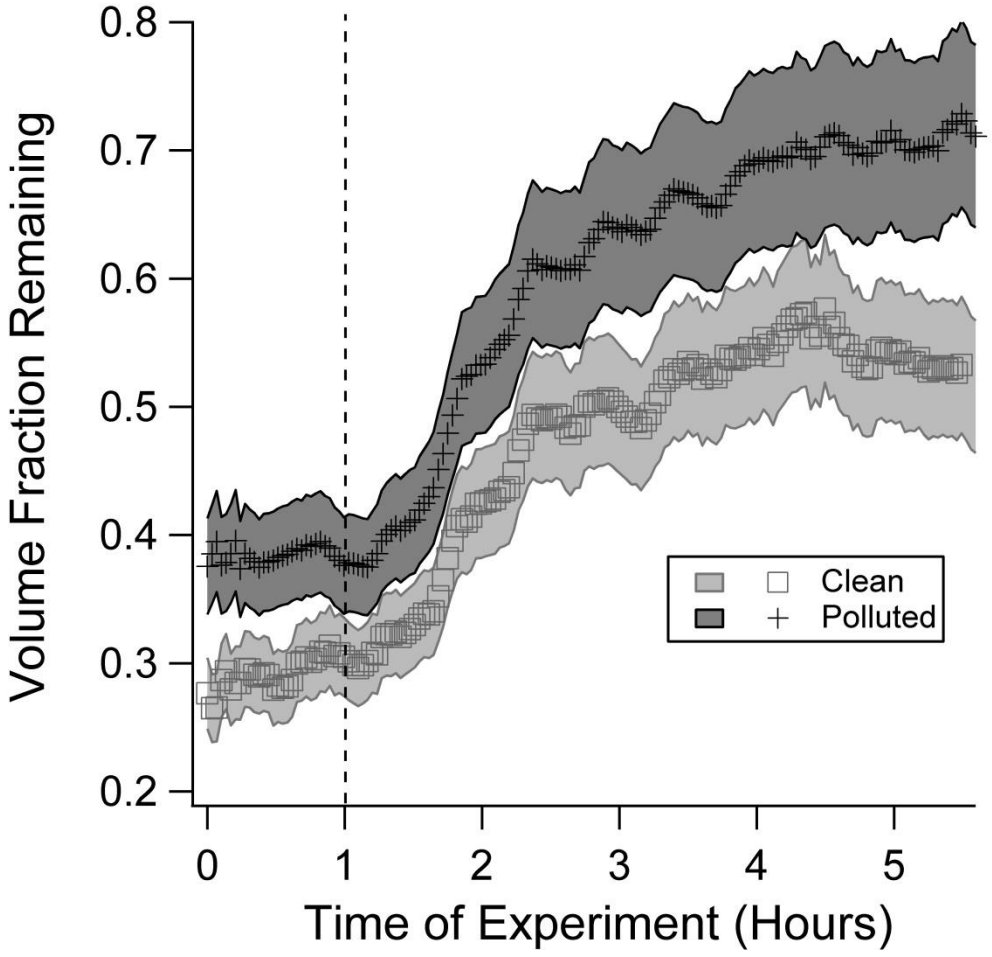

Figure 6.3: Volume fraction remaining of the aerosol versus time in experiment. The average values for clean fuels (grey) and polluted fuels (black) are shown with their standard deviations as shaded areas. The dotted line represents the time the lights are turned on in the experiment.

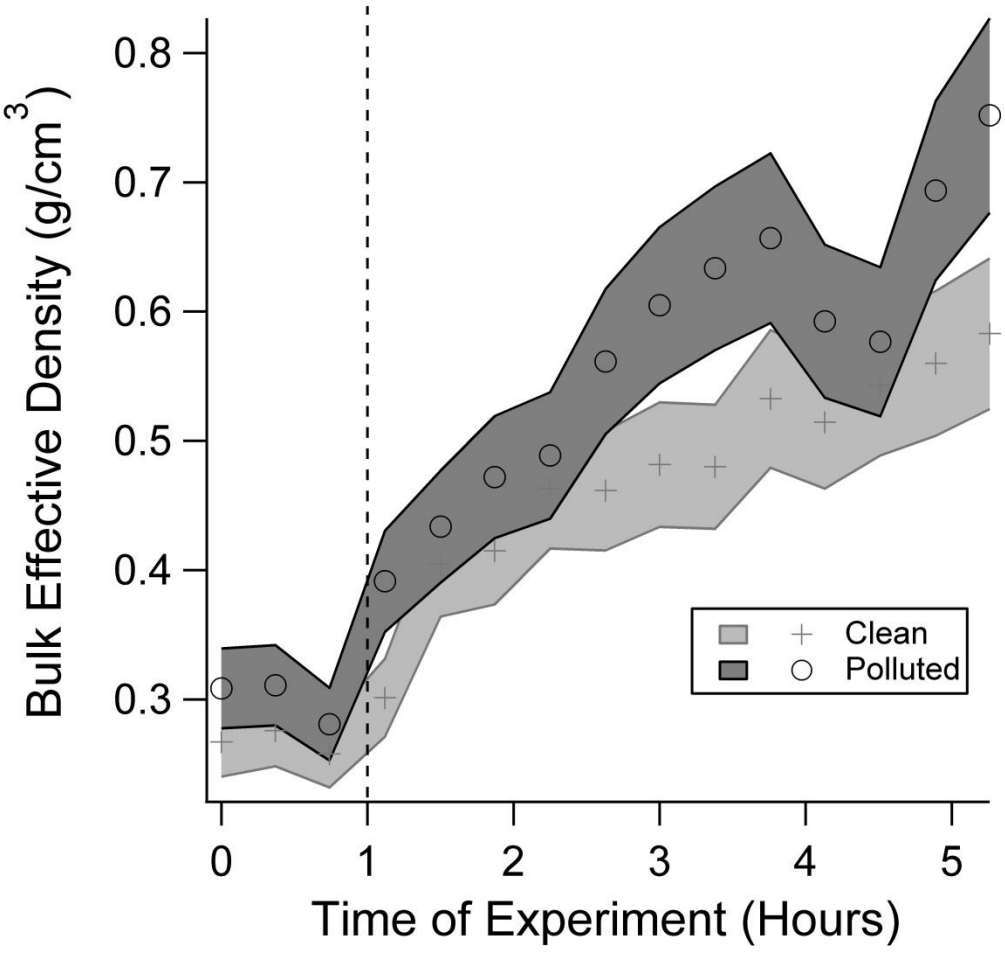

Figure 6.4: Average bulk effective density for clean fuels (grey) and polluted fuels (black). The standard deviations are represented as shaded areas. The dotted line represents the time the lights are turned on in the experiment.

7 Conclusions

The overall goal of this dissertation was to constrain the climatic impacts of biomass burning. The goal was achieved through analyzing how surface tension, particle morphology, light absorption, and growing conditions affect the parameterization and estimation of biomass burning emissions' direct and indirect climate effects. An environmental chamber with simulated photochemical aging was used to achieve the stated goal.

Chapter two investigated how surface active compounds in biomass burning aerosols effects the perceived hygroscopicity of the aerosol. This study was the first environmental chamber study to show that surface active compounds exist in biomass burning aerosol and that their characteristics evolve with photochemical aging. Two different species of biomass show differing trends of surface activity: chamise has an increasing surface tension depression with photochemical aging while manzanita has a decreasing surface tension depression. When accounting for the presence of surfactants, the hygroscopicity parameter κ is shown to be lowered by up to 30%, depending on the photochemical aging of the system. Thus, the common assumption that surface active compounds are negligible for the CCN activity is improper when applied to biomass burning aerosol.

Chapter three evaluated how particle morphology affects the κ hygroscopicity parameterization of biomass burning aerosols and how particle morphology evolves with

photochemical aging. The results indicate that the particles are non-spherical and that the degree of non-sphericity lessens with aging. An assumption that is applied when using the κ hygroscopicity parameterization is that the electrical mobility diameter is a measure of the volume of the particle. This work shows that assumption is incorrect for biomass burning aerosol and can overestimate the true volume of the particles by up to 50%. When correcting κ for the true volume of the particle, estimates of the hygroscopicity are underestimated by 15-50% at fresh emission.

Chapter four applied the corrections from chapters two and three to form a more accurate κ parameterization of hygroscopicity. Results indicate that by applying κ without any surface tension or morphology corrections overestimates κ by up to 30% at fresh emission and 5% upon six hours of photochemical aging. This work therefore indicates that the age of the biomass burning emissions must be taken into account when trying to model biomass burning's climatic impacts.

Chapter five explored biomass burning aerosol light absorption and how the absorption evolves with photochemical aging. This study used a PILS-WSOC-UVVis system to measure the light absorption in a semi-online manner where previously only filter studies have been conducted. The results indicate that the absorption characteristics are similar to carboxylic acids commonly found in atmospheric aerosols. The results also indicate that light absorption of the particles can evolve with photochemical aging and follow trends similar to surface tension results discussed in chapter two.

Chapter six presents evidence that the air quality of a region during the growth of biomass can impact that biomass' emissions upon burning. Biomass of the same species from a polluted area and a non-polluted area were examined in the environmental chamber and exposed to photochemical aging. This work shows that biomass grown in an area of chronic air pollution has more gas and particle-phase emissions on a per mass burned basis. Results also indicate that there is a significant difference in the volatility of the aerosol emitted. Therefore, in addition to factors such as fire properties and biomass species, the growth area of biomass participating in biomass burning events should be taken into consideration when estimating biomass burning's climatic impacts. The results of this chapter are preliminary but show a promising path for future work to explore.

Continuing work on biomass burning is necessary in order to fully understand how this important source of aerosol and trace gases to the atmosphere affects climate. This work, however, provides some constraint on the climatic impacts of the phenomena. Future work should focus on exploring the presence of surfactants in biomass burning aerosol, if fire properties affect particle morphology, and if any other factors are impacted by air pollution during biomass growth.